AD-A055 592 BOEING CO SEATTLE WASH F/G 20/14
EMP COUPLING ANALYSIS FOR H.M.S. SHEFFIELD.(U)
MAY 78 R S CARTER, D E YOUNG N60921-77-C-0185
UNCLASSIFIED D194-10043-1 NL

1 OF 2
AD
A055 592

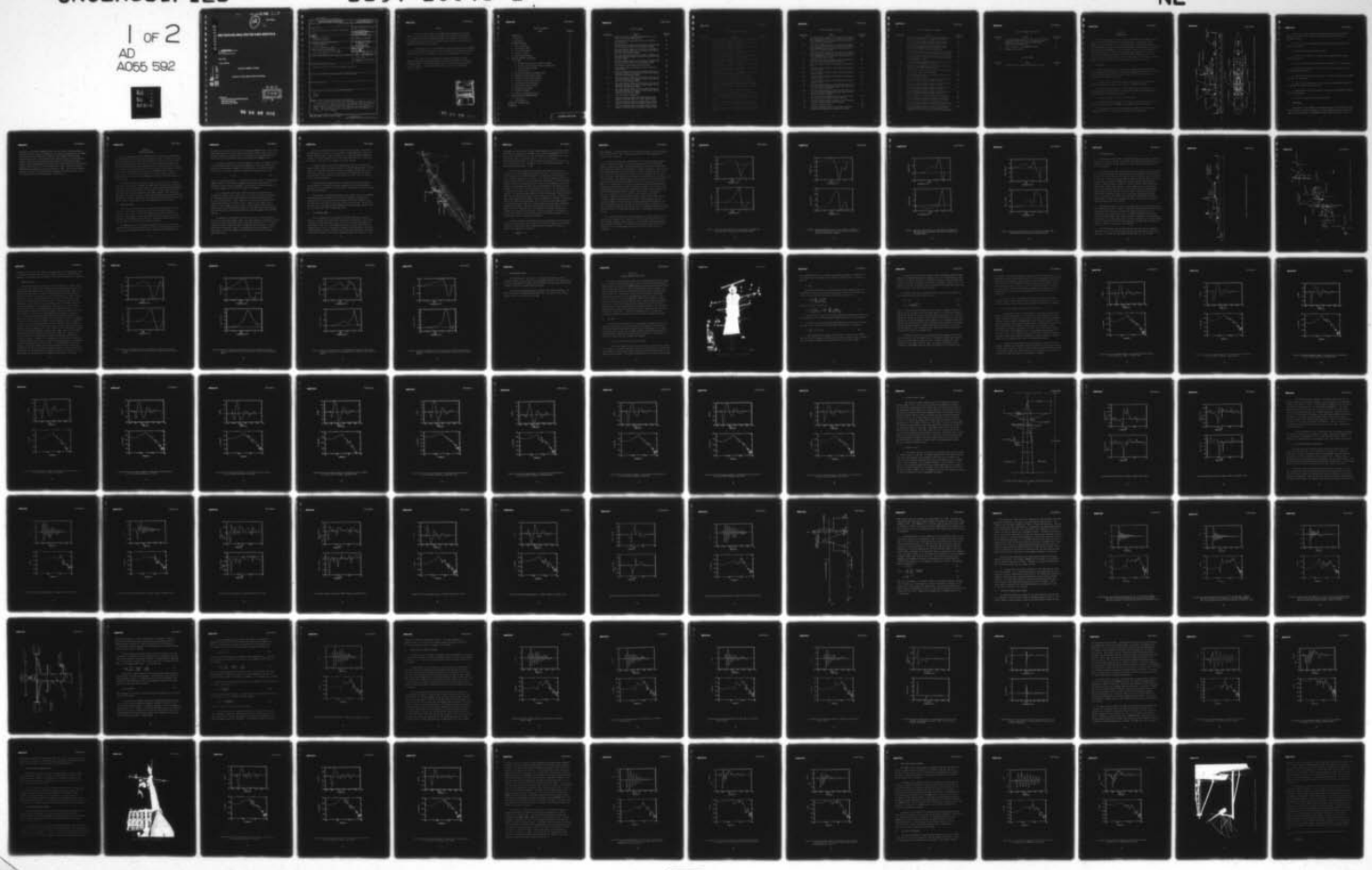

(12)

D194-10043-1

EMP COUPLING ANALYSIS FOR H.M.S. SHEFFIELD

THE BOEING COMPANY
P.O. BOX 3707
SEATTLE, WASHINGTON 98124

MAY 1978

FINAL REPORT

CONTRACT N60921-77-C-0185

Approved For public release; distribution unlimited

Prepared for
NAVAL SURFACE WEAPONS CENTER
White Oak Laboratory
Silver Spring, MD 20910

UNCLASSIFIED

SECURITY CLASSIFICATION OF THIS PAGE (When Data Entered)

REPORT DOCUMENTATION PAGE

READ INSTRUCTIONS BEFORE COMPLETING FORM

1. REPORT NUMBER	2. GOVT ACCESSION NO. / 3. RECIPIENT'S CATALOG NUMBER
4. TITLE (and Subtitle): EMP Coupling Analysis for H.M.S. Sheffield.	5. TYPE OF REPORT & PERIOD COVERED: Final Report.
	6. PERFORMING ORG. REPORT NUMBER: D194-10043-1
7. AUTHOR(s): Dr. Robert S. Carter; Dr. Donald E. Young	8. CONTRACT OR GRANT NUMBER(s): N6921-77-C-0185
9. PERFORMING ORGANIZATION NAME AND ADDRESS: The Boeing Company, P.O. Box 3707, Seattle, Washington 98124	10. PROGRAM ELEMENT, PROJECT, TASK AREA & WORK UNIT NUMBERS: 62734N; F34384; ZF34384001; WA3016
11. CONTROLLING OFFICE NAME AND ADDRESS: Naval Surface Weapons Center, WOL, White Oak, Silver Spring, Md 20910, Attn: Code WA-51	12. REPORT DATE: May 1978
	13. NUMBER OF PAGES: 118
14. MONITORING AGENCY NAME & ADDRESS (if different from Controlling Office)	15. SECURITY CLASS. (of this report): Unclassified
	15a. DECLASSIFICATION/DOWNGRADING SCHEDULE

16. DISTRIBUTION STATEMENT (of this Report)

Approved for public release; distribution unlimited.

17. DISTRIBUTION STATEMENT (of the abstract entered in Block 20, if different from Report)

18. SUPPLEMENTARY NOTES

19. KEY WORDS (Continue on reverse side if necessary and identify by block number)

EMP
EMPRESS
WIRANT

20. ABSTRACT (Continue on reverse side if necessary and identify by block number)

This report presents the results of an electromagnetic modeling analysis of the British destroyer H.M.S. Sheffield. EMP coupling models were developed for selected masts, antennas, and cabling aboard ship. Calculating of EMPRESS induced responses to these items were made using the computer code WIRANT. The calculated responses were compared to test data obtained on these two items by NSWC.

DD FORM 1 JAN 73 1473 EDITION OF 1 NOV 65 IS OBSOLETE

UNCLASSIFIED

SECURITY CLASSIFICATION OF THIS PAGE (When Data Entered)

059 690

JCB

PREFACE

This is the final report on the EMP coupling analysis of the H.M.S. Sheffield. This analysis effort was performed for the Naval Surface Weapons Center (NSWC) under Contract N60921-77-C-0185. The purpose of this effort was to demonstrate the applicability of computer-aided analysis to the solution of EMP coupling problems in ship systems.

NSWC conducted tests on the Sheffield under vertically-polarized EMPRESS excitation for one angle of incidence. The test data will be compared by NSWC to the analysis results. The analysis results only are presented in this report.

This report has been prepared by the Systems Vulnerability and Hardening Branch of the Logistics Support and Services Division in the Boeing Aerospace Company. The Program Manager was D. E. Isbell; the Project Engineer was J. W. Schomer. The principal investigators were Dr. D. E. Young and Dr. R. S. Carter.

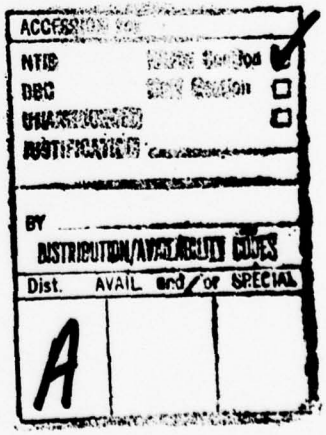

TABLE OF CONTENTS

LIST OF FIGURES

LIST OF FIGURES (Continued)

LIST OF FIGURES (Continued)

LIST OF FIGURES (Continued)

LIST OF FIGURES (Continued)

LIST OF TABLES

SECTION 1
INTRODUCTION

This report contains the results of an electromagnetic pulse (EMP) coupling analysis of the H.M.S. Sheffield, a British destroyer. Voltage and current responses on selected ship's systems are calculated for a free-field excitation of the Sheffield provided by the Navy's Electromagnetic Pulse Radiating Environment Simulator for Ships (EMPRESS). These calculated responses will be compared to measured data obtained by Naval Surface Weapons Center (NSWC) in the Sheffield under actual EMPRESS radiated EMP fields. The EMPRESS excitation at the ship location was a vertically-polarized, 2800 V/M peak electric field with an incident angle of 62^{o} off the bow 85^{o}, measured from the center line of the ship.

1. OBJECTIVES

The basic objective of this program was to demonstrate the applicability of the computer aided EMP analysis techniques, developed for analysis of aircraft, to the problem of predicting EMP-induced responses on naval ship systems. Specifically, the objectives were to:

a. Examine survey data obtained during an on-ship survey of the H.M.S. Sheffield conducted in January 1977 (Contract No. N60921-77-M-1160).

b. Construct electromagnetic coupling models that relate an exernal electromagnetic (EM) environment to the induced responses on selected antennas, cables, and masts on the H.M.S. Sheffield.

c. Produce transfer functions from the models.

d. Calculate induced voltages and currents on the selected items using the measured source field of the EMPRESS at the H.M.S. Sheffield's location.

The selected items for which predictions were made in this program are identified in Figure 1. The following responses were calculated:

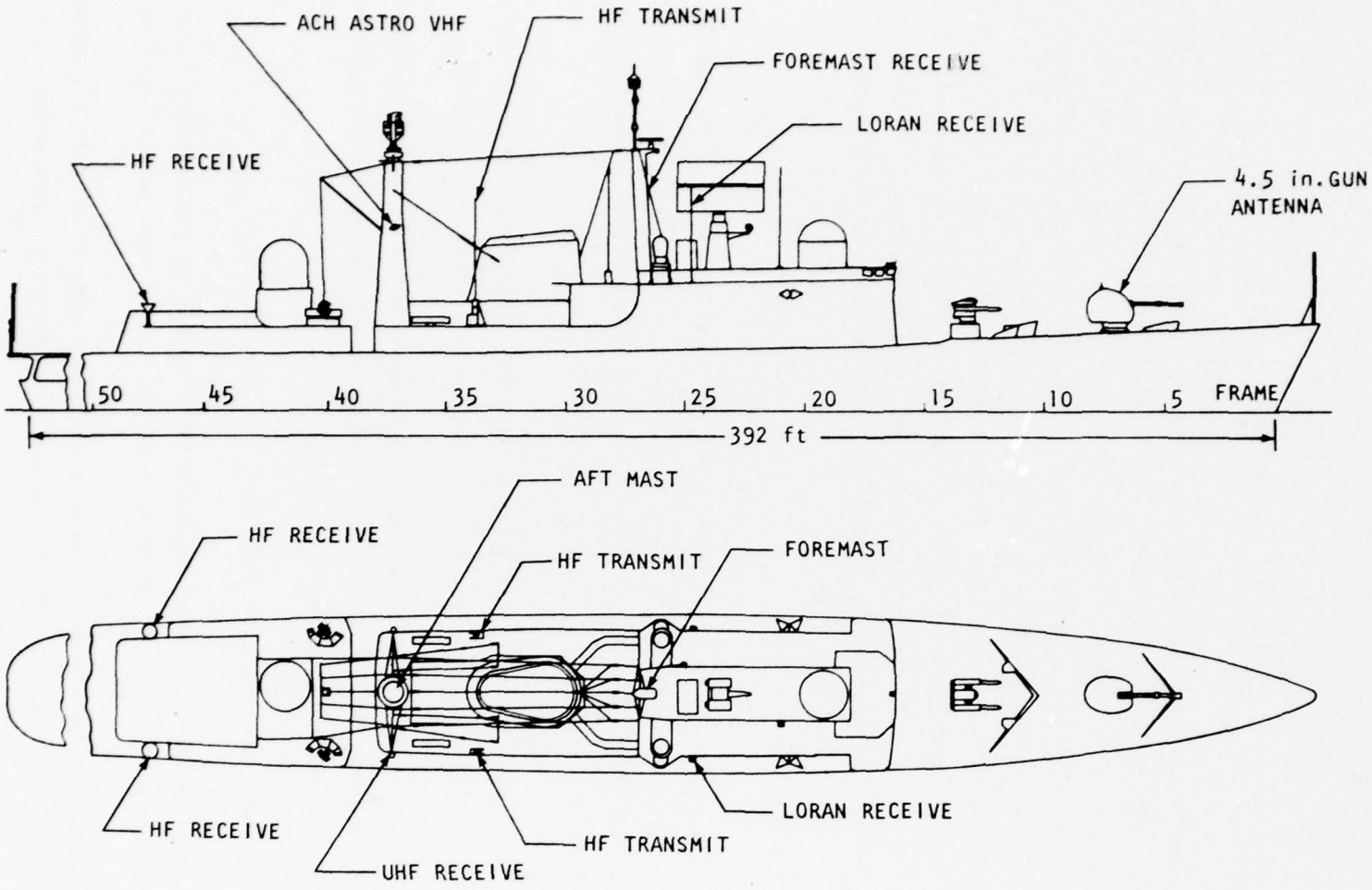

Figure 1 Locations of H.M.S. Sheffield Antennas, Masts, and Cables Analyzed for EMP Coupling

a. Aft mast surface current distribution on each of the four sides at heights of 1, 5 and 9 meters and the total currents on each of the five horizontal yardarms.

b. 4.5-inch gun mount whip antenna bulk cable current at three points inside the gun mount.

c. UK/SRA-102 antenna bulk cable currents.

d. Short circuit current at the base of the foremast wire MF receive antenna (starboard).

e. Foremast surface current distribution at heights of 1, 5 and 9 meters.

f. Open circuit voltage and short circuit current at the base of the HF transmitting whip (port).

g. Open circuit voltage and short circuit current at the base of the LORAN receiver whip (starboard).

h. Open circuit voltage, short circuit current, and matched load current at the MCO for the ACH Astro VHF antenna.

i. Matched load current and voltage in the MCO for the UK/SRA-101 antennas (port and starboard).

j. Current on cables in the operations room.

2. BACKGROUND

The purpose of this program was to make predictions of voltage and current levels induced at various locations on the H.M.S. Sheffield by the electric and magnetic fields produced by the EMPRESS simulated EMP environment. A brief

description of the Navy's EMPRESS facility and its electric field measured at the ship's location is given in Appendix A. The ship was subjected to the EMPRESS fields during a test conducted by the Naval Surface Weapons Center between September 16-25, 1977. The predictions were made by using a wire grid modeling computer code which was developed several years ago at the Boeing Aerospace Company, Seattle, Washington, and has been used on many previous aircraft programs. Examples include the B-1, F-111, 747, and YC-14. It was also used to predict EMPRESS-induced responses on the U.S.S. Valcour in 1975. This wire grid modeling technique is based on a method of moments solution for induced currents on the wire grid model and is described further in Section II.1.

SECTION II
TECHNICAL APPROACH

Prior to commencement of the modeling activity, the physical descriptions of the Sheffield and its antennas were examined in detail. Included in this were ship's drawings and the data collected by a Boeing survey crew in January 1977. The survey data consist of notes and sketches of the antennas and cables plus more than 100 photographs taken onboard the ship. Discussions with the survey crew were also held at the beginning of this program to clarify details on antenna connectivity. The documentation on the vertical EMPRESS field, provided by NSWC, was also reviewed since the final time domain and frequency domain predictions are to be made for the EMPRESS environment to facilitate comparisons with test data.

The analytical models were kept as simple as possible. Minor scatterers such as most of the HF wire antennas and upper deck structure were not included. Similarly, cross coupling to other cables was ignored except through a generalized loss term. These secondary effects are expected to be small and, in general, will tend to give more loss than the simple models predict. When simplifying the models, it was always done in a manner which gave maximum coupling, neglecting shadowing, for example. Therefore, when comparing the analytical predictions with the test data, the analytical results are expected to be over estimates.

1. MODELING METHODS

All of the models presented in this report are frequency domain transfer functions. The transfer functions are ratios of the voltage, current, or surface current response to an incident plane wave electric field with unit amplitude. The response spectrums were obtained by multiplying the transfer functions by the EMPRESS incident spectrum. A numerical inverse Fourier transform was then used to obtain the time domain responses.

The EMPRESS spectrum as displayed in Appendix A is the sum of a direct incident field plus a water reflected field. Since the reflection angle is near the horizon, the reflected field is nearly identical to the incident field.

Therefore, the incident field is half of the measured EMPRESS field. Most of the models developed on this task include a ground plane either at water level or at an upper deck level so that the fields in the absence of any scattering object have direct and reflected plane waves which represent the EMPRESS field.

The transfer functions of response (voltage or current) to incident electric field were generated by the computer code WIRANT [1]. This code solves for the currents on wire segments induced by an incident field. The method of moments [2] is used to reduce the solution to a simple matrix equation of the form

$$ZI = V \qquad (1)$$

where I is the current matrix, V is the excitation matrix, and Z is a generalized impedance matrix. The current is expanded as a series of pulse functions (constant current on each wire segment). Good results are usually obtained if the segment lengths are less than one sixth of a wavelength.

A wire grid model of the H.M.S. Sheffield could be constructed which included all antennas, masts, cables, etc., for which an analysis was required. All important structures would be included in the model to account properly for the scattered fields. If this model were to be valid up to 50 MHz, each segment length should be less than 1 meter. Hence, it would require many segments of this length to construct this wire grid model of the entire ship. However, practical considerations (computer run time and central memory) dictate that the total number of wire segments be less than 160 segments for a CDC 6500 computer.

The modeling of the Sheffield, therefore, consists of several submodels, each with a restricted frequency range. The upper frequency of each model is determined by the segment length and the one-sixth wavelength constraint. The lower frequency limit of a particular model is dependent upon the number of segments which limits the physical extent of the Sheffield that can be modeled. A discussion of two of the submodels of the Sheffield will help in clarifying these restrictions.

The lowest frequency model must include the entire length of the ship if the dominant ship resonance is to be included. If 100 segments are used, the nominal segment length is about 15 meters. This implies an upper frequency of 3.3 MHz. The lower frequency limit is zero since the entire ship is included. This model is described in more detail in the next section.

A higher frequency model of the ship which is valid up to 15 MHz would require segment lengths less than 3.33 meters. With 160 segments each 3.33 meters long, one is limited to modeling the fore and aft masts, the HF antennas, and some of the upper deck structures. Therefore, this submodel does not contain the fundamental ship resonance but would contain the first several resonances of the masts and antennas.

Using the above two models, the first several ship and mast resonances can be obtained. The higher order ship resonances were not included but are not expected to be significant. A discussion of the merging of the two solutions will be presented later.

The modeling of individual substructures may require one or more submodels depending upon their physical size. Usually, an asymptotic solution such as physical optics or the infinite wire current can be used to extend a wire grid model up to the upper limit of the incident field spectrum. The main mast surface current, for example, should approach the physical optics solution when the mast becomes more than 2 wavelengths long.

2. LOW FREQUENCY MODEL

The low frequency wire grid model of the H.M.S. Sheffield is shown in Figure 2. The ship was oriented with the stern at the coordinate system origin extending in length along the X axis. The ship's structure was divided into many segments where each of the segments was a metal cylinder upon which the induced currents flow. The model has 91 segments and 60 junctions. The radius of each segment was chosen so that the total area of the cylinder's surface was electrically equivalent to the ship's surface area which it represents. Since

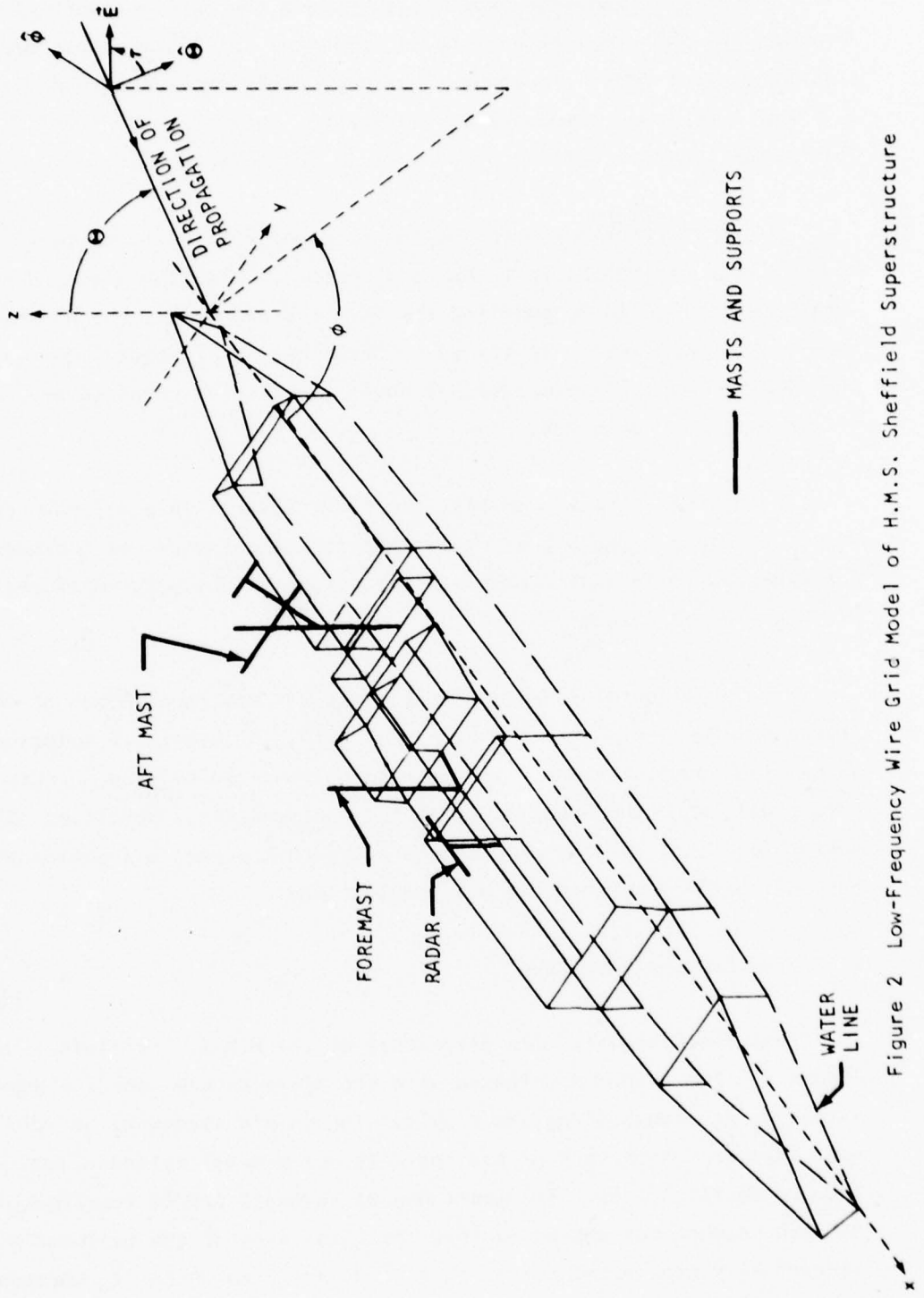

Figure 2 Low-Frequency Wire Grid Model of H.M.S. Sheffield Superstructure

this model was used only for the low-frequency analysis, only the major elements of the ship's structure were included. The incident electromagnetic field is shown in the coordinate system. The polar angle θ is measured from the Z axis, the azimuth angle $\hat{\phi}$ is measured from the X axis in the X-Y plane and the polarization angle τ is the angle which the electric field makes with the $\hat{\theta}$ unit vector in the $\hat{\theta} - \hat{\phi}$ plane. Hence, vertical polarization has $\tau = 0^{\circ}$ and horizontal polarization $\tau = 90^{\circ}$.

The low frequency model was to determine the currents and fields for frequencies near the fundamental resonance of the ship. The length of the ship is 125 meters and the resonant frequency is 2.5 MHz (full wave) whereas the first half-wave resonance is at 1.2 MHz. Thus, segment lengths were chosen so that the model would be valid up to frequencies near 3 MHz. The maximum segment length is given by the condition that the current in the segment be essentially constant. As mentioned previously, this was obtained when the length ℓ of the segment is $\ell < \lambda/6$ where λ is the wavelength of interest. This corresponds to a length of 16.7 meters. This condition was satisfied for all the segments except several of the long horizontal segments which were 27.4 meters. Hence, currents in these segments may not be constant as the frequency nears 3 MHz. Currents in these long segments were monitored closely to determine if the model was breaking down as the frequency was increased. Thus, by using the low-frequency model up to frequencies near 3 MHz, the currents produced near the ship's fundamental resonances were found. Two other considerations enhance the quality of this model. First, the "fatness" of the ship reduces the resonant frequency and second, the excitation of the ship was in the vertical mode. The segments in the vertical direction were short compared to the resonant wavelength so that the constant current assumption was satisfied.

The model considers the sea water to be a good conductor at the frequencies of analysis and represents the sea water as a perfectly conducting ground plane. That this is valid can be seen by calculating the frequency for which the conductivity condition is satisfied,

$$\frac{\sigma}{2\pi f \varepsilon_o \varepsilon_r} >> 1. \qquad (2)$$

For sea water, $\sigma = 4$ mhos/m and $\varepsilon_r = 81$ so that the sea water is a good conductor for $f << 8.9 \times 10^8$ Hz. This condition was satisfied for all frequencies of interest in this analysis.

In order to determine the transfer function for the low frequency model (LFM), the model was excited by a unit amplitude plane wave for frequencies between 0.1 MHz and 4.0 MHz. The real and imaginary parts of the current have been plotted for several selected segments in Figures 3 through 5. Figure 3 shows the real and imaginery parts of the current transfer function 2.4 meters up the main or aft mast. The resonance associated with the length of the mast can be seen at 2.8 MHz. The influence of the ship's structure broadens the resonance. Due to restrictions on the maximum frequency for which the LFM is accurate, currents above 3 MHz should be viewed with caution (the current was set to zero at 4.2 MHz). It is significant to note that no resonances associated with the ship's length are seen in the mast current. The ship's resonance is near 1 MHz. This is not unexpected since the mast is perpendicular to any currents which may have been associated with the ship's resonance. The currents in the gunwales are shown in Figures 4 and 5 in order to check further for the ship's resonance. Segment 4 is located amidships and segment 8 in the bow. Currents in neither segment exhibit the ship's resonance. This indicates that the vertical excitation of the ship does not have any appreciable coupling to the horizontal modes of the ship, or that the horizontal modes are shorted out by the sea water when they reach the bow and stern. A resonance probably associated with the aft mast is present near 2.4 MHz, but no low-frequency resonances are present.

The interaction between the aft and foremasts is shown in Figure 6. The current on the foremast has a strong dip in the real and imaginary parts near the resonance frequency of the aft mast. This coupling was expected because of the proximity of the masts. The influence of the foremast upon the main mast current is not as strong because the aft mast current is larger near the resonance.

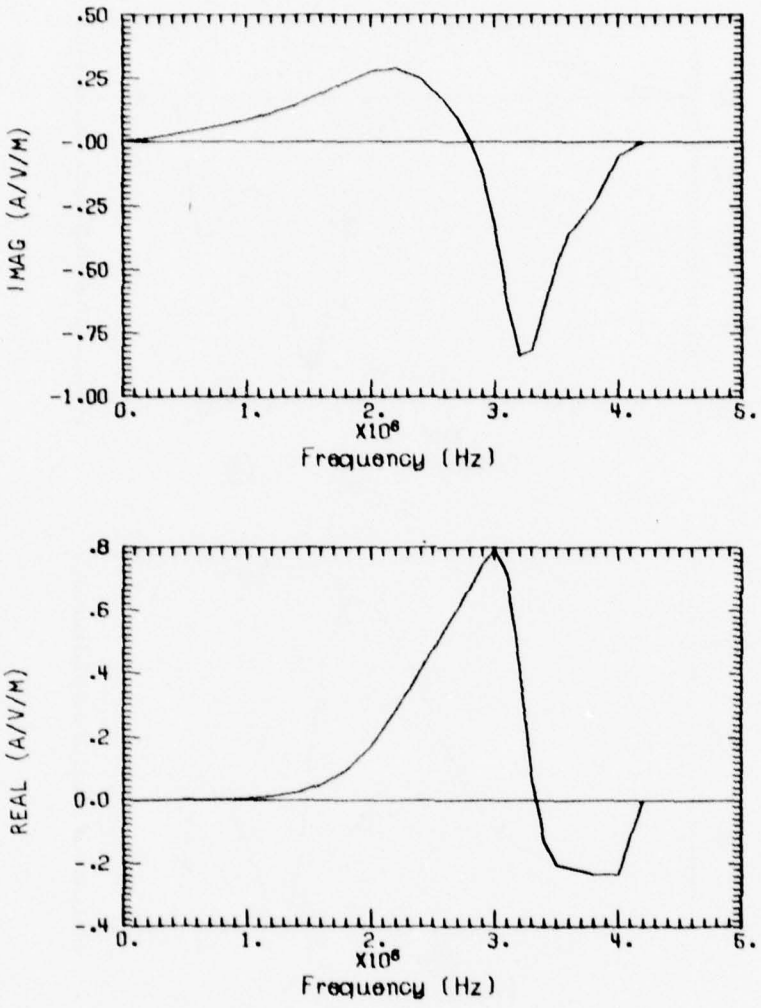

Figure 3 Real and Imaginary Parts of the Current on Segment 85 - Aft Mast (H.M.S. Sheffield Low-Frequency Model)

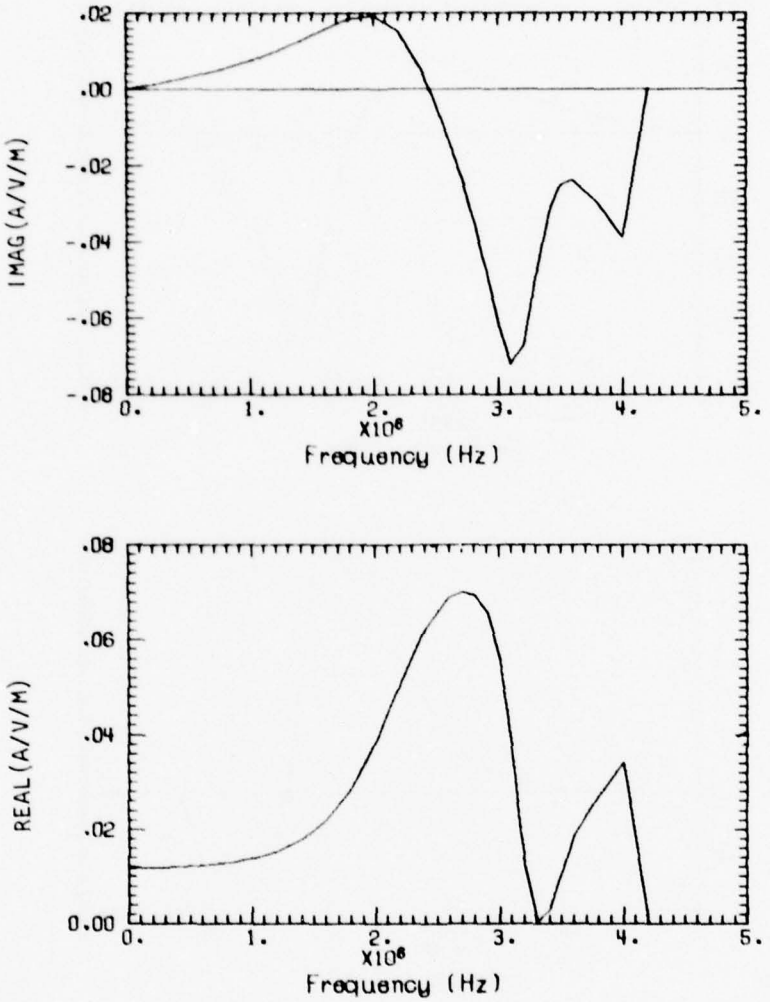

Figure 4 Real and Imaginary Parts of the Current on Segment 4 - Mid Ship Section, Main Deck, Illuminated Side (H.M.S. Sheffield Low-Frequency Model)

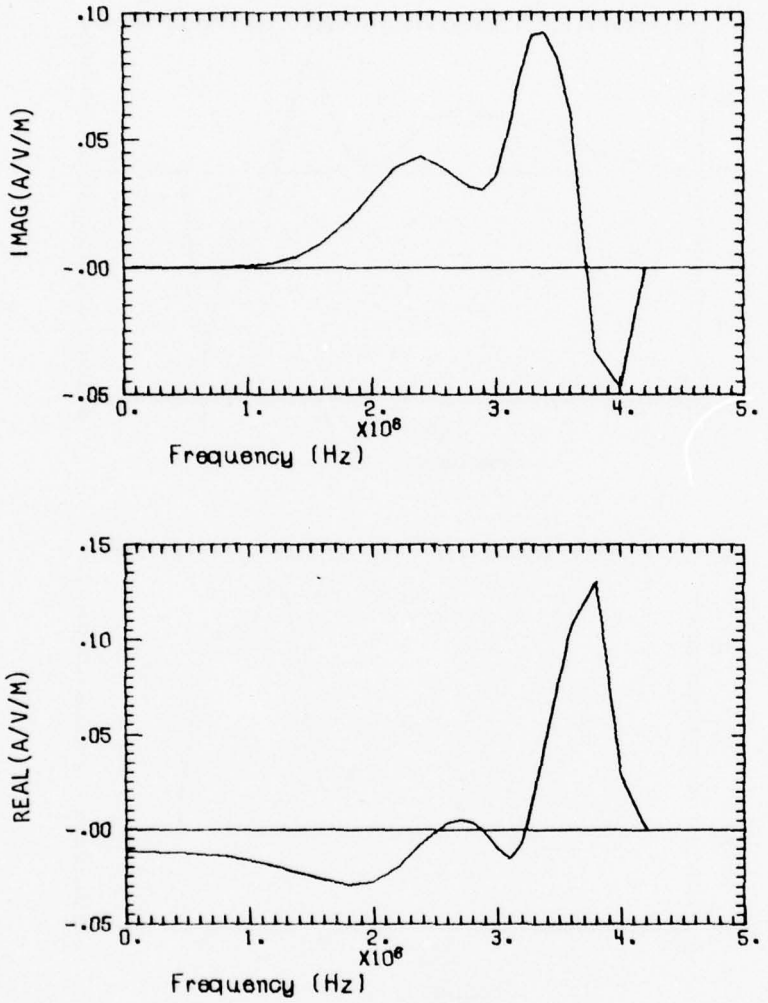

Figure 5 Real and Imaginary Parts of the Current on Segment 8 - Bow Section on Illuminated Side (H.M.S. Sheffield Low-Frequency Model)

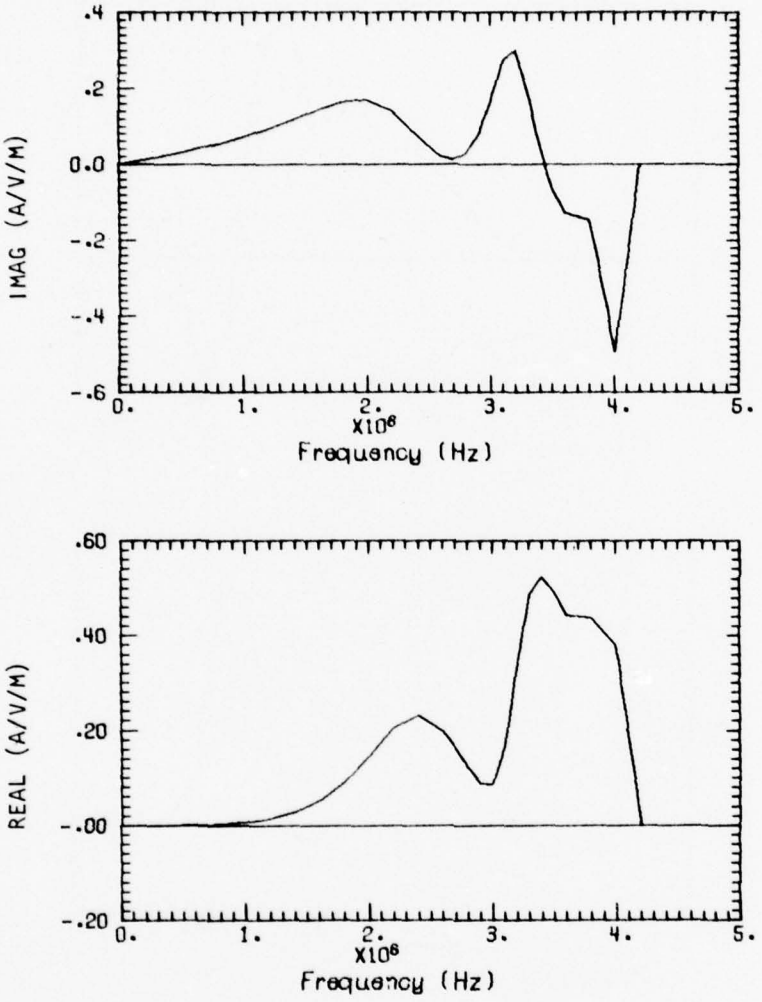

Figure 6 Real and Imaginary Parts of the Current on Segment 88 - Foremast (H.M.S. Sheffield Low-Frequency Model)

3. MID-FREQUENCY MODEL

A mid-frequency model (MFM) of the Sheffield was constructed to extend the analysis from 3 MHz to 15 MHz. In addition to extending the frequency range, the model must include the aft and foremasts in order that mast current densities can be calculated.

In constructing the MFM, advantage was taken of the fact that the scattered fields are only important for positions within one wavelength of the scattering object. This greatly reduces the amount of the structure that need be included in the model. The items which were analyzed that are near the foremast were the wire MF receive antenna, the LORAN receiver whip, and the foremast surface currents. Nearby structure includes the radar, several HF whips, 909 director, smoke stack, and HF transmit antenna. Items studied which are near the aft mast are the ACH Astro VHF antenna, the HF transmitting whip, the UK/SRA-102 antenna cable, and the aft mast surface currents. Important structure near the aft mast includes the 909 director, smoke stack, and several antennas. Hence, by considering only those structures whose scattered fields interact significantly with the subject antennas and masts, the structures required for the mid-frequency model were limited.

With the above points in mind, the ground plane for the mid-frequency model was established as shown in Figure 7. The ground reference plane follows the fore top deck and then drops down to include the smoke stack and aft mast and finally goes up to model the director. In the wire grid model, these steps were not included because their lengths were small compared to the wavelengths of interest in the mid-frequency model. The wire grid model for the mid-frequency region is shown in Figure 8. As discussed above, the model only included that structure which was nearby those items analyzed.

The mid-frequency model was oriented the same way as the low frequency model with the stern at the coordinate system origin extending in length along the X-axis. The model had 126 segments and 87 junctions. The currents

Figure 7 Mid-Frequency Model Reference Ground Plane

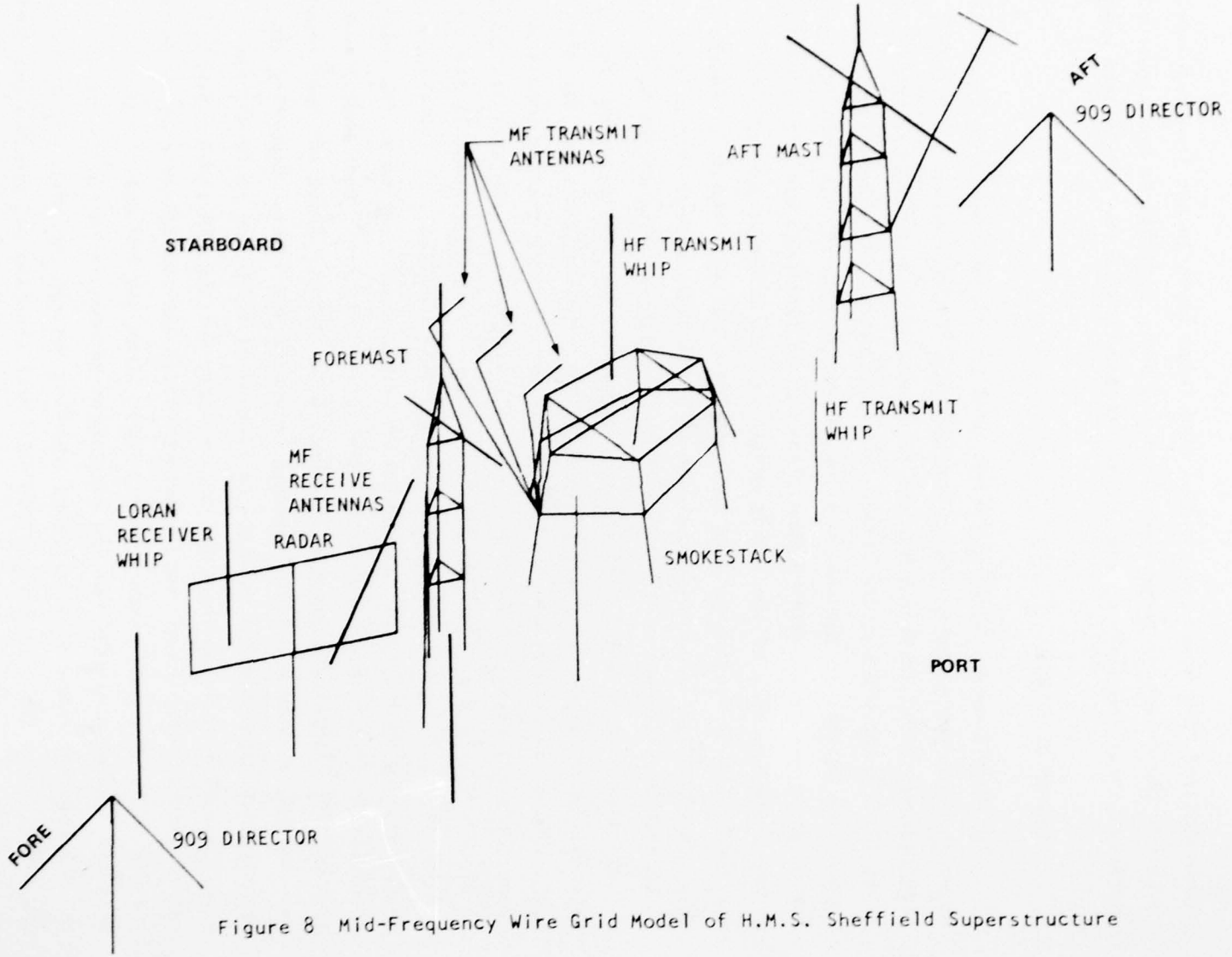

Figure 8 Mid-Frequency Wire Grid Model of H.M.S. Sheffield Superstructure

calculated for this model were merged with those found in the low-frequency model to extend the frequency range from 0.1 to 15 MHz. Currents on the masts were compared in the frequency overlap region to assure that the models were compatible.

4. MERGING OF MODELS

The low-frequency model (LFM) was used for frequencies up to about 3 MHz at which point the segment lengths approach the 1/6 wavelength restriction. The mid-frequency model (MFM) extends the frequency up to near 15 MHz. Hence, near 3 MHz the LFM and MFM must be merged. The structures which have significant length with respect to the ship are the aft and foremasts; i.e., those structures for which we expect the MFM "ground plane" to be least representative of the ground plane produced by the ship's structure. In order to correct for this inaccuracy, L, R, C elements were added to these masts in the MFM. Hence, the ship can be thought of as an element which loads these masts. The circuit by which each base segment of the MFM aft mast was loaded was a series L, R, C circuit placed in parallel with the base segment. The initial values for L, R, C were estimated by comparing the LFM and MFM transfer functions for the aft mast. These values were adjusted until agreement between the two models was found. The aft mast transfer functions for the current at the base are compared in Figure 9 (LFM) and Figure 10 (MFM). The low-frequency current is capacitive and increases as $j\omega$, both the models exhibit this behavior. As the frequency increases, the real part of the current increases as ω^2 peaking at the resonance frequency where the imaginary part of the current is zero. Both models resonant at about 3 MHz showing analogous responses below 3 MHz. These aft mast models were merged by using a weighted average between 2 and 4 MHz. Comparing the transfer functions for the foremast in Figures 11 (LFM) and 12 (MFM), the capacitive current is dominant at low frequency but the LFM shows a significant interaction between the aft mast scattered field and the foremast as evidenced by the dip in the foremast current near 3 MHz. Since the MFM doesn't have this behavior, one must assume that the structures between the masts shield them in the MFM and that there is significant coupling between the masts via the ship's upper deck. The LFM probably has too much mast coupling and the MFM too little. These models were merged by using a weighted average between 2 and 4 MHz.

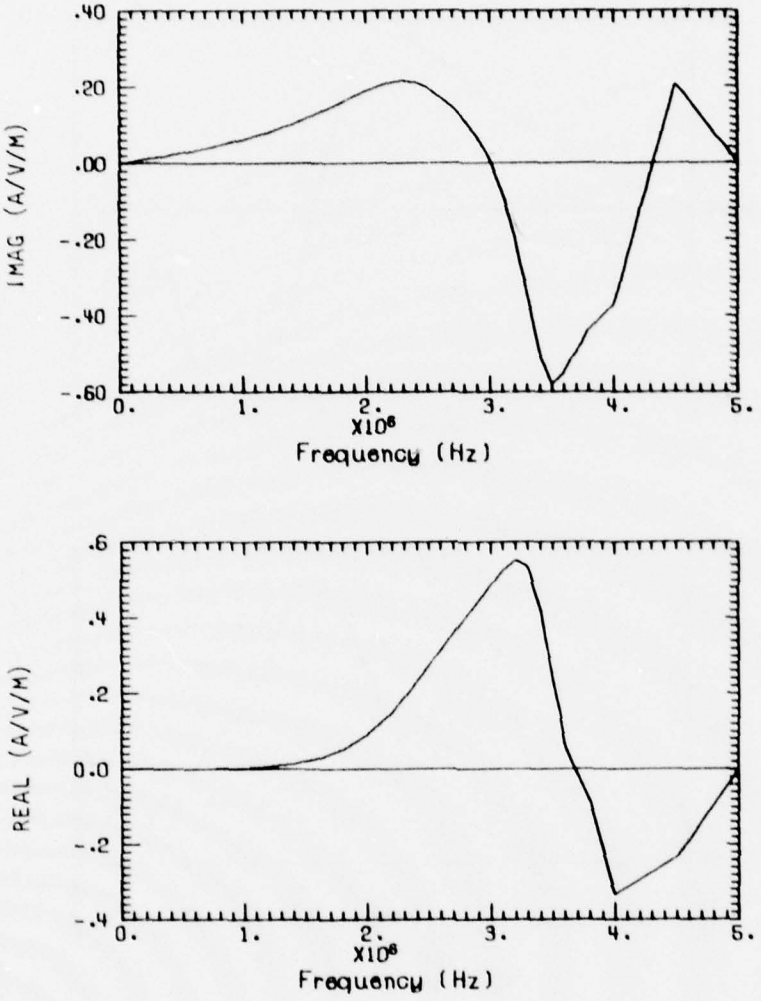

Figure 9 Real and Imaginary Parts of the Transfer Function for the Total Current at the Base of the Aft Mast (H.M.S. Sheffield Low-Frequency Model)

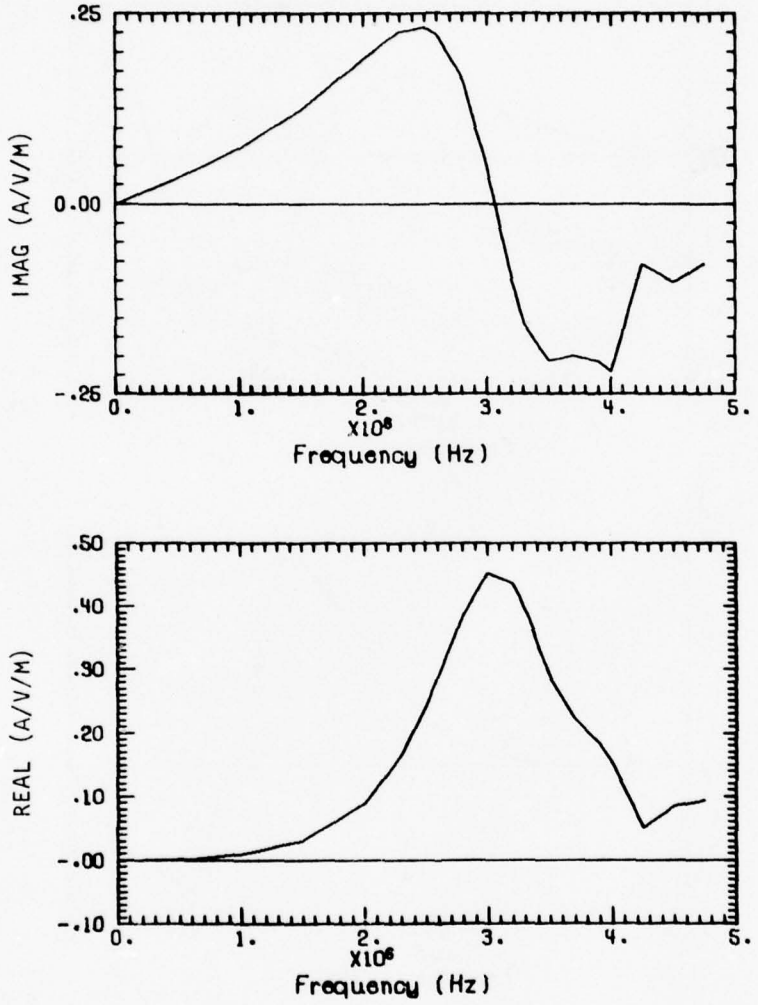

Figure 10 Real and Imaginary Parts of the Transfer Function for the Total Current at the Base of the Aft Mast (H.M.S. Sheffield Mid-Frequency Model)

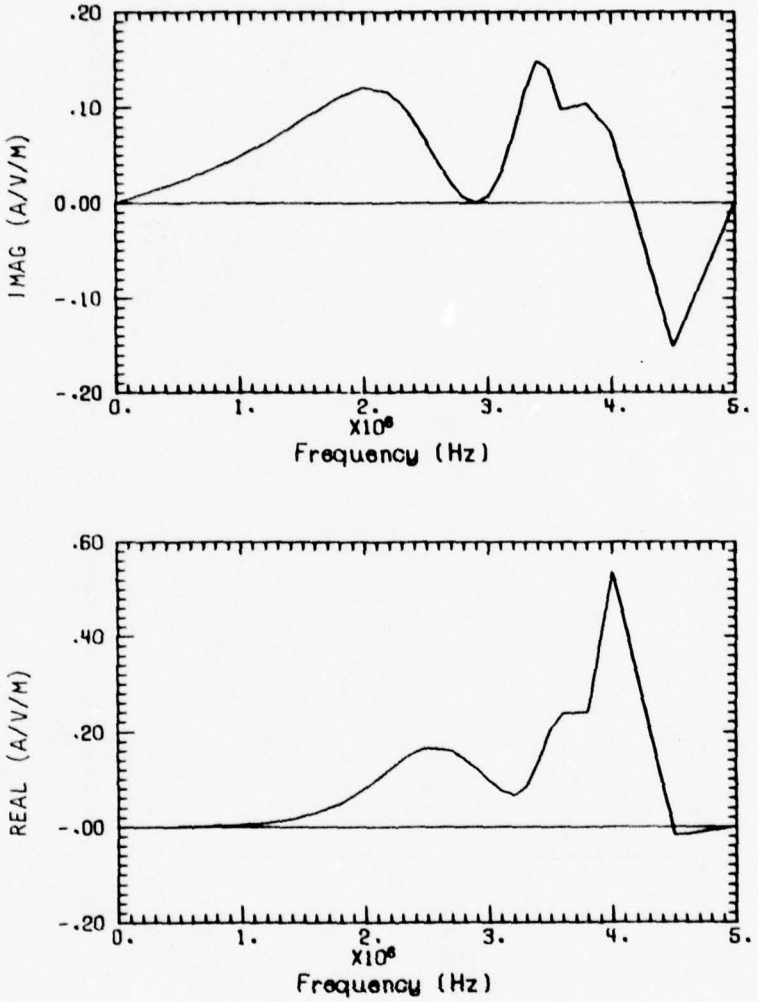

Figure 11 Real and Imaginary Parts of the Transfer Function for the Total Current at the Base of the Foremast (H.M.S. Sheffield Low-Frequency Model)

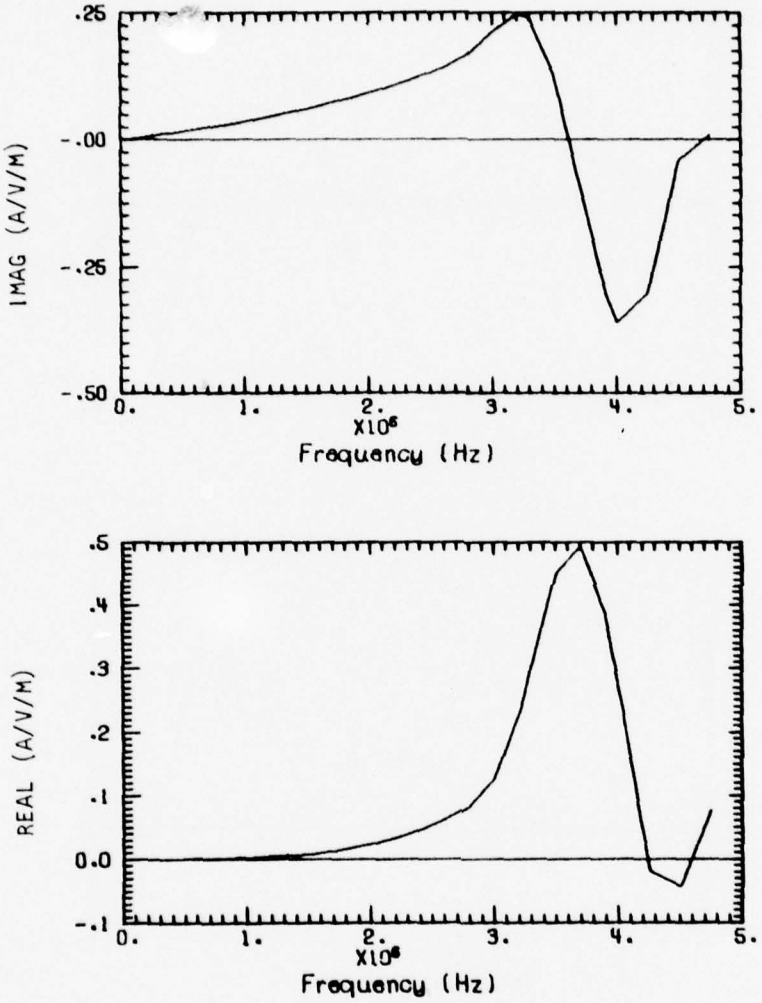

Figure 12 Real and Imaginary Parts of the Transfer Function for the Total Current at the Base of the Foremast (H.M.S. Sheffield Mid-Frequency Model)

5. HIGH-FREQUENCY MODELS

As the frequency of the analysis is increased, the effect of nearby scattering objects on the subject structure becomes minimal. The high-frequency antenna or cable models calculate the interaction of the structure with only the incident field (over a ground plane) excitation.

These individual models extend the analysis from 15 MHz to 100 MHz. The HFM is merged with the MFM between 12 and 15 MHz. The extent to which these models merge is a verification of the HFM.

SECTION III
COUPLING ANALYSES AND RESULTS

The analysis and predicted results of the individual models are presented in this section. The time domain results were all obtained by multiplying the model transfer functions by the EMPRESS spectrum and then numerically performing the inverse Fourier transform. Before performing the inverse transform, the spacial origin was shifted to the prediction point so that the response would start at zero time. The quality of the inverse transform was examined by computing the response for up to 200 nanoseconds before time zero. If the transfer function is causal and adequately sampled in the frequency domain, then the negative time response should be zero. Nonzero results are generally due to either insufficient sampling or the merging of two solutions over a frequency band in which the two solutions are quite different. For all of the models of this section, the numerical "noise" for negative time was well below the positive time results. Insufficient sampling, when it occurred, was corrected by adding more frequencies where the spectral resolution was poor.

1. AFT MAST

The aft mast of the Sheffield is a rectangular cylinder (see Figure 13) which for vertical electric field excitation is the dominant ship structure. The aft mast has five horizontal yardarms which are designated in this report as the two upper yardarms, the two middle yardarms and the lower yardarm which has the ACH Astro VHF antenna. Surface current densities on the mast and currents on each of the five yardarms were computed.

a. Surface current density, analysis method.

The electromagnetic response of the aft mast is basically the response of a monopole. A circular monopole excited by a parallel electric field has two basic modes; the common mode or dipole current and the differential mode or loop type of current density. The dipole current density is the usual mode associated

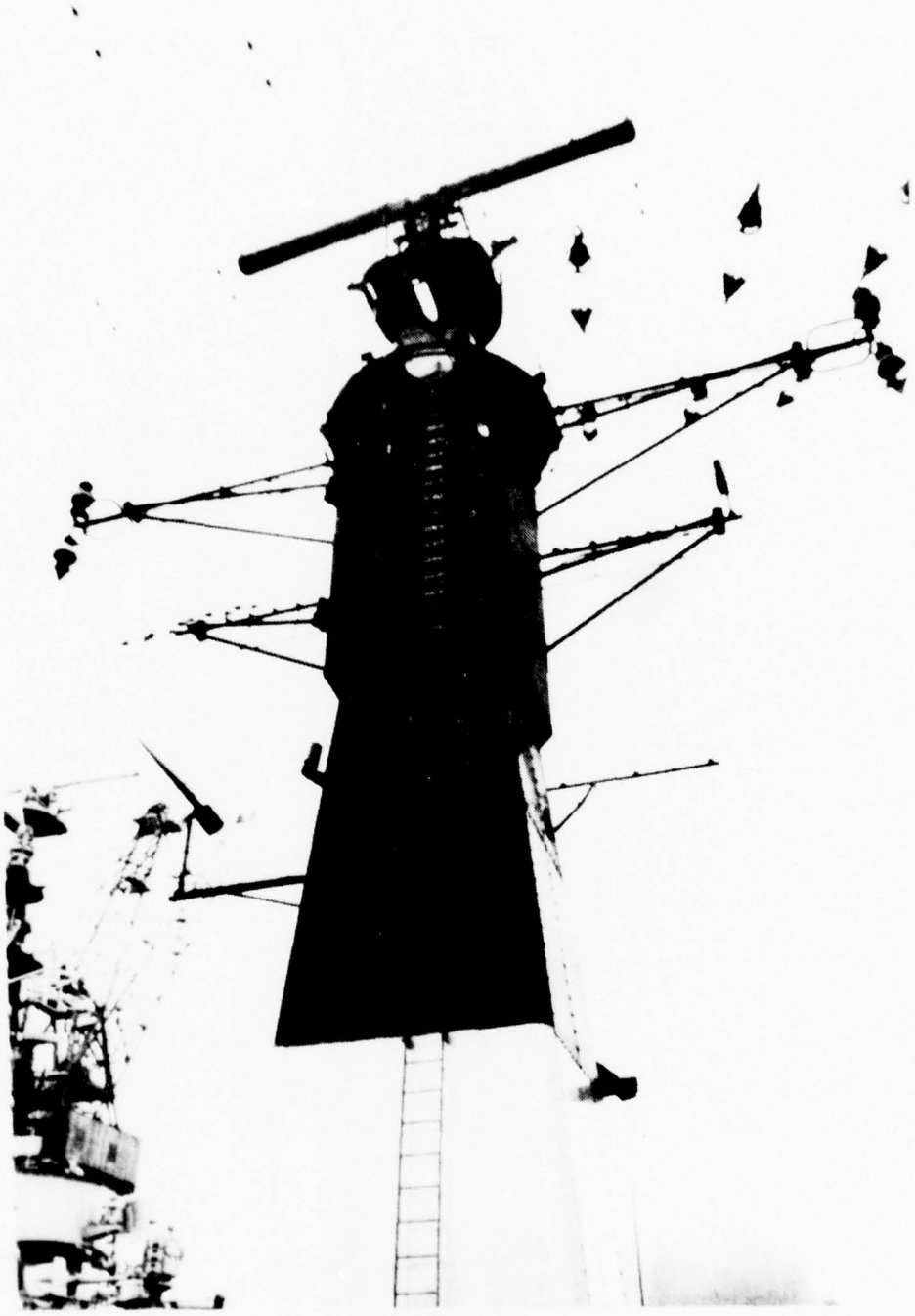

Figure 13 View of Aft Mast Looking Aft

with a dipole antenna and is uniformly distributed around the circumference. At the antenna surface the magnetic field that this dipole current, I, produces is given by

$$H = \frac{I}{2\pi a} \tag{3}$$

The differential modes are those modes which have ϕ variation about the circumference. These modes are nearly the same as the differential modes on an infinite cylinder which has an axial current density given by [3]

$$J = \frac{2\, H^{inc}}{\pi Ka} \sum_{n=-\infty}^{\infty} \frac{j^{-n}\, e^{jn\phi}}{H_n^{(2)}(Ka)} \tag{4}$$

Equation (4) can be rewritten as

$$J = \frac{2\, H^{inc}}{\pi Ka\, H_o^{(2)}(Ka)} + \frac{4\, H^{inc}}{\pi Ka} \sum_{n=1}^{\infty} \frac{\cos n\phi}{j^n H_n^{(2)}(Ka)} \tag{5}$$

The first term of equation (5) is the common mode (uniform ϕ variation) and is considerably different from the dipole common mode which is length dependent.

For small Ka, the dominant differential mode term is the n=1 or cosϕ term. The total current density on a dipole surface for small Ka is, therefore,

$$J = \frac{I}{2\pi a} - 2\, H^{inc} \cos\phi \tag{6}$$

In the formulation of equation (4), the field is incident at $\phi = 180^{o}$ so that the differential mode current density is positive (upward) on the illuminated side and negative (downward) on the shadow side like in a loop response.

The aft mast surface current density of the low-frequency Sheffield model (Figure 2) is approximately given by equation (6). For the mid-frequency model (Figure 8) the mast is gridded as a triangular cylinder so that the common mode current is computed by summing the three vertical segments. Equation (6) is only approximate for the two Sheffield models because there are other ship structures which contribute to the total scattered field.

The general approach to include the other structures is to compute the scattered field by the vector potential, i.e.,

$$\overline{H} = \nabla \times \overline{A} \tag{7a}$$

$$\overline{A} = \mu \int \frac{\overline{I}(r')e^{-jkR}}{4\pi R}\, ds. \tag{7b}$$

where I is the current distribution on the wire model. Depending upon the complexity of the wire model, the differential modes may or may not be included. The aft mast of the low-frequency Sheffield model, for example, is a simple wire segment and, therefore, has only a common mode current, the current in the wire. The aft mast of the mid-frequency model, however, is a triangular cylinder and exhibits the differential current flow through the three vertical wire segments. Differential mode currents of approximately equal amplitude flow up the two vertical segments on the illuminated side, and the sum of these two currents flow down the segment on the shadow side.

The potential mast surface current densities were computed by using the vector potential. For the special case of sinusoidal currents, the scattered fields can be computed in closed form [4]. A computer program which takes advantage of this special case was used. The program expands the current (computed by the WIRANT code) over each half-segment as a sinusoid by using

the current at the midsection and the charge at the end of the segment. For the low-frequency model, the differential mode on the mast was added to complete the solution. The mid-frequency model contains the mast differential mode, but the observation point which represents the mast surface must be carefully chosen. If the observation point is too close to one of the wire segments, the fields are overestimated. The observation point, therefore, was selected so that the integration over the vertical mast segments gave a result equal to that of equation (6).

The total spectrum was obtained by merging the low and mid-frequency solutions between 2 and 4 megahertz and by merging the mid-frequency solution with the infinite cylinder solution (equation (4)) between 12 and 15 megahertz.

b. Aft mast surface current density predictions.

The aft mast surface current densities are presented in Figures 14 through 25 at mast heights of 1, 5, and 9 meters. At each height the current density is shown for each of the four sides of the mast. Each of the responses are quite similar, having a 2.8 MHz damped sinusoid response associated with the mast resonance. The differential mode, which is proportional to the incident field, causes the slight response variations on the four sides. On the illuminated side (port), for example, the early time current density follows the initial pulse of the EMPRESS field. For the shadow side (starboard) the reversal in sign of the differential mode ($2\ H^{inc}$) nearly cancels the monopole response at early time so that the combined rise time is increased. The peak values at the 12 locations vary from 12 to 26 amperes-per-meter.

The nonzero responses of the current densities, which have a low-frequency behaviour, indicate that the merging between the low and mid-frequency solutions was not perfect. Better results probably would be obtained by having a low-frequency model which would be valid up to 5 megahertz in order that the merging could take place above the 2.8 megahertz resonance.

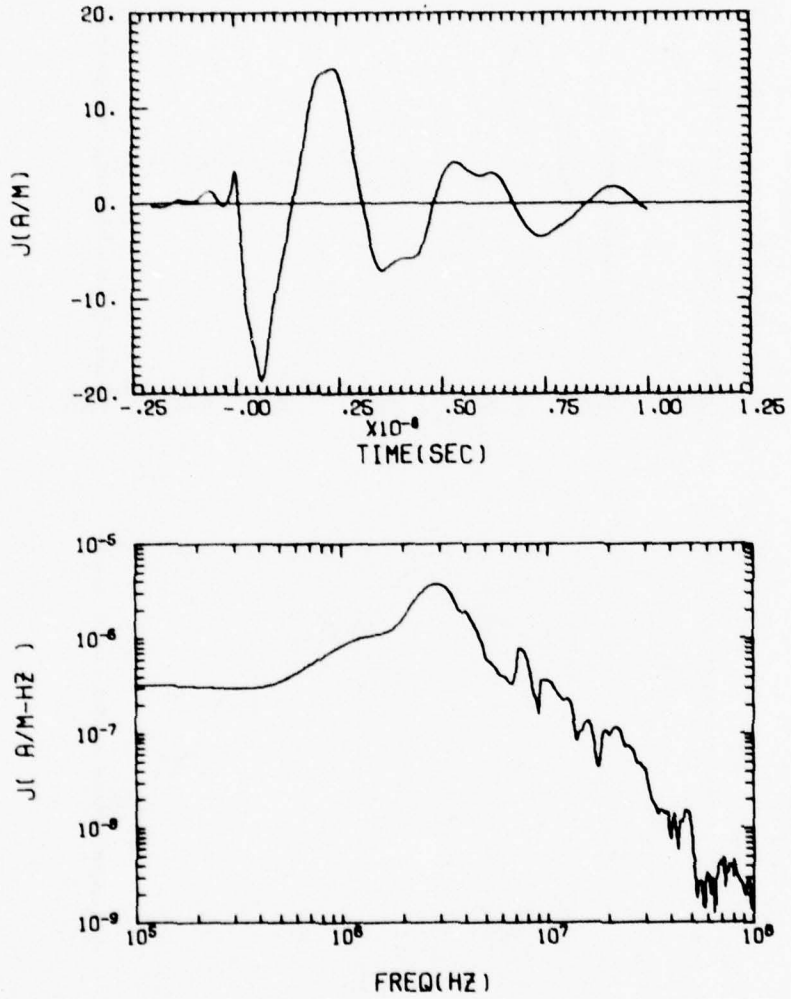

Figure 14 Time and Frequency Domain of Longitudinal Current Density on the Aft Mast (z=1 Meter, Forward Side)

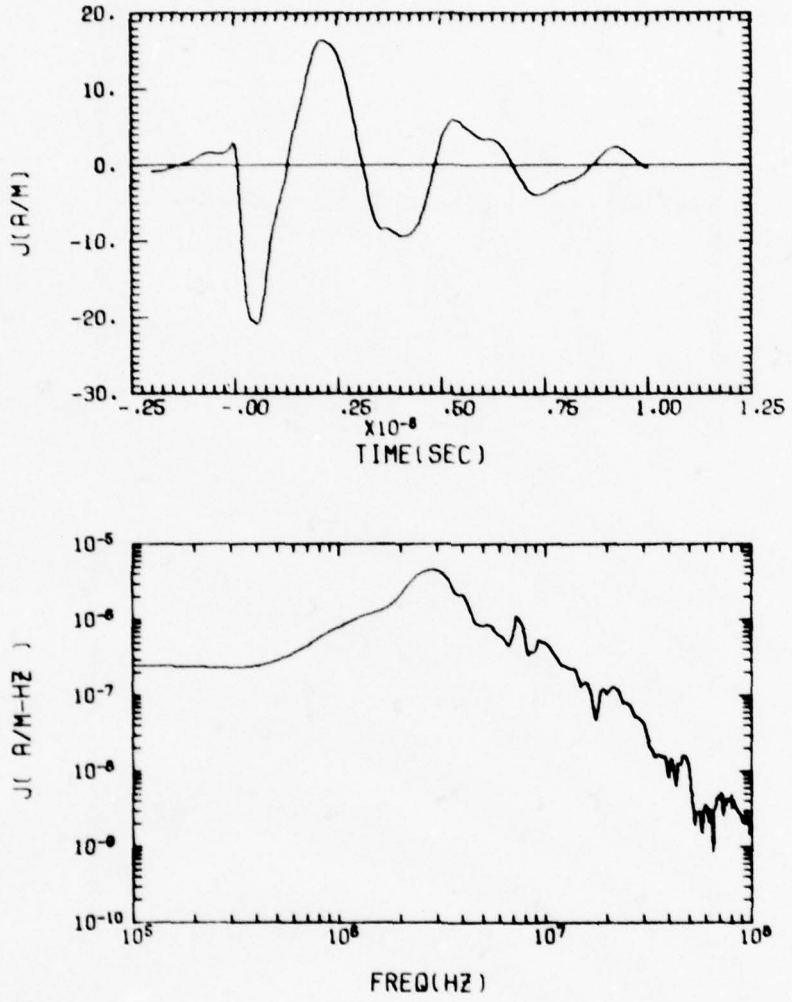

Figure 15 Time and Frequency Domain of Longitudinal Current Density on the Aft Mast (z=5 Meters, Forward Side)

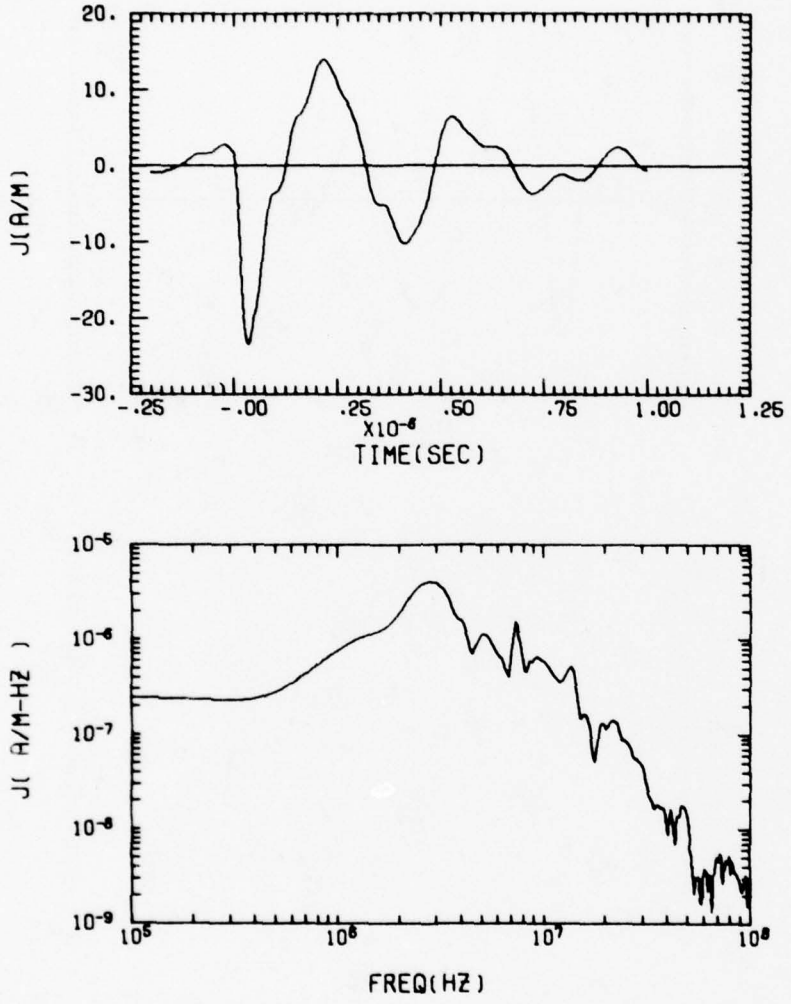

Figure 16 Time and Frequency Domain of Longitudinal Current Density on the Aft Mast (z=9 Meters, Forward Side)

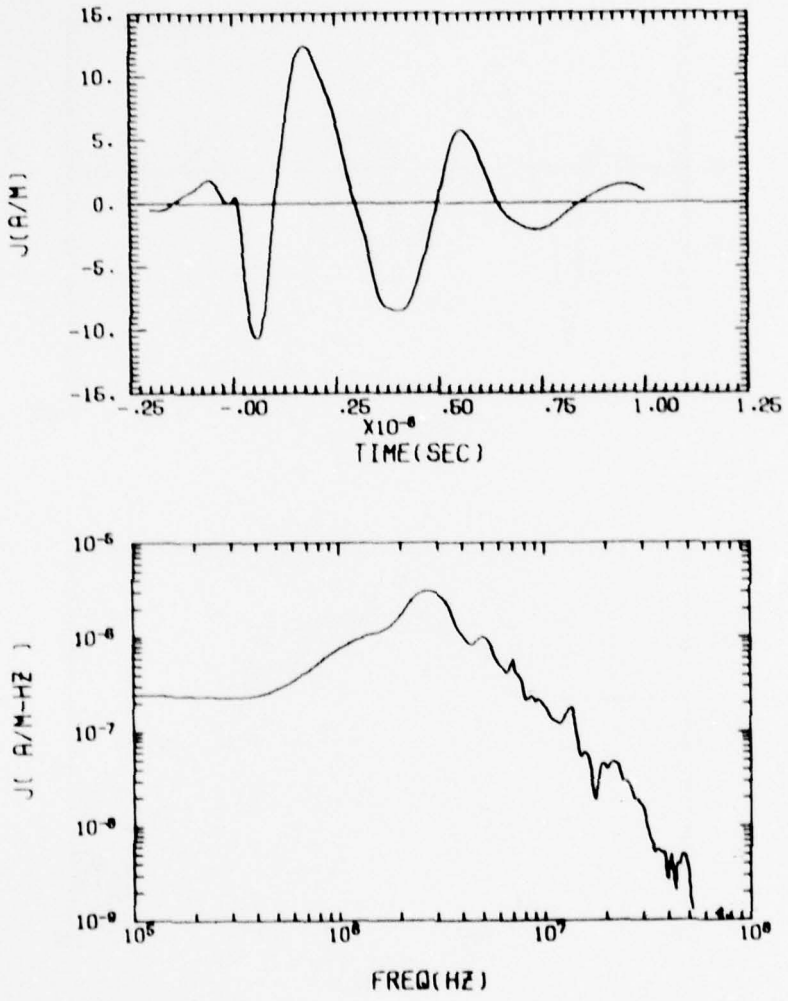

Figure 17 Time and Frequency Domain of Longitudinal Current Density of the Aft Mast (z=1 Meter, Aft Side)

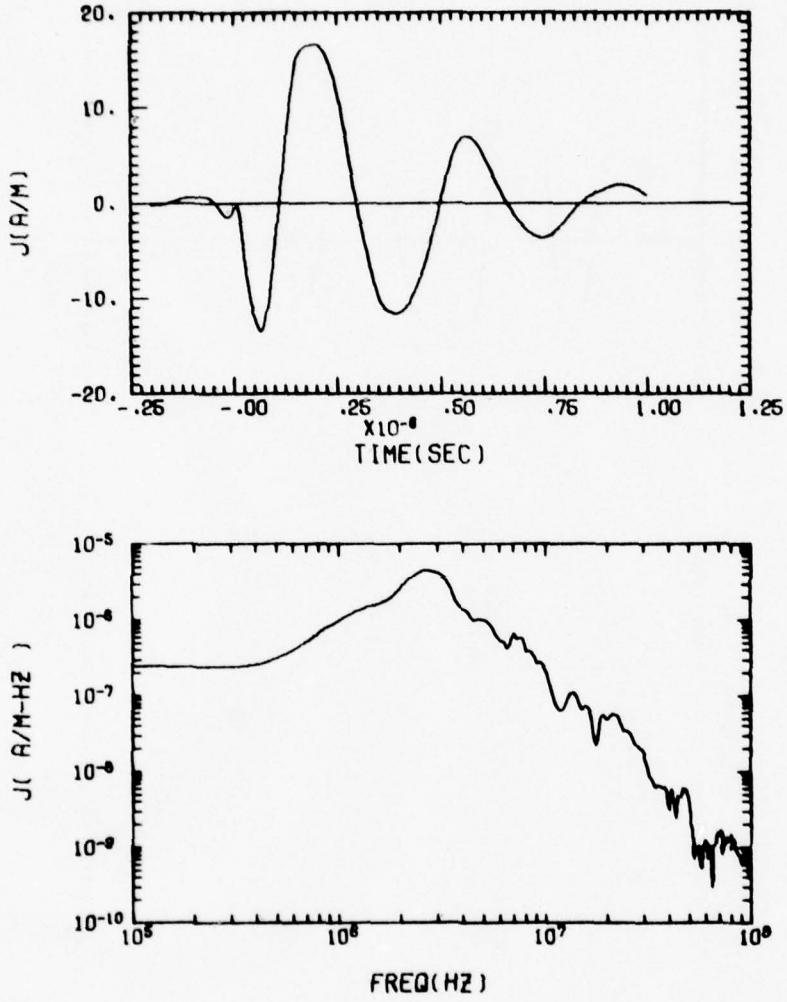

Figure 18 Time and Frequency Domain of Longitudinal Current Density on the Aft Mast (z=5 Meters, Aft Side)

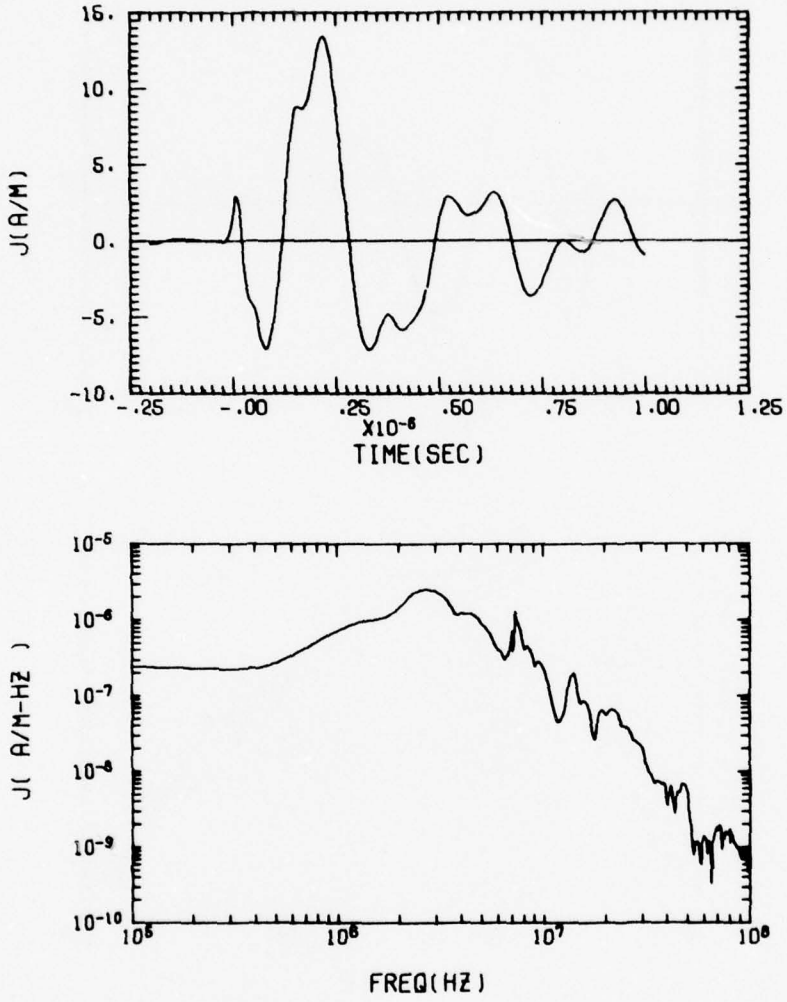

Figure 19 Time and Frequency Domain of Longitudinal Current Density on the Aft Mast (z=9 Meters, Aft Side)

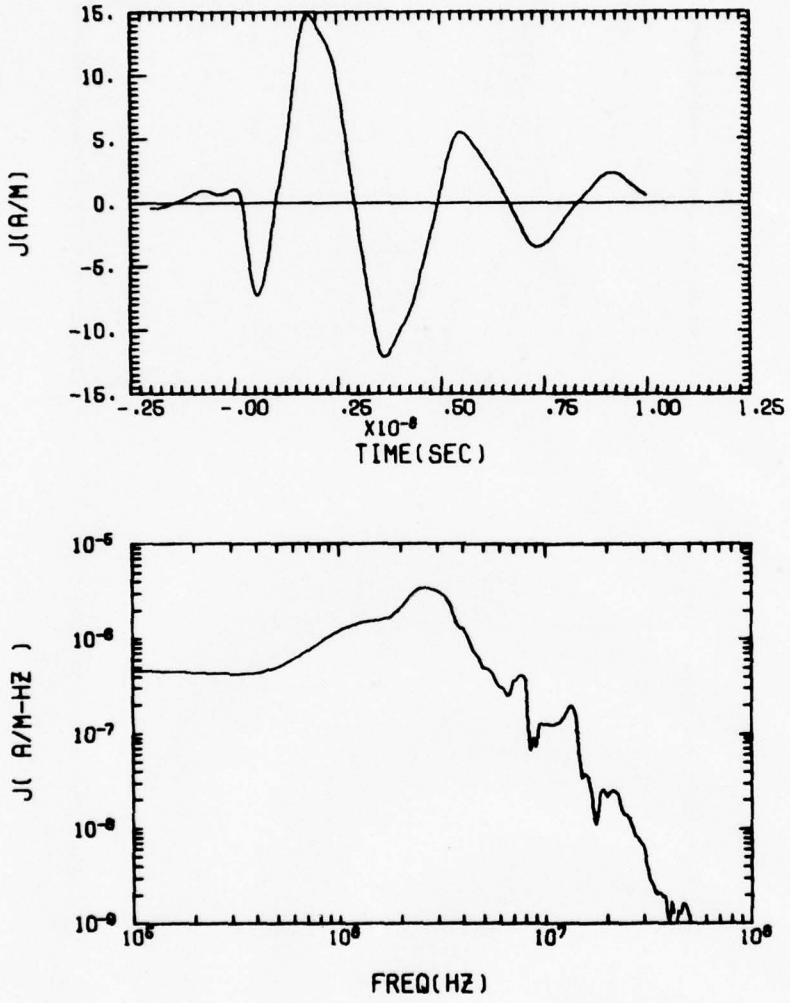

Figure 20 Time and Frequency Domain of Longitudinal Current Density on the Aft Mast (z=1 Meter, Starboard Side)

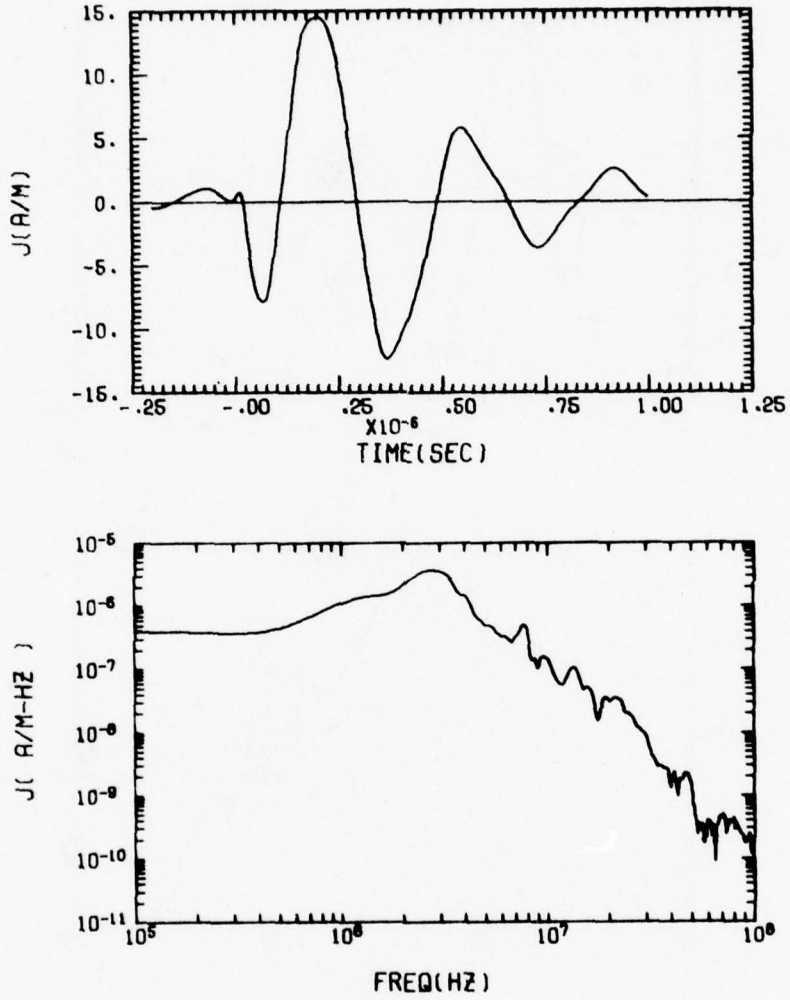

Figure 21 Time and Frequency Domain of Longitudinal Current Density on the Aft Mast (z=5 Meters, Starboard Side)

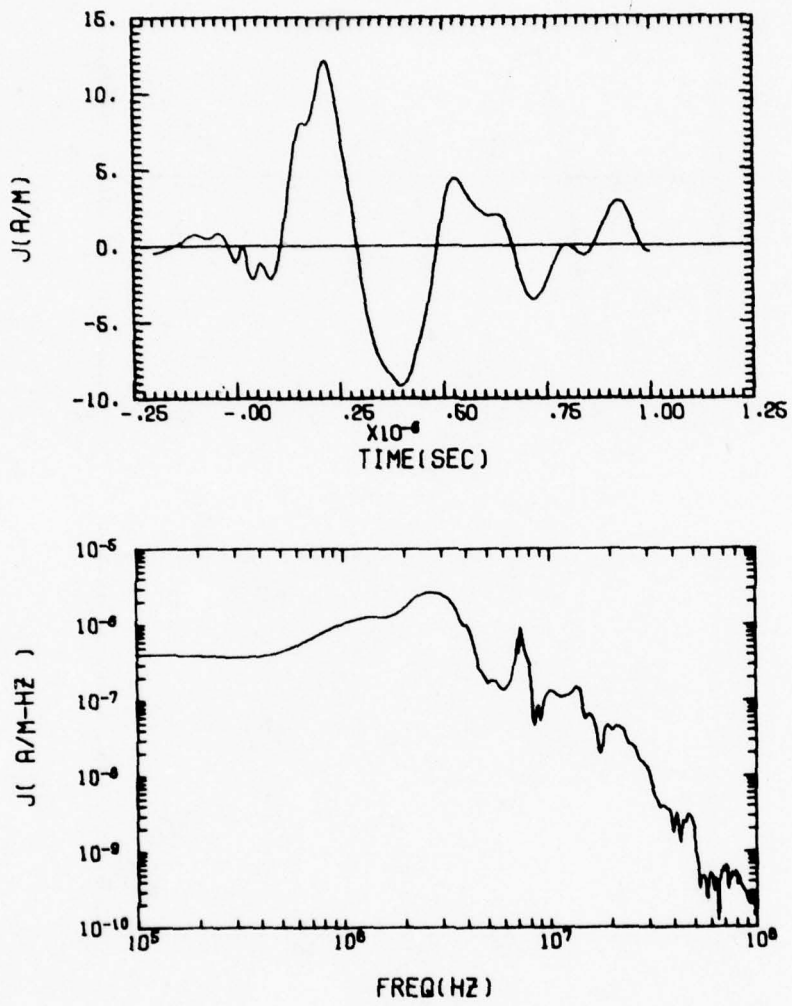

Figure 22 Time and Frequency Domain of Longitudinal Current Density on the Aft Mast (z=9 Meters, Starboard Side)

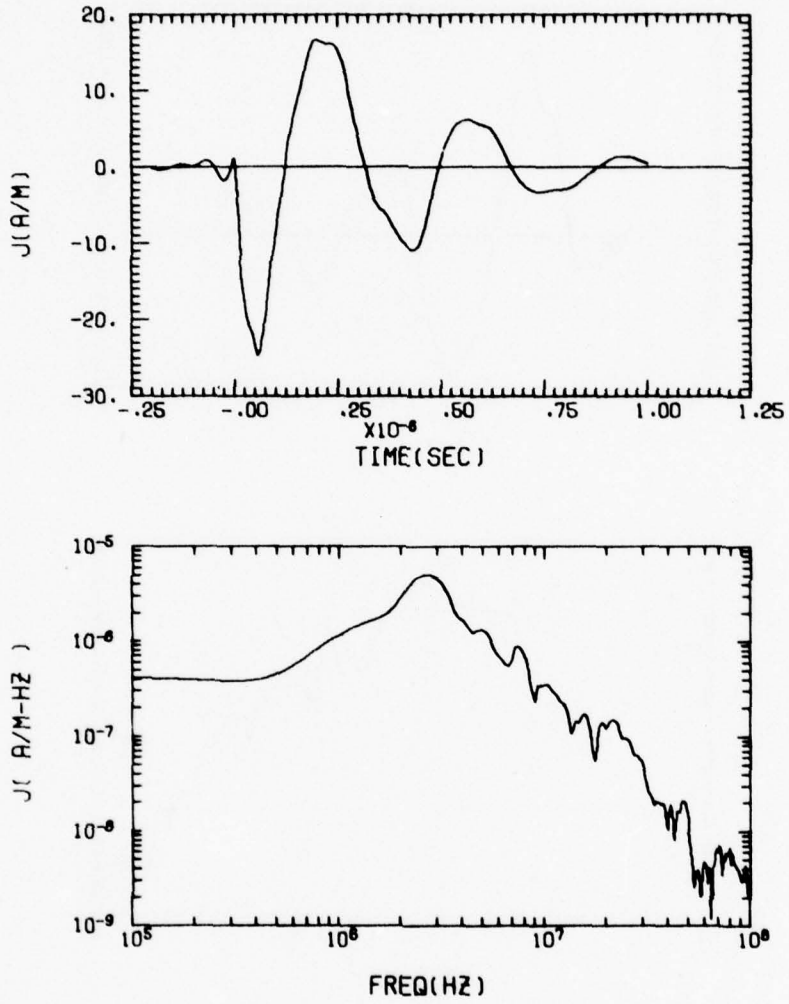

Figure 23 Time and Frequency Domain of Longitudinal Current Density on the Aft Mast (z=1 Meter, Port Side)

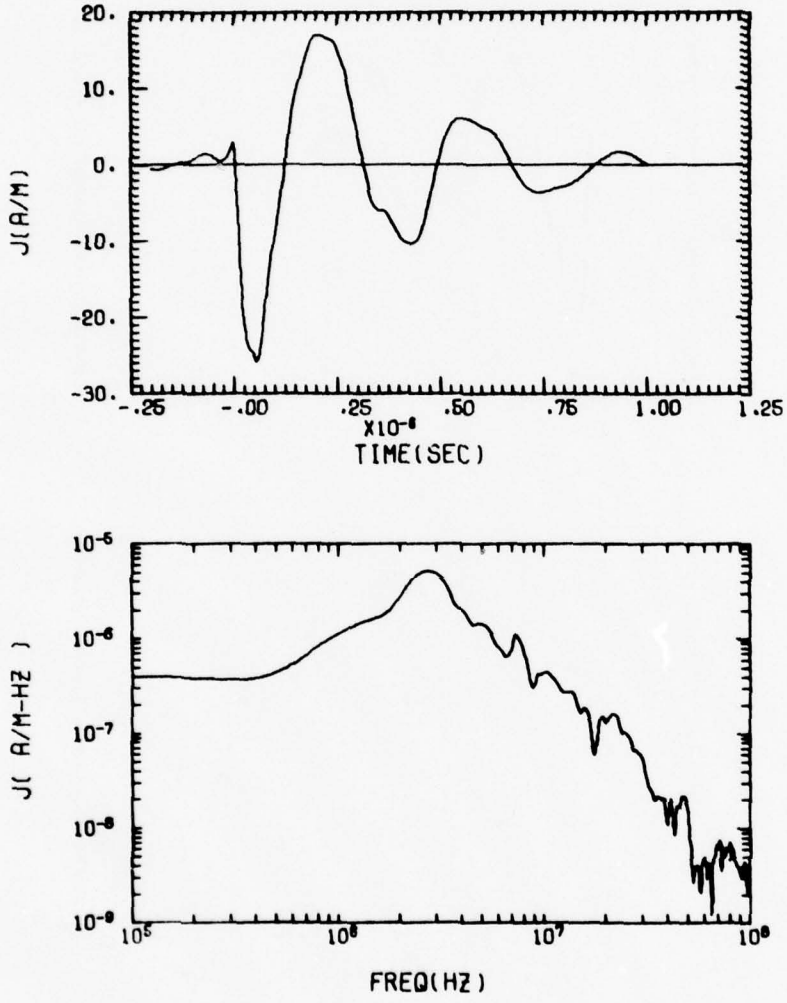

Figure 24 Time and Frequency Domain of Longitudinal Current Density on the Aft Mast (z=5 Meter, Port Side)

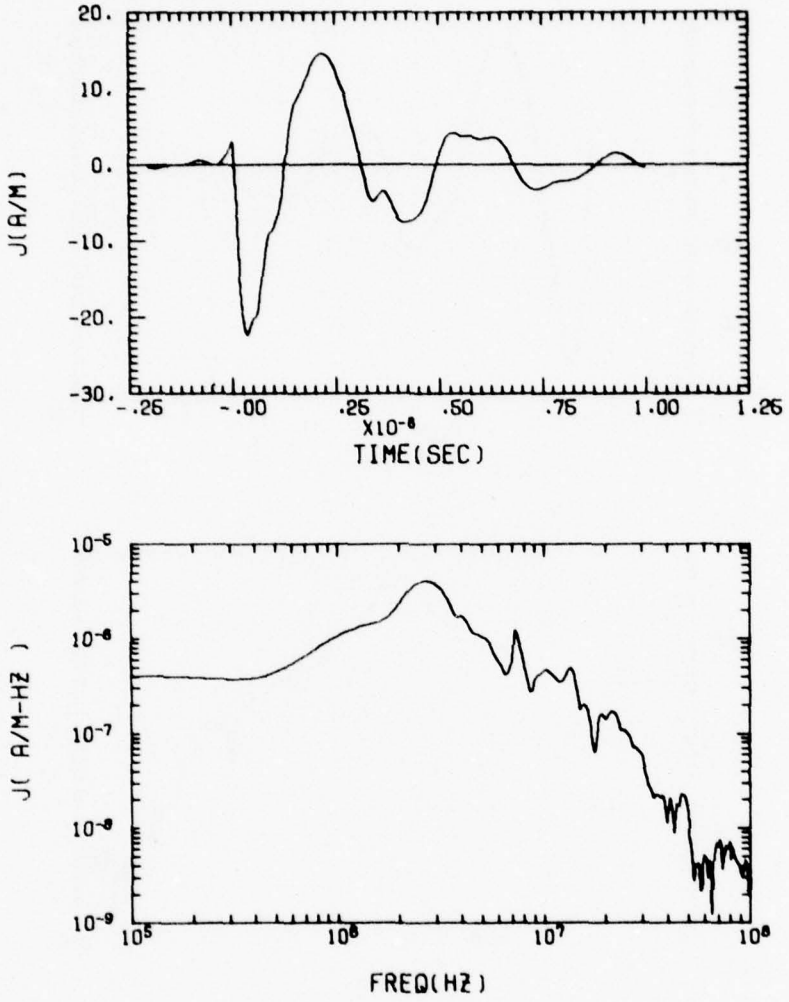

Figure 25 Time and Frequency Domain of Longitudinal Current Density on the Aft Mast (z=9 Meters, Port Side)

c. Yardarm analysis method.

The upper and middle yardarms consist of a horizontal arm and two slanted support struts. Currents on the yardarms are induced by two modes, the dipole mode (associated with the length) and the loop mode (associated with the area between the horizontal arm and the supports). The original modeling concept was to consider each yardarm separately driven by the aft mast surface current and normal electric field as computed from the low and mid-frequency Sheffield models. The yardarms, however, are physically close to each other so that it was decided to include their mutual coupling by griding the aft mast and yardarms as illustrated in Figure 26. This model is valid up to 30 megahertz. The upper and middle yardarm currents are predicted by observing the current in the appropriate segment of the model. The model automatically picks up the dipole and loop response. The lower yardarm also has a slanted support which is too small to conveniently be included in the model. The support forms a small loop with the horizontal arm and the loop is driven by the mast surface current. This loop response was added to the lower yardarm current of the wire model. The lower yardarm also contains a simple model of the ACH Astro VHF antenna which is discussed in Section III.8.

d. Yardarm results.

The transfer functions of the port and starboard upper yardarm currents are shown in Figures 27 and 28. The upper yardarms currents are seen to respond to the aft mast resonance at 3.2 megahertz (this model was not loaded at the base as the mid-frequency Sheffield model was and, therefore, the mast resonance is at a higher frequency). The strongest resonance is at 10.5 megahertz which appears to be a combined upper-middle-lower yardarm resonance since it appears in all of the yardarm responses but only weakly in the lower segments of the mast. The upper yardarm resonance is at 13.3 megahertz, and the 21.5 megahertz resonance is possibly a harmonic of the 10.5 megahertz resonance.

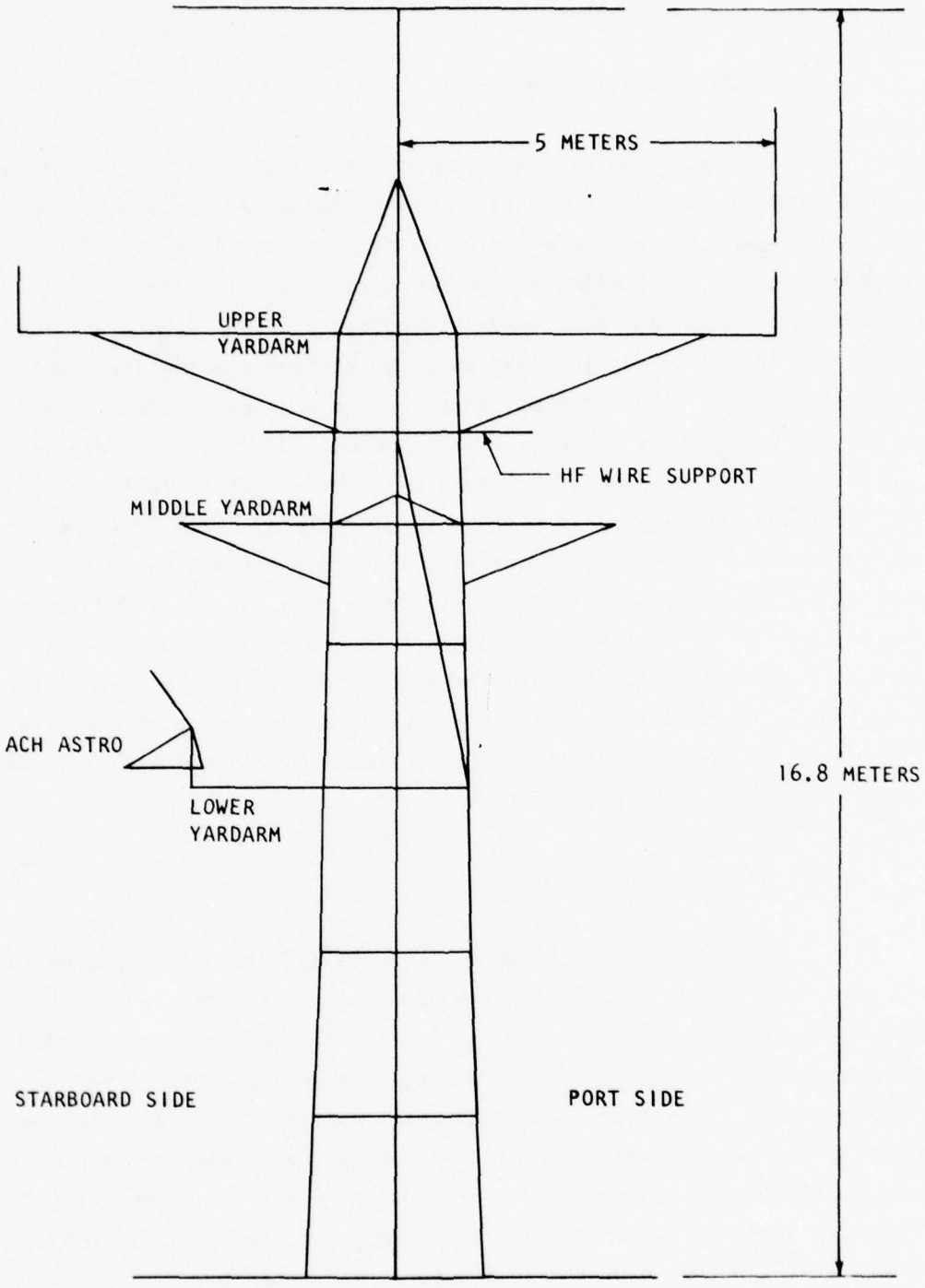

Figure 26 Aft Mast Model with Yardarms and ACH Astro Antenna

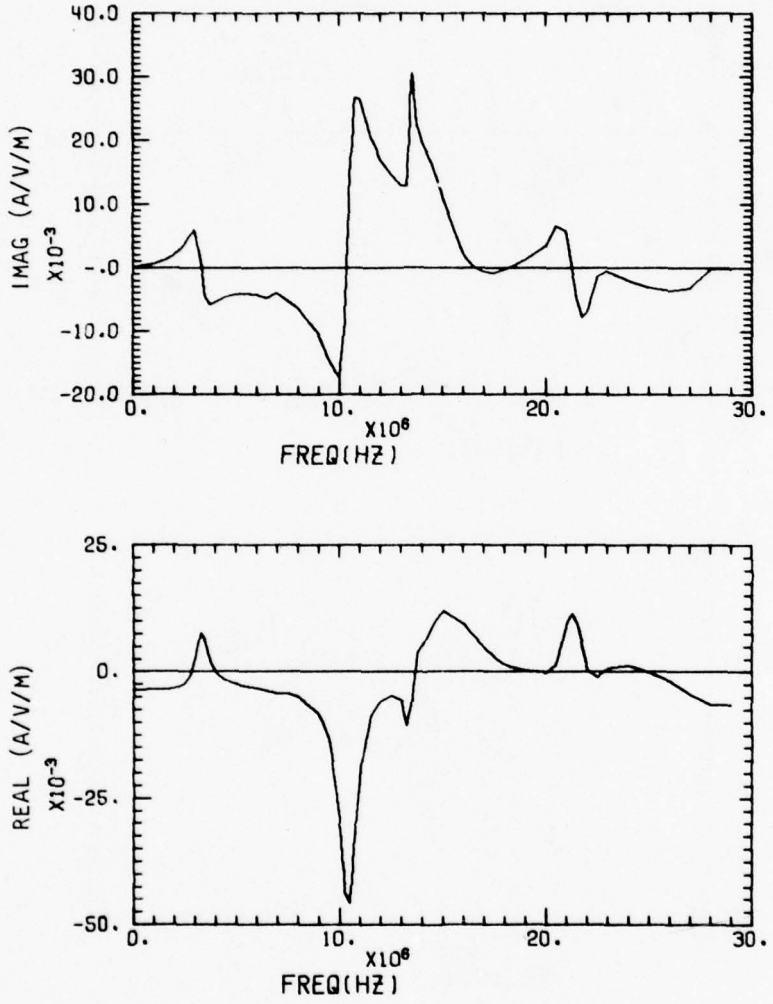

Figure 27 Transfer Function of Upper Yardarm (Port Side)

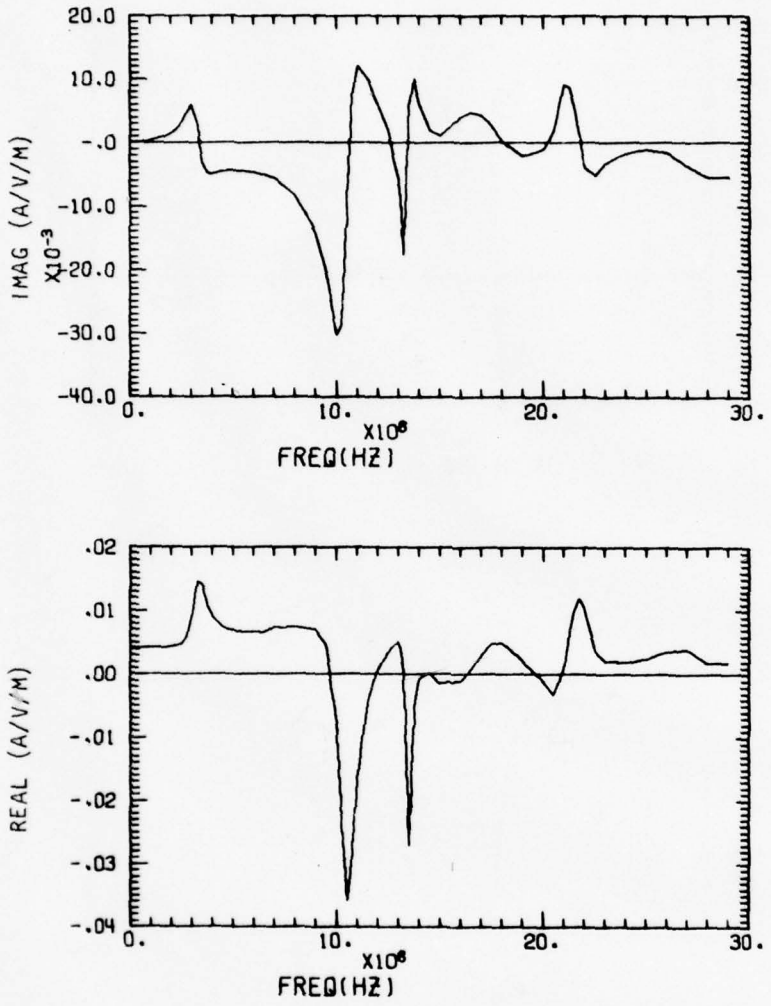

Figure 28 Transfer Function of Upper Yardarm (Starboard Side)

The time and spectral responses of the upper yardarms are shown in Figures 29 and 30. The dominant response is at 10.5 megahertz with peak values of 8.6 and 10.5 amperes. There is a slight Gibb's phenomena at time zero due to the assumption that the current is constant above 28 megahertz. The middle yardarm transfer functions are shown in Figures 31 and 32. They show strong coupling to the mast resonance plus an added resonance at 7 megahertz which is due to the aft HF antenna wire support. Since the middle yardarms act primarily as loops, their time and spectral responses (Figures 33 and 34) are almost identical to the aft mast surface current densities. That is, Figure 33 compares with Figure 24 and Figure 34 compares with Figure 21. There is a polarity difference due to the arbitrary choice of positive current flow. The peaks are 11 and 10.8 amperes.

The lower yardarm current is dominated by the 10.5 megahertz resonance (see Figure 35) and to a lesser degree by the upper yardarm (13.3 megahertz) and its own resonance (18 megahertz). The time and spectral responses; shown in Figure 36, are predominantly at 10.5 megahertz with a peak value of 10.5 amperes.

2. 4.5-INCH GUN MOUNT WHIP ANTENNA CABLE

The housing for the 4.5-inch gun mount, which lies ahead of the superstructure on the main deck, is made primarily of fiberglass. It contains a large number of cables, including a coaxial antenna feeder cable that leads to the base of a short whip antenna on the top of the turret. However, during the analysis and test the antenna was not attached. The bulk (common mode) current was predicted at three points along the cable inside the gun mount: at the antenna base, at the center of the run, and at the exit point from the gun mount.

A wire grid model of the antenna cable and some of the nearby structure over a ground plane was constructed (Figure 37). The antenna cable runs up the side of the turret (segments 1 through 6) and returns to ground by a metal strap (segments 7 through 13). The cable then runs from the gun mount to the operations room 33.5 meters distant. Thie cable run was treated as a shorted transmission line

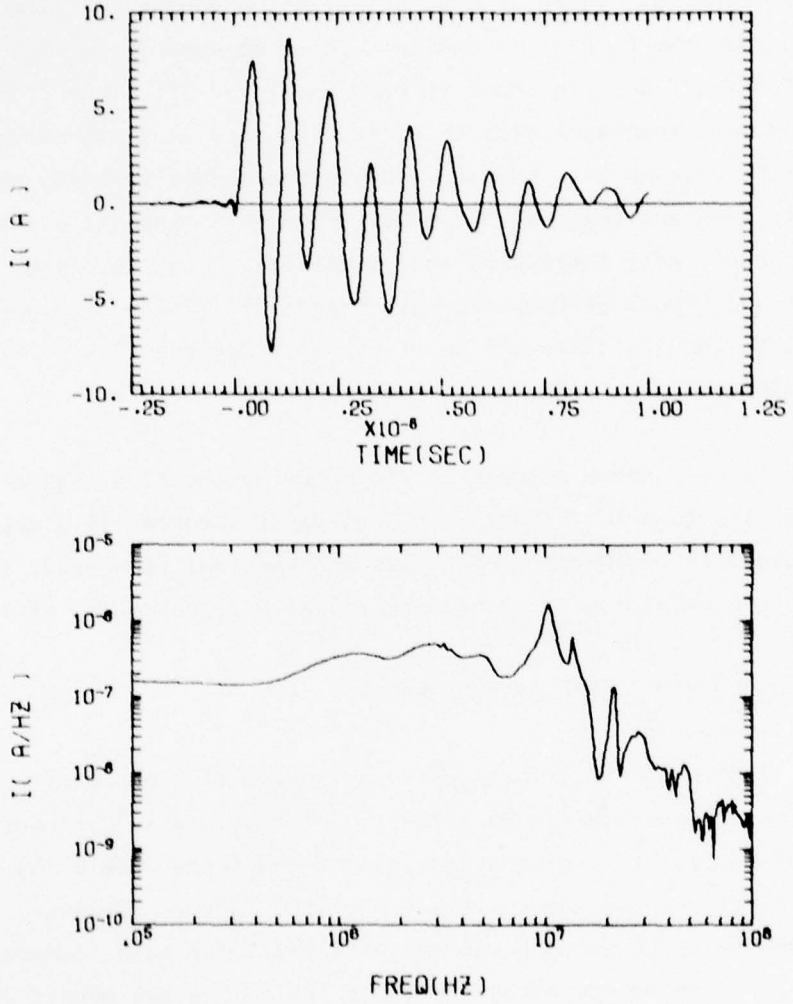

Figure 29 Time and Frequency Domain of Upper Yardarm (Port Side)

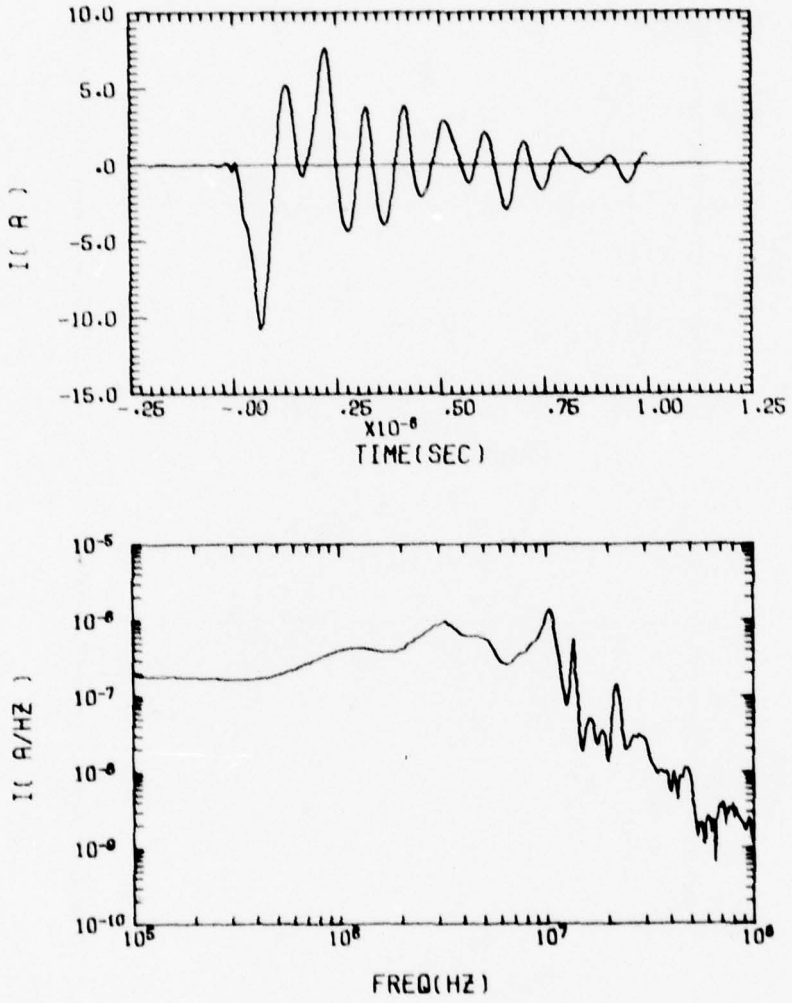

Figure 30 Time and Frequency Domain of Upper Yardarm (Starboard Side)

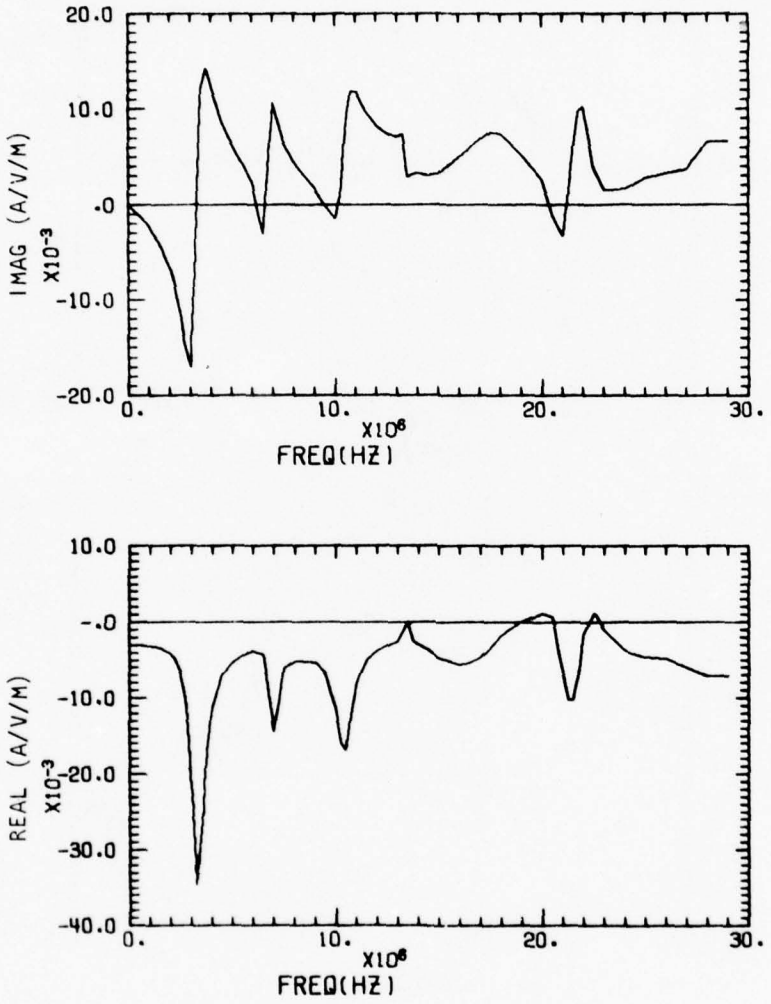

Figure 31 Transfer Function of Middle Yardarm (Port Side)

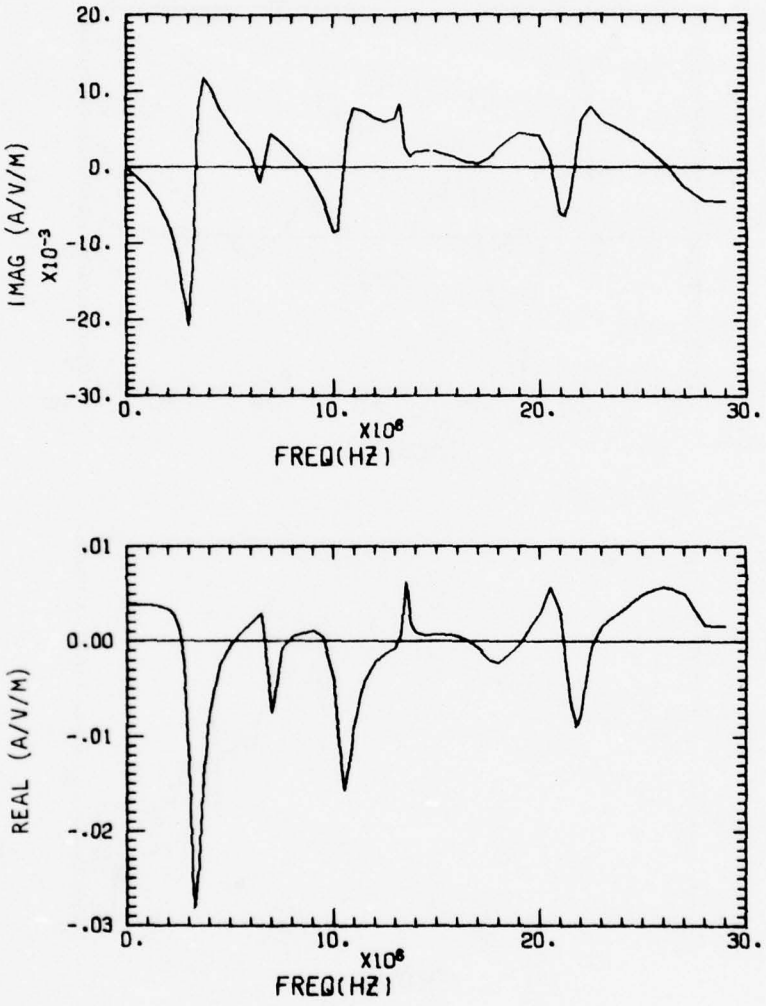

Figure 32 Transfer Function of Middle Yardarm (Starboard Side)

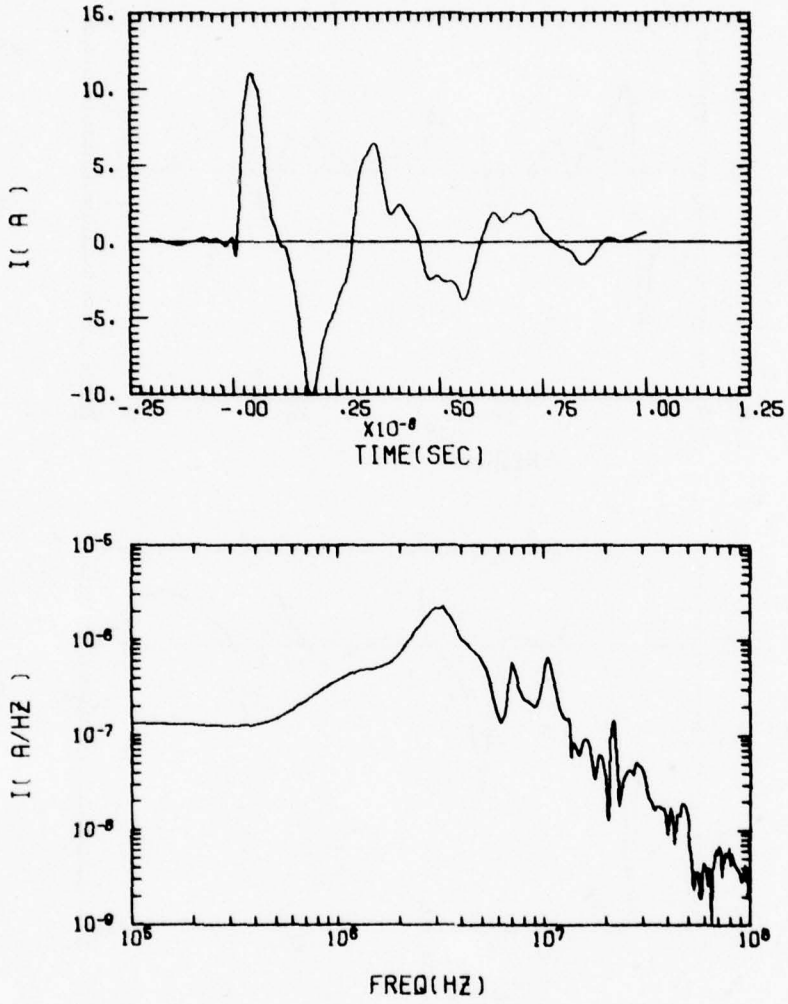

Figure 33 Time and Frequency Domain of Middle Yardarm (Port Side)

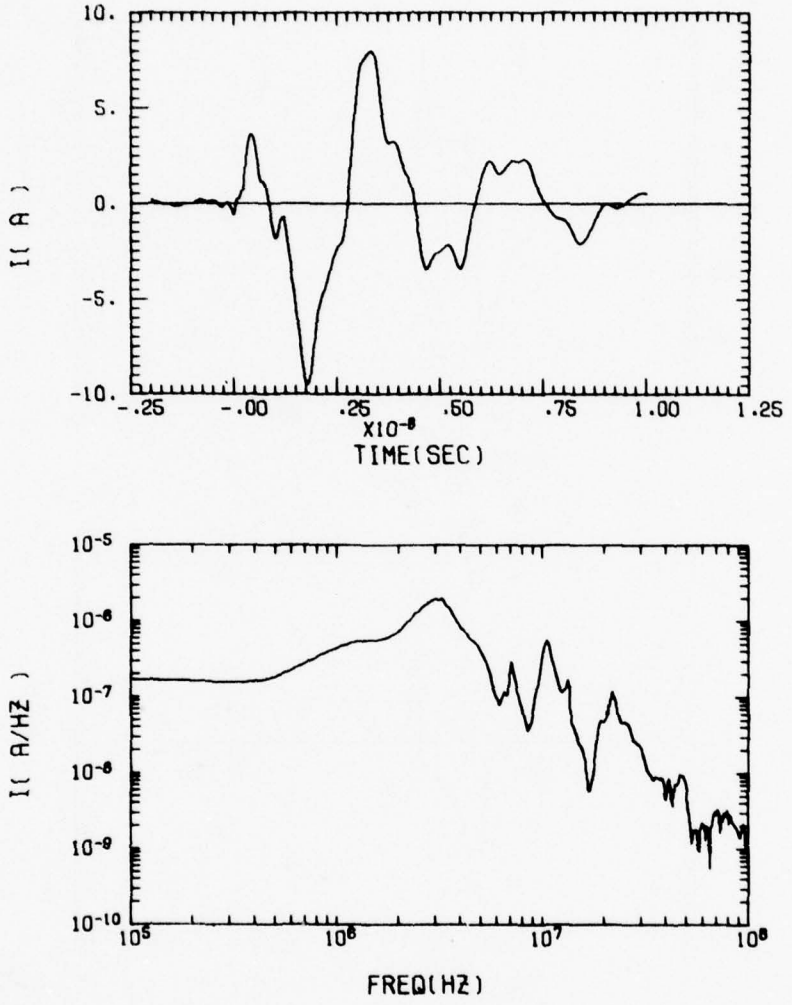

Figure 34 Time and Frequency Domain of Middle Yardarm (Starboard Side)

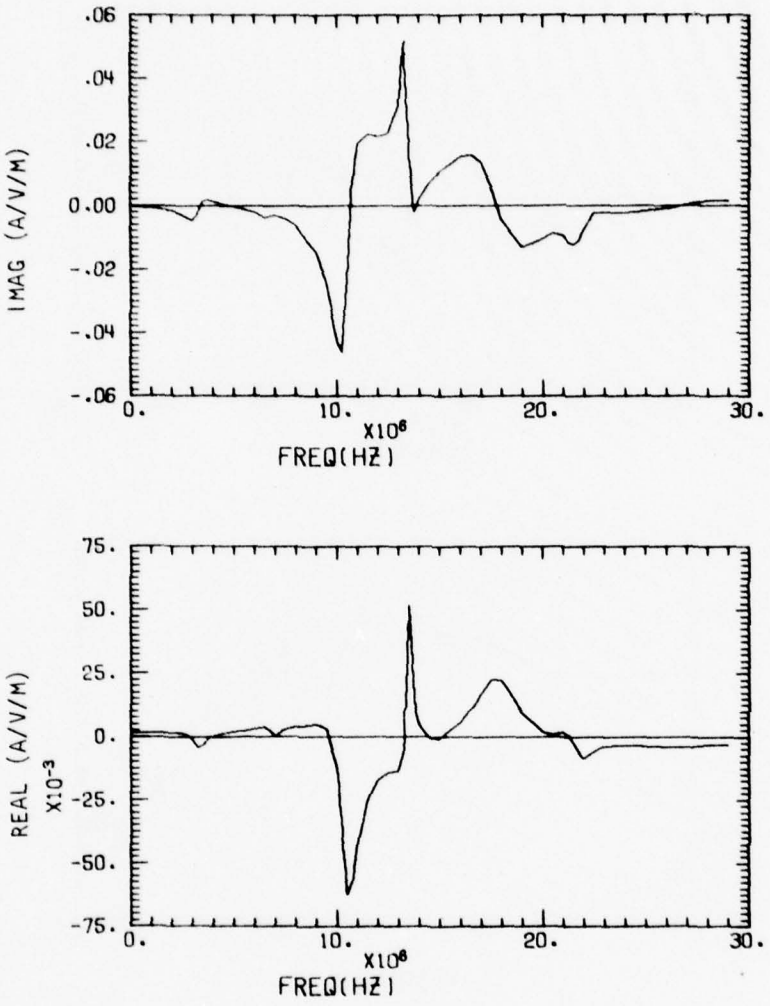

Figure 35 Transfer Function of Lower Yardarm (Starboard Side)

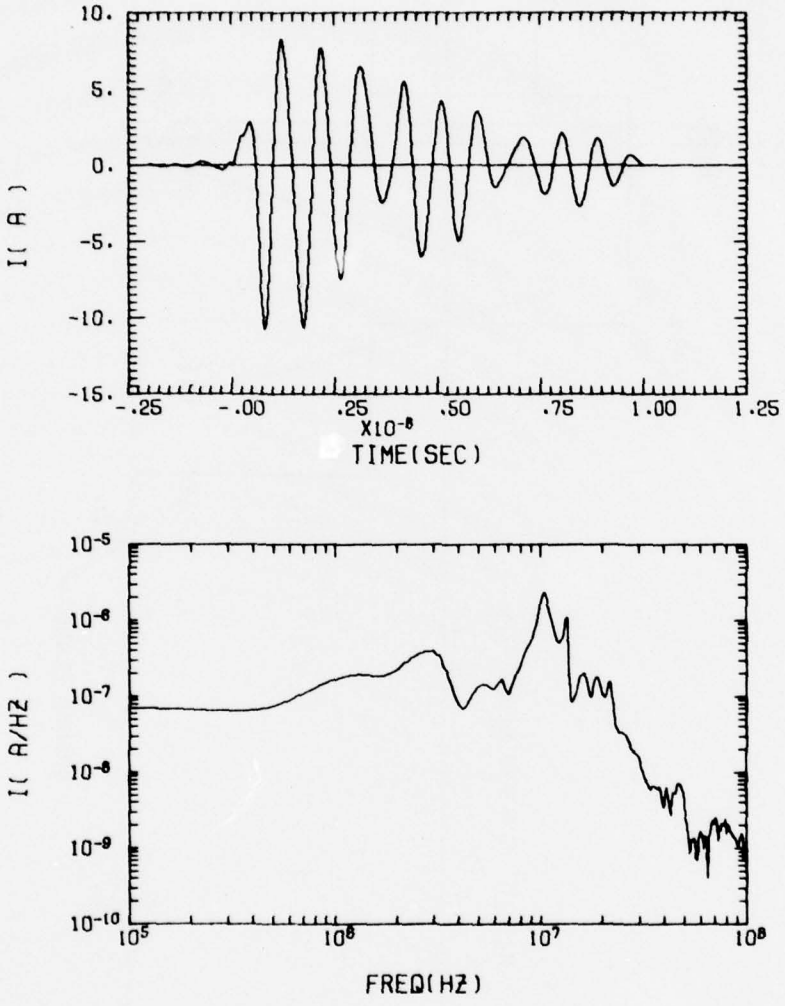

Figure 36 Time and Frequency Domain of Lower Yardarm (Starboard Side)

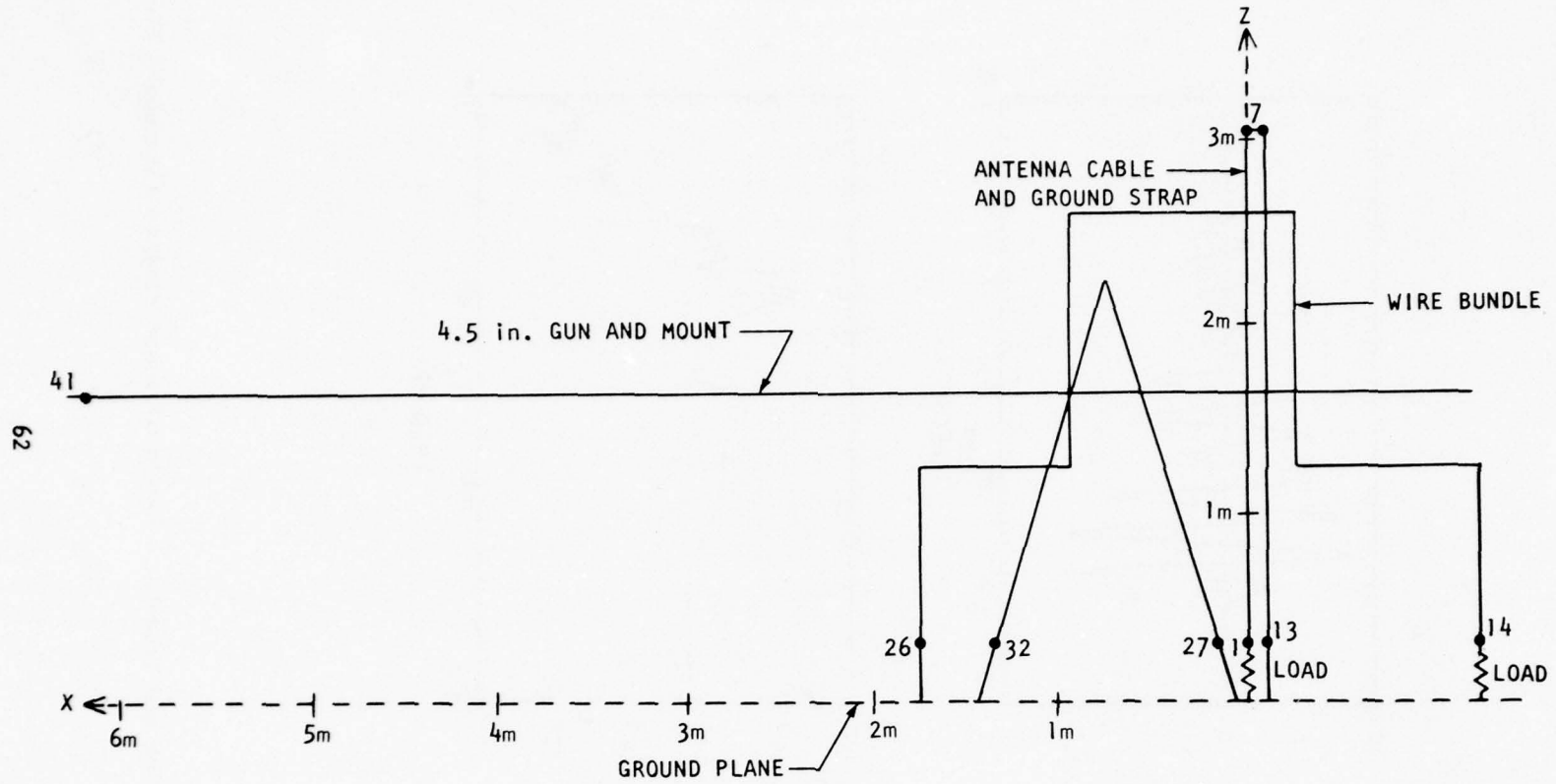

Figure 37 Wire Grid Model for the 4.5-Inch Gun Mount Whip Antenna Cable

over a ground plane and included in the base segment as a load. The model also included a large loaded cable bundle (segments 14 through 26) and the 4.5-inch gun (segments 27-41). The EMPRESS field is incident upon the gun mount with $\theta = 85^{o}$, $\phi = 62^{o}$, and $\tau = 180^{o}$. The gun mount lies far enough ahead of the superstructure that scattered fields can be neglected and only the incident plane wave field need be considered.

The antenna cable is routed together with a large number of cables in its run from the gun mount to the operations room. These other cables form a "ground plane" with respect to the antenna cable which is considered as a transmission line over this ground plane. The loading of the model to represent the transmission line from the gun mount to the operations room was done by adding an impedance Z_c to the self-impedance term for the cable base segment. When the antenna cable is grounded in the operations room, the transmission line impedance is $Z_c = Z_o \tanh \gamma L$, where Z_o is the characteristic impedance, γ is the propagation constant, and L is the length of the cable. Values for the characteristic impedance and propagation constant were obtained from an empirical study of electronic subsystems [5]. The propagation constant is written in the standard complex frequency form

$$\gamma = \alpha + j\beta \tag{8}$$

where $$\alpha = \frac{0.1}{2Z_o} \frac{\sqrt{f}}{10^3} + \frac{0.35f\sqrt{\varepsilon}}{c} \tag{9}$$

$$\beta = \frac{2\pi f}{c} \sqrt{\varepsilon} \tag{10}$$

and f is the frequency, c the speed of light, ε the relative dielectric constant. The first term in the loss factor α is due to internal wire resistance and the second term is based on empirical observation. Since the volume between the cables contains a combination of dielectric material and free space, the dielectric constant was set to 2.3. Measurements indicate that a resonable value for Z_o is 30 ohms [5].

The antenna bulk cable current was predicted at three locations inside the gun mount; 0.38 meters, 1.70 meters, and 2.95 meters up from the floor. The frequency and time domain responses are shown in Figures 38 through 40. The bulk current nearest the floor (0.38 meters) is dominated by the quarterwave resonance of the antenna cable at 19 MHz. The transmission line resonances at lower frequencies are seen to modulate the time domain slightly. The peak bulk current is 9.5 A. As one moves up the cable, the peak bulk cable current decreases to 7.5 A at 1.70 meters up. The quarterwave resonance at 19 MHz still stands out along with the low-frequency modulation. It is expected that the current decreases as the prediction point moves up the cable since the quarterwave resonance current should approach zero at the top. As the quarterwave resonance current decreases, the current associated with the transmission line at 2 MHz remains constant. This is evident in Figure 40 at a location of 2.95 meters from the floor where the bulk cable current rings at 19 MHz but the low-frequency component is significant.

The bulk current measurements were made along the cable with a Singer 91550-2 current probe. The transfer impedance for this probe is very near one over the frequency range 0.1 to 50 MHz. Therefore, the analytical predictions have not been corrected since the change is small.

It is expected that the currents predicted in this model will be larger than those measured. This is because the model can only approximate the large amount of structure surrounding the antenna cable. This additional structure will shadow the cable and load it and hence decrease the current and the resonant frequency. The large cable bundle into which the antenna cable feeds would also introduce a more complex loading than that used in the model. These corrections could be put into a more complex model but were beyond the scope of the effort intended for this program.

3. UK/SRA-102 ANTENNA CABLE CURRENT

Four SRA-102 antennas are located on the upper yardarms of the aft mast as illustrated in Figure 41 and as shown in the photograph of Figure 13. The coaxial cables to each antenna are laced to the upper yardarms, enter the mast,

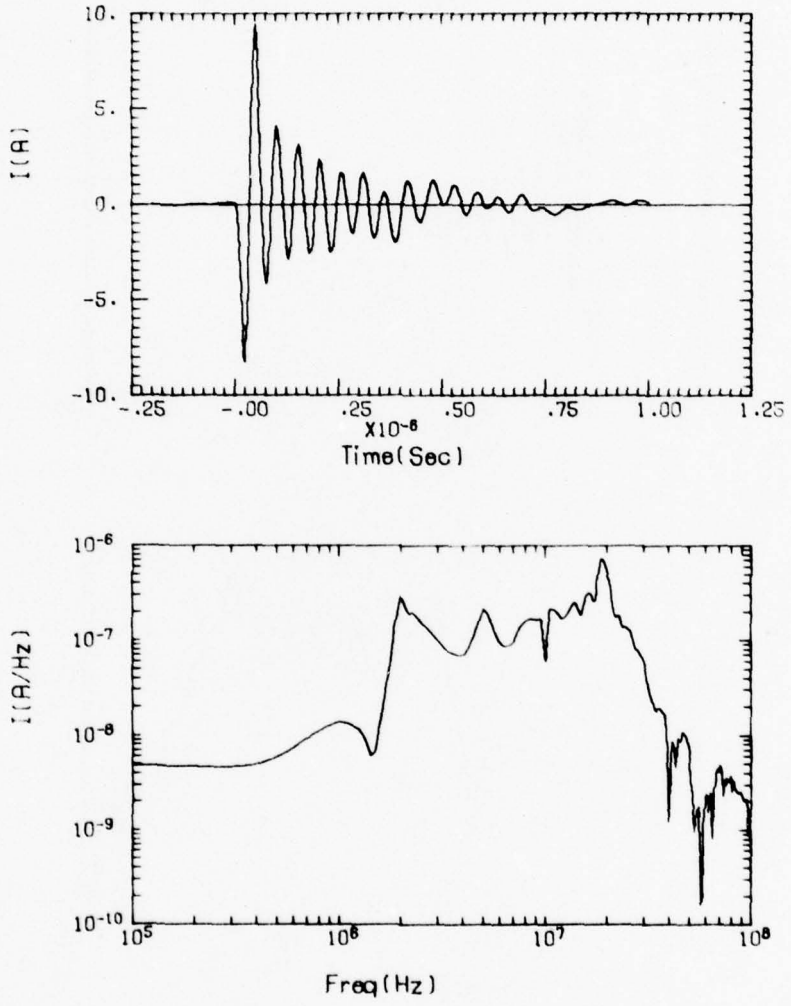

Figure 38 Time and Frequency Domain for the 4.5 Inch Gun Mount Antenna Bulk Cable Current at 0.38 Meters up from the Floor (EMPRESS Facility Excitation and Cable Shield Grounded in Operations Room)

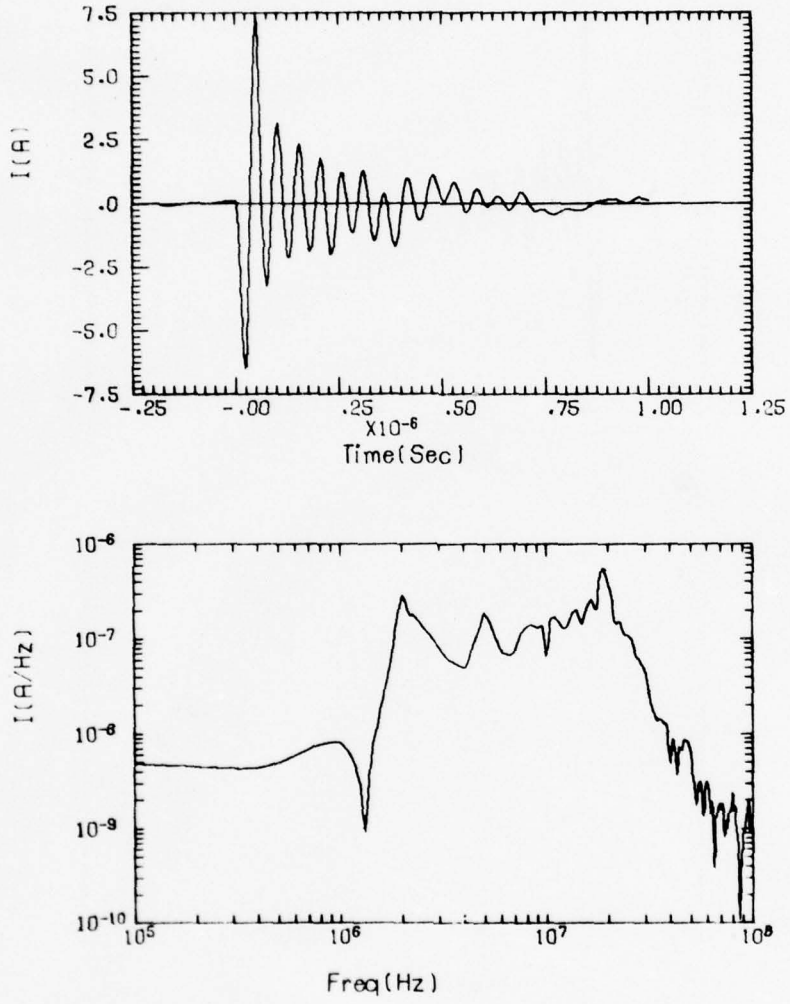

Figure 39 Time and Frequency Domain for the 4.5-inch Gun Mount Antenna Bulk Cable Current at 1.70 Meters up from the Floor (EMPRESS Facility Excitation and Cable Shield Grounded in Operations Room)

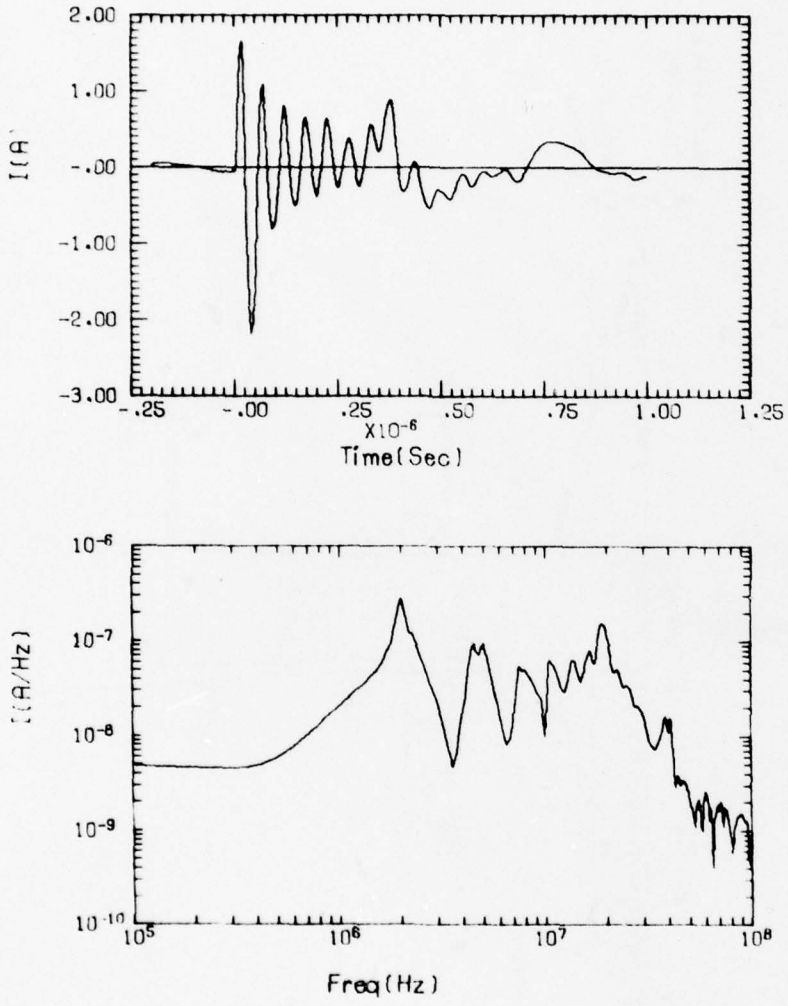

Figure 40 Time and Frequency Domain for the 4.5-Inch Gun Mount Antenna Bulk Cable Current at 2.95 Meters up from the Floor (EMPRESS Facility Excitation and Cable Shield Grounded in Operations Room)

Figure 41 Aft (Main) Mast of the SHEFFIELD, Showing UK/SRA-102 Antenna Cable with Measurement Locations

and are routed down the interior of the mast as illustrated in Figure 41. Bulk cable currents on the outer braid of the coax were measured at the locations shown in Figure 41. Analysis of only one of the four cables was required by the work statement. The selected cable is one which connects to an antenna on the port yardarm.

The exact length of the cable from the mast entry point to its final destination in the V/UHF office was not measured but is estimated, from ship cable routing diagrams, to be about 61 meters. The characteristic impedance Z_c, of the cable with respect to the interior mast wall is estimated to be 40 ohms. The propagation coefficient, γ, is assumed to be

$$\gamma = \frac{0.1}{2Z_c}\sqrt{\frac{f}{10^6}} + \frac{0.35f}{3\times10^8} + j\frac{2\pi f}{3\times10^8} \qquad (11)$$

The first two terms of equation (11) are based upon empirical data of aircraft cable runs having many branches. The third term is the usual free space propagation factor. The coaxial cable is most likely shorted to the equipment in the V/UHF office so that the impedance at the mast entry point, Z_B, looking towards the mast interior, is

$$Z_B = Z_C \tanh \gamma L \qquad (12)$$

The impedance at this point is driven by the current picked up on the external portion of the cable.

The drive of the external cable can be represented as a Norton source; i.e., a short circuit current and a parallel impedance. The short circuit current of the external cable is estimated to be about 0.3 times the computed total yardarm current. That is, if both antenna cables on the port yardarm were shorted to the mast at the mast entry point, the total yardarm current would divide among the two cables and the yardarm. The estimate that 3/10 of the current flows in one cable is probably high.

The source impedance, Z_A, of the external cable is essentially the impedance of the transmission line formed by the cable and the yardarm. The cable at the antenna end is believed to be grounded to the yardarm so that the impedance at the mast entry point looking out towards the antenna is

$$Z_A = Z_0 \tanh \gamma' d \tag{13}$$

Based upon physical observation, the characteristic impedance, Z_o, is estimated to be 33 ohms and the length d, 4.22 meters. The propagation coefficient, γ', was estimated as

$$\gamma' = \frac{0.1}{2Z_o}\sqrt{\frac{f}{10^6}} + \frac{0.11f}{3\times10^8} + j\frac{2\pi f}{3\times10^8} \tag{14}$$

This is the same propagation coefficient as for the interior cable except that the second term is smaller since there is no cable branching. The first and second terms were chosen to be equal at 17 megahertz, the external cable resonance.

Based upon the above Norton equivalent circuit parameters the cable current at the mast entry point, I_E, is

$$I_E = \frac{0.3\ I_{sc}\ Z_A}{Z_A + Z_B} \tag{15}$$

The current at any other location, x, along the cable is given by the transmission line equation for a cable shorted at one end; namely,

$$I(x) = I_E \frac{\cosh\gamma(L-x)}{\cosh\gamma L} \tag{16}$$

where x is equal to zero at the mast entry point.

The time and spectral responses of the cable current at the mast entry point are shown in Figure 42. The responses are almost identical to the port upper yardarm current (Figure 29) except with a reduction in magnitude. The peak time domain response is 1.8 amperes. The responses further down the cable

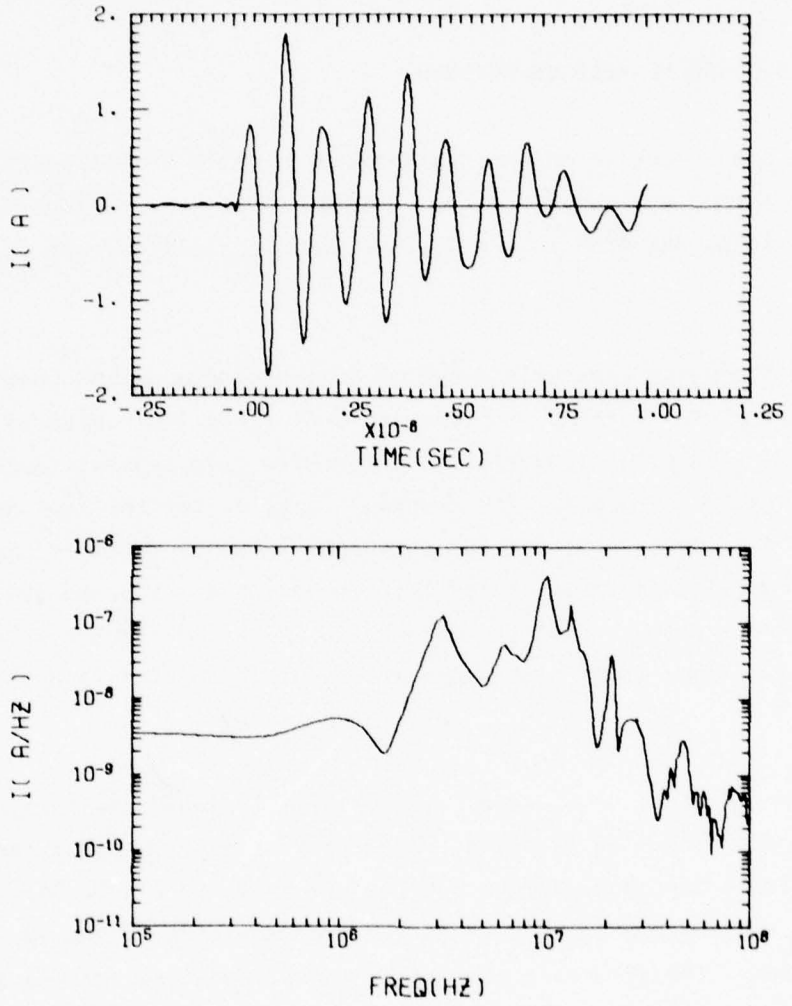

Figure 42 Time and Frequency Domain of UHF Cable at Mast Entry Point

(Figures 43 through 45) change only slightly. The high frequencies are attenuated more as a function of distance so that by 8.5 meters (Figure 46) the peak time domain response has dropped to 1.55 amperes.

4. FOREMAST WIRE MF RECEIVE ANTENNA

The foremast receive antenna is located at frame 26 starboard. The antenna is 10.75 meters long and runs from the foremast yardarm to a high voltage standoff at the base. It is required to predict the short circuit current at the base of the antenna.

A high-frequency wire grid model of just the antenna was constructed for the interaction of the antenna with the incident field (no scattered fields). This model consisted of 21 linearly connected wire grid segments each of length 1/2 meter over a ground plane. The transfer function for the real and imaginary parts of the base segment current for the high-frequency model is shown in Figure 47. The current is capacitive at low frequency with a resonance near 7 MHz. This is the quarterwave resonance of the antenna at which the current at the base is maximal. Other higher order resonances are seen but they are reduced considerably in amplitude.

The mid-frequency model (see Section II.3) includes the foremast wire receive antenna as shown in Figure 8. The transfer functions for the real and imaginary parts of the base segment current are shown in Figure 48. The field which excites the antenna in the MFM is the superposition of the incident and scattered fields. The structure near the antenna loads the antenna by increasing antenna capacitance and mutual inductance. This loading decreases the antenna resonance frequency and the scattered field changes the magnitude and phase of the current with respect to the incident field. Hence, the transfer function of Figure 48 has a resonance near 6.5 MHz and the scattered field interaction is evident driving the real part negative near resonance. This dip in the transfer function is due to the interaction of the antenna with the port foremast antenna. The port antenna was shorted at its base whereas if it were loaded,

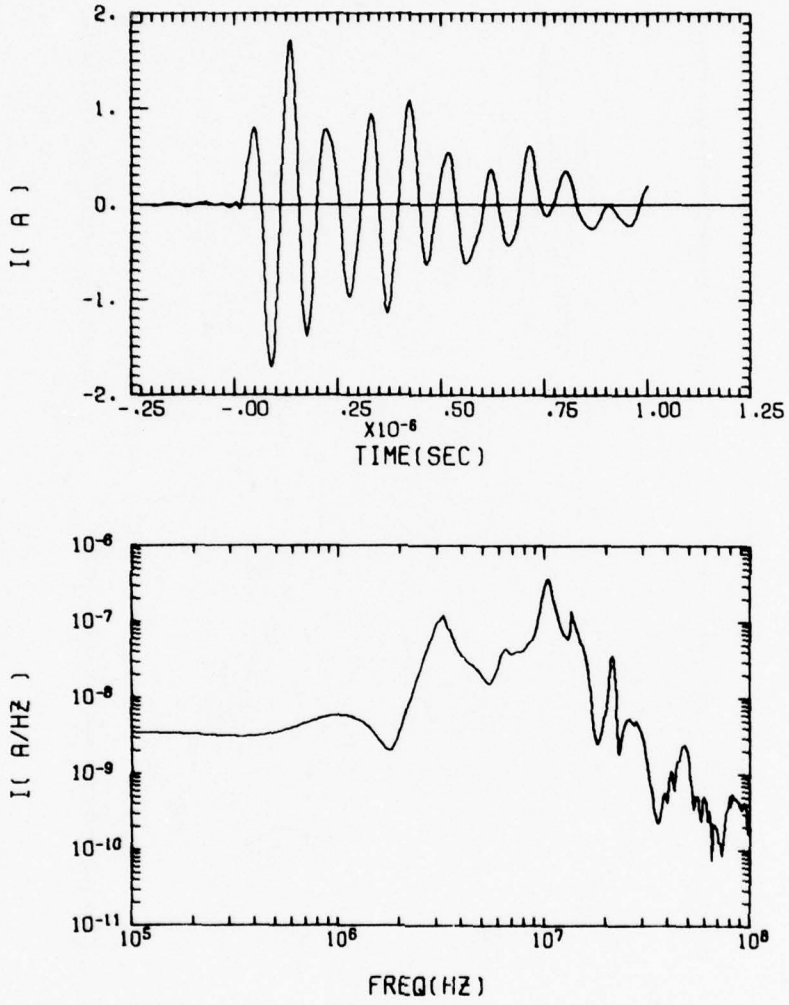

Figure 43 Time and Frequency Domain of UHF Cable at 2.8 Meters Inside of Mast

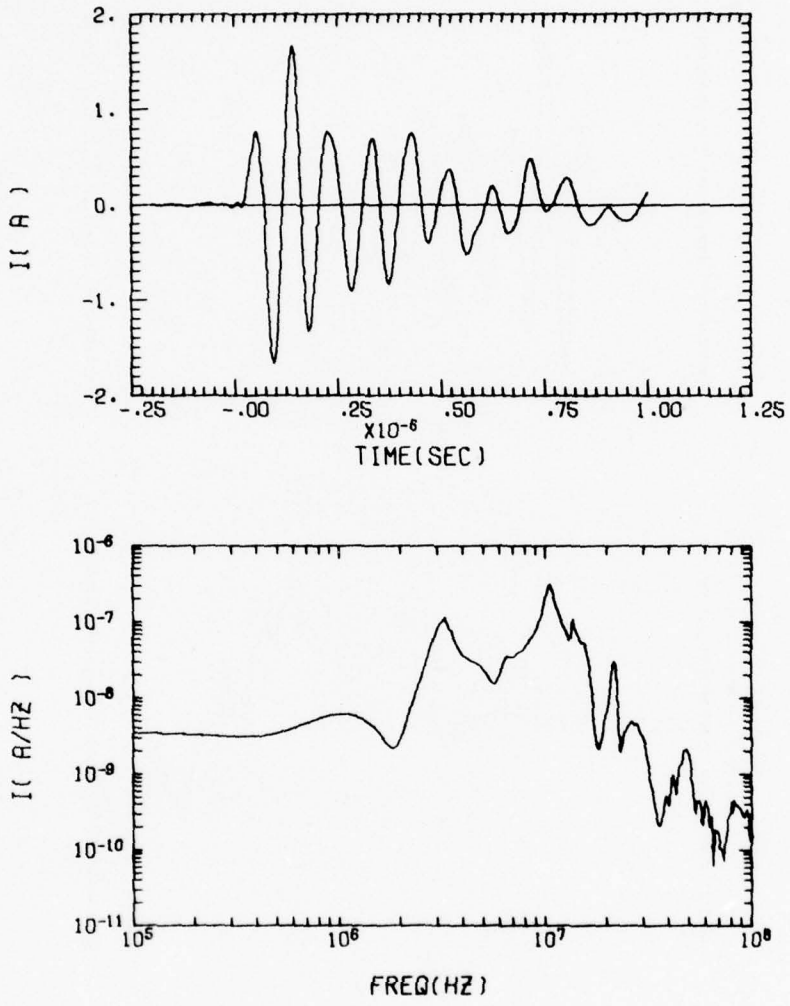

Figure 44 Time and Frequency Domain of UHF Cable at 4.6 Meters Inside of Mast

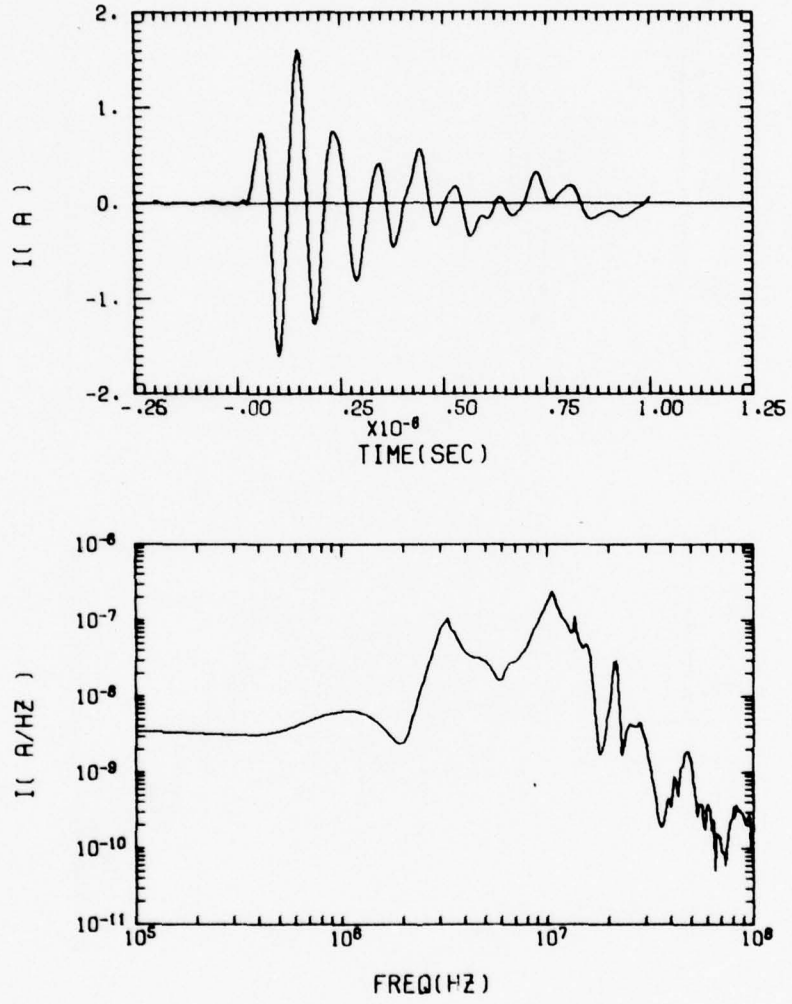

Figure 45 Time and Frequency Domain of UHF Cable at 6.5 Meters Inside of Mast

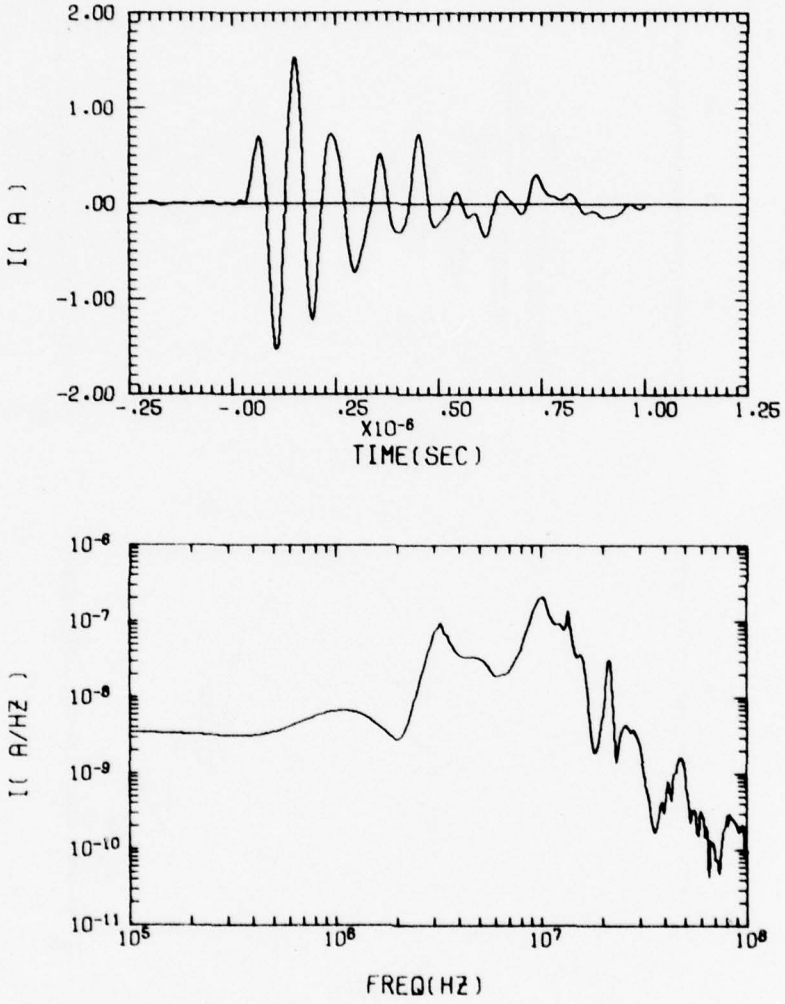

Figure 46 Time and Frequency Domain of UHF Cable at 8.5 Meters Inside of Mast

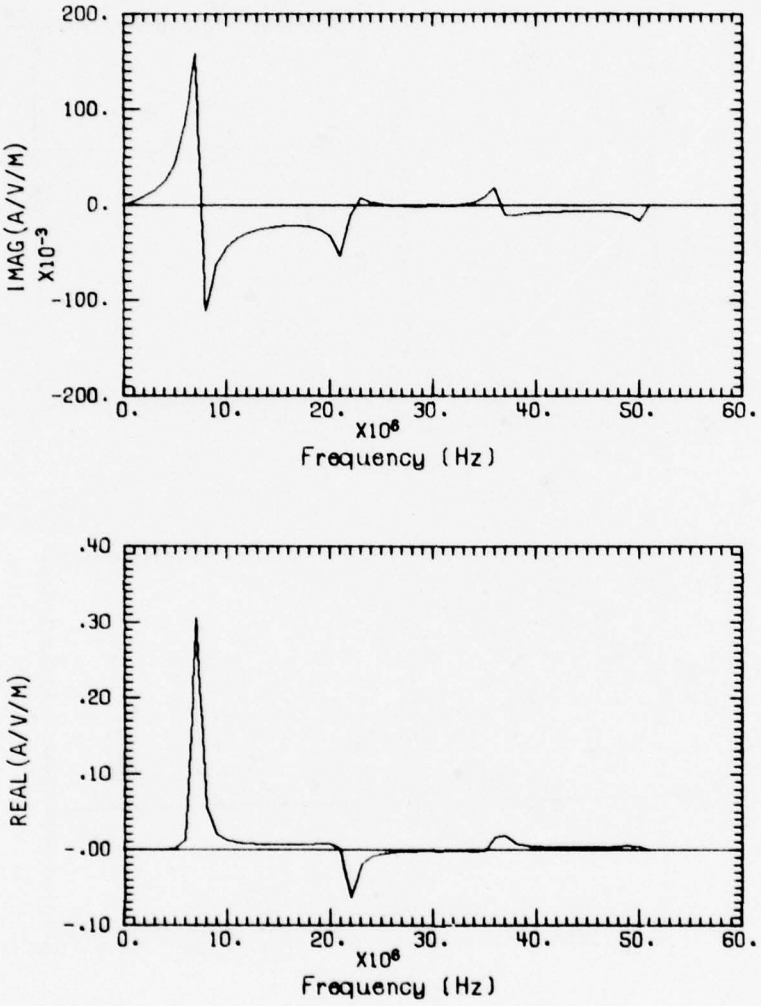

Figure 47 Real and Imaginary Parts of the Transfer Function for the Foremast Wire MF Receive Antenna (Short Circuit Current at Base of Antenna)

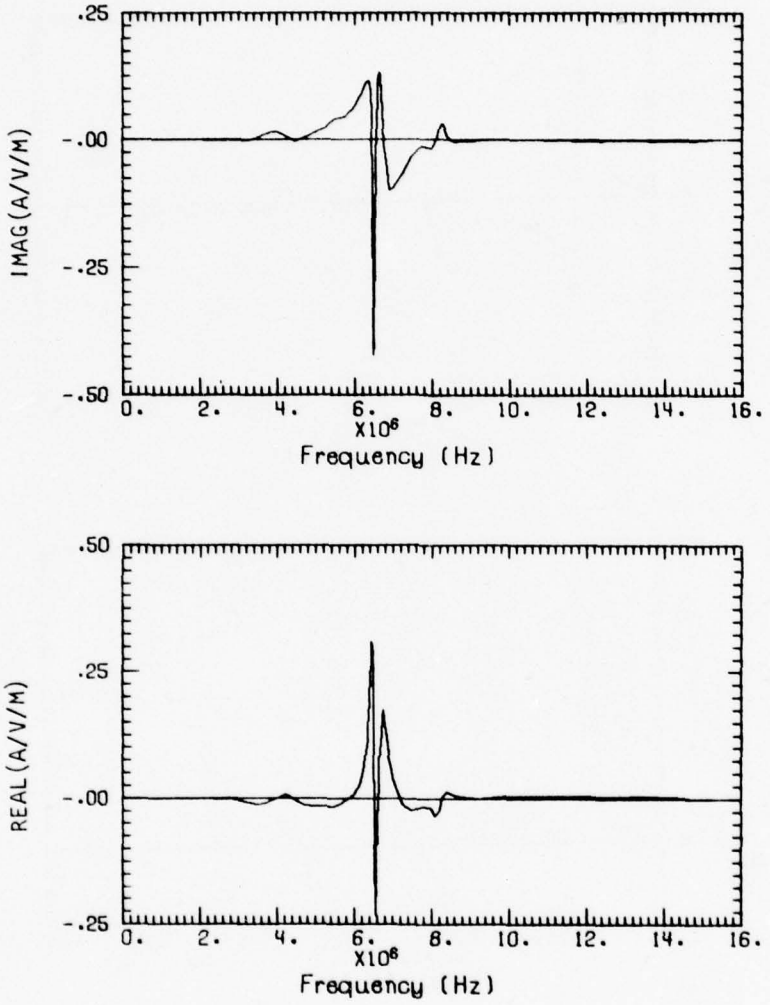

Figure 48 Real and Imaginary Parts of the Transfer Function for the Foremast Wire MF Receive Antenna (Short Circuit Current at Base of Antenna)

the interaction would be weaker. These transfer functions for the mid-frequency and high-frequency models were merged between 12 to 15 MHz. By comparing the amplitudes, it is clear that the quarterwave resonance near 6.5 MHz dominates the transfer function; however, the higher order resonances were included for completeness. The transfer function is completed when the LFM contribution is included. The LFM foremast transfer function was found by first calculating the electric field at those positions in the LFM (see Figure 2) occupied by the foremast antenna. This electric field was then integrated along the length of the antenna to give the open circuit voltage at the base. The antenna impedance was derived from the MFM calculations which extended down to 0.5 MHz. Consequently, the LFM transfer function for the short circuit current is given by $I(f) = V(f)/Z(f)$. This transfer function was merged with the MFM between 2 and 4 MHz. The foremast receive antenna transfer function over the entire frequency domain was obtained from these three models and appropriate merging.

The short circuit current at the antenna base was determined by multiplying the transfer function by the EMPRESS spectrum. The time and frequency domain responses are shown in Figure 49. The quarterwave resonance at 6.5 MHz dominates the spectrum with the next resonance peaking near 20 MHz. The current initially follows the incident electric field until the reflected current arrives at the base and the antenna current oscillates at the quarter wavelength resonant frequency peaking at 17 A. The small ripples on the early time waveform are caused by the three-quarter wavelength resonance at near 20 MHz. The structure surrounding the antenna creates a cavity effect which accounts for the high Q of the current.

The open circuit voltage at the base of the antenna was predicted and the frequency and time domain results are shown in Figure 50. The open circuit voltage was calculated by forming the product of the short circuit current and antenna impedance at each frequency, $V_{oc}(f) = I_{sc}(f) \times Z_a(f)$. The antenna Thevenin impedance was found as part of the WIRANT program. The open circuit voltage response follows the incident field excitation with the half-wave antenna resonance at 13 MHz superimposed as a ringing. The peak open circuit voltage is

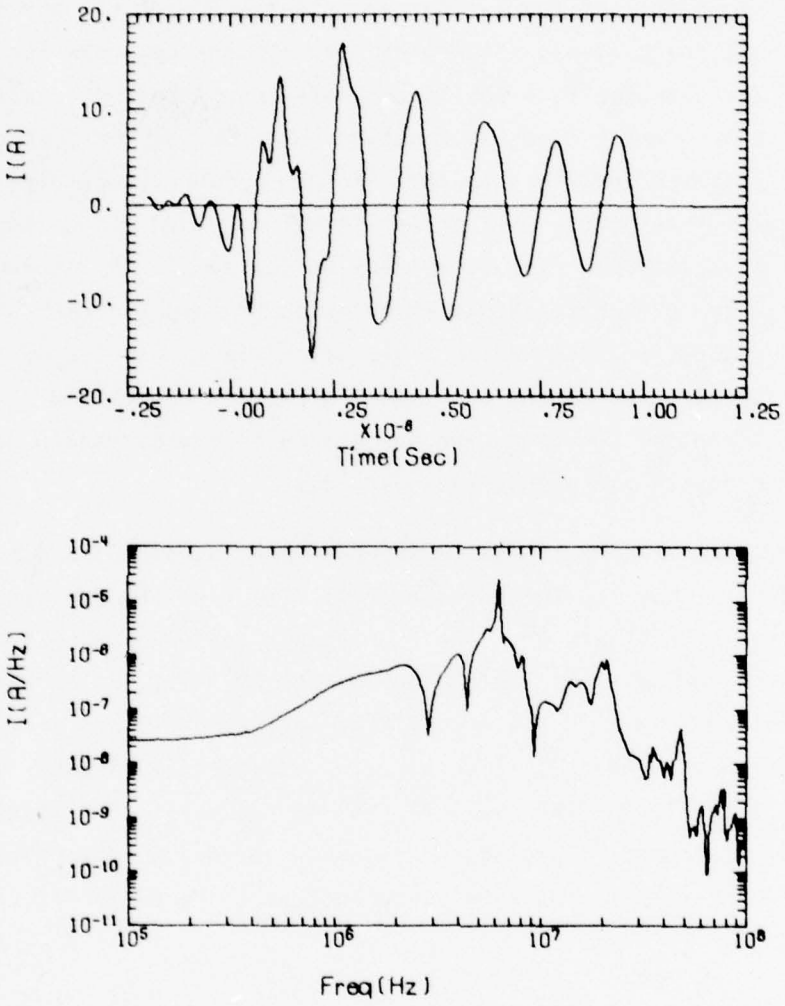

Figure 49 Time and Frequency Domain for Short Circuit Current at the Base of the Foremast Receive Antenna

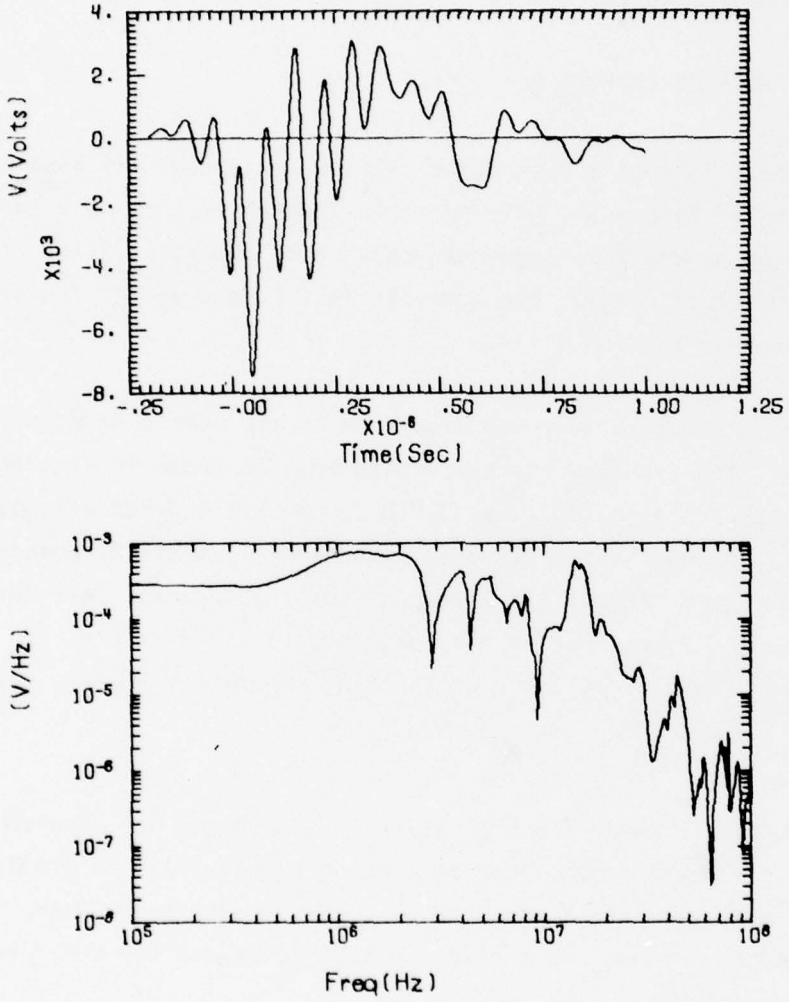

Figure 50 Time and Frequency Domain for Open Circuit Voltage at the Base of the Foremast Receive Antenna

7.4 kV and nonlinear effects which might limit this voltage have not been included in the model. The effect of measurement probe capacitance is small (see Section II.6), and the results were not modified to include probe effects.

5. FOREMAST SURFACE CURRENT DENSITY

The foremast is nearly a circular cylinder except at its base as shown in the photograph of Figure 51. The mast was modeled in the low-frequency Sheffield model as simple wire segments and as a triangular cylinder in the mid-frequency Sheffield model. The analysis is the same as for the aft mast which is discussed in Section III.1.

The axial surface current was predicted on the port side at heights of 1, 5, and 9 meters. The time and spectral responses are shown in Figures 52, 53, and 54. The foremast resonance is at 3.8 MHz, and the 2.8 MHz aft mast resonance is also predominant. The peak response is lowest (27 amperes/meter) at the one meter height since the base of the foremast fans out and has a circumference of 8.2 meters. At the heights of 5 and 9 meters, the circumference is 2.9 meters and the peak values are 47 and 42 amperes-per-meter, respectively.

6. HF TRANSMITTING WHIP ANTENNA

The HF transmit whips are 9.1 meters in length and are located at frame 34 on the port and starboard. The port antenna was analyzed to predict both the short circuit current and open circuit voltage at the base. The method used to analyze the antenna was similar to that described for the foremast receive antenna (III.4).

The high-frequency wire grid model of the antenna consisted of 18 linearly connected segments extending 9.1 meters off the ground plane. This model was run for frequencies of interaction up to 100 MHz. The transfer function has a simple dipole resonances at 8, 24, 40 MHz, etc. The HF transmit whips were included as part of the MFM and the current in the base segment was calculated. The MFM transfer function

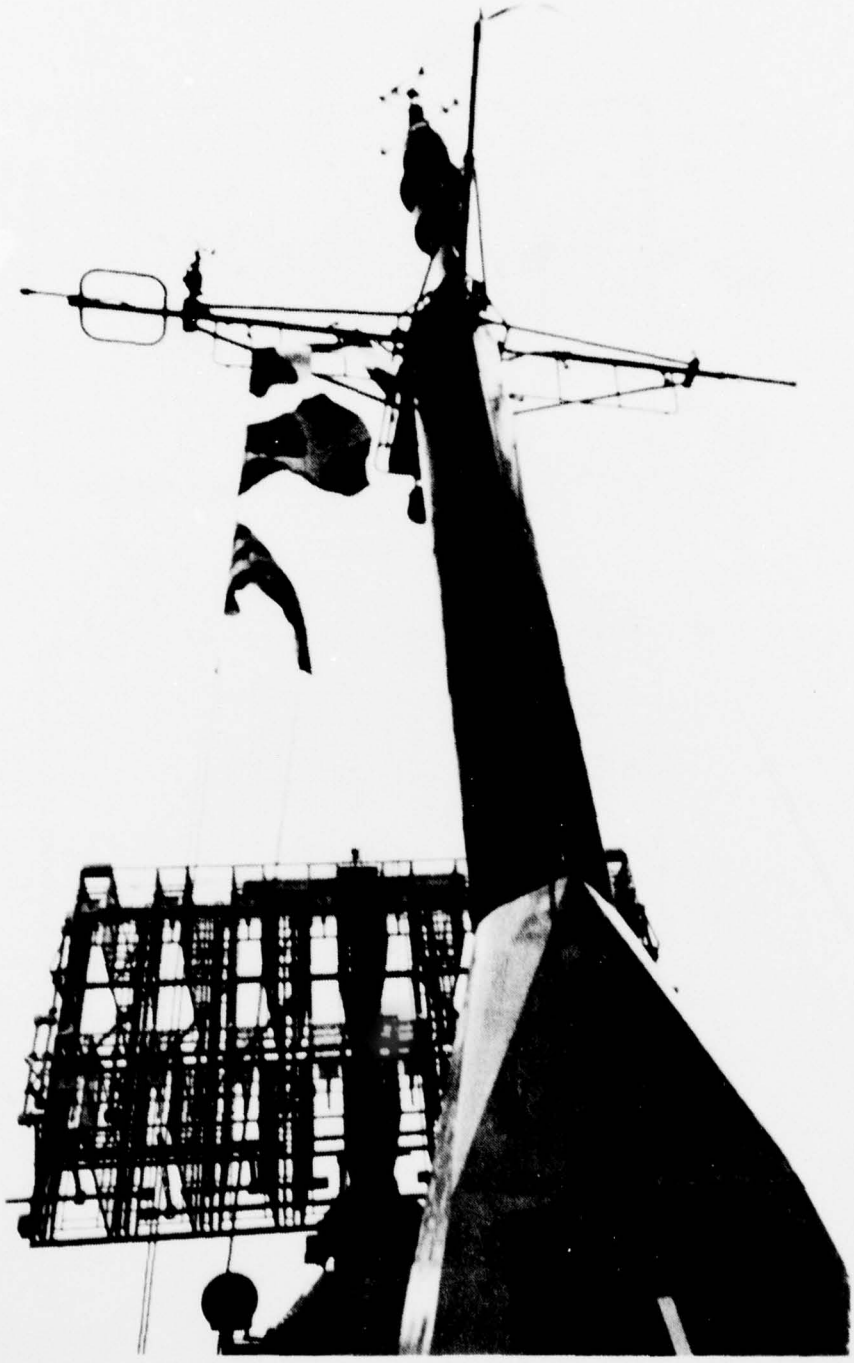

Figure 51 Foremast, Looking Forward

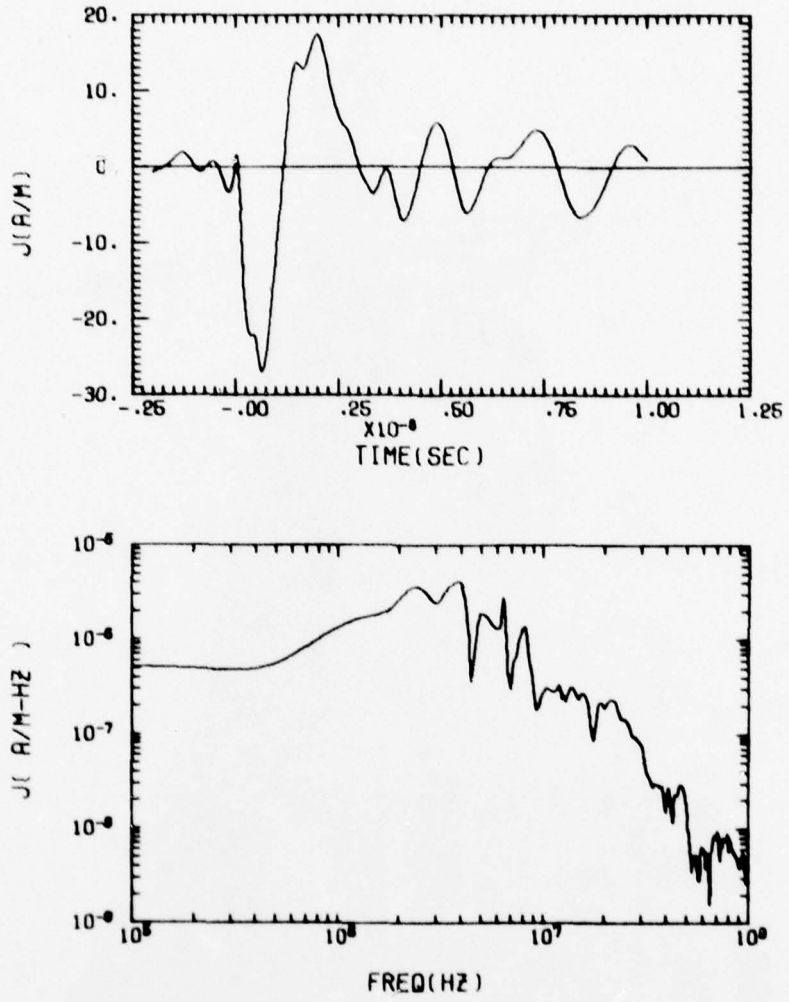

Figure 52 Time and Frequency Domain of Longitudinal Current Density on the Foremast (z=1 Meter, Port Side)

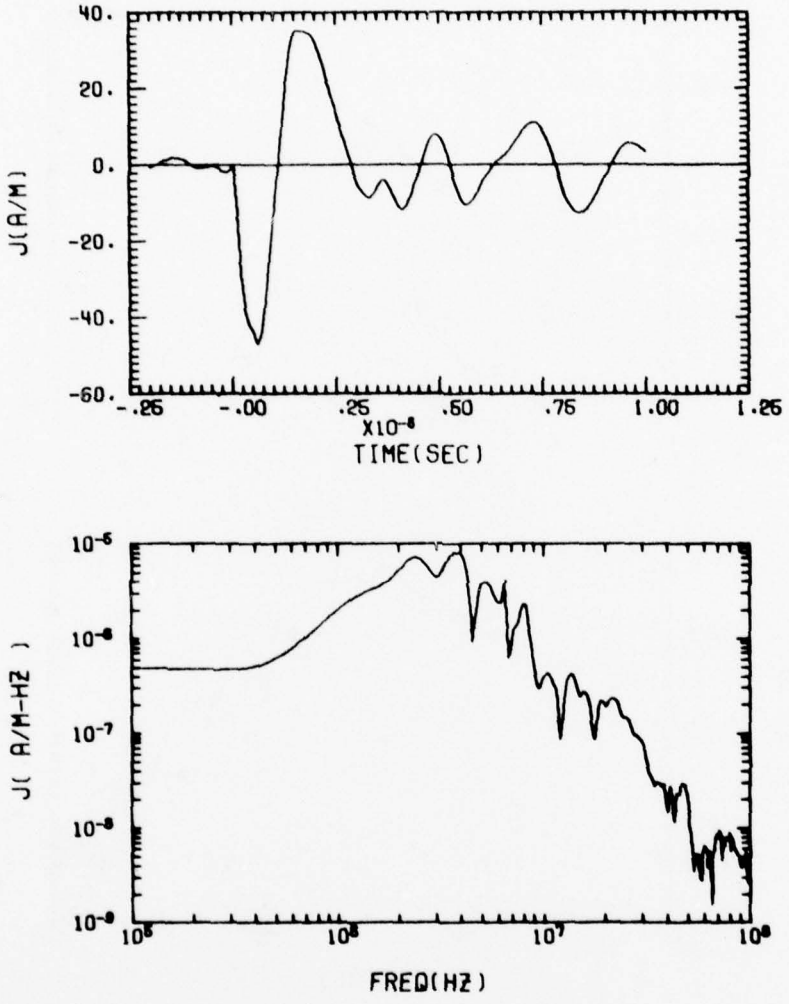

Figure 53 Time and Frequency Domain of Longitudinal Current Density on the Foremast (z=5 Meters, Port Side)

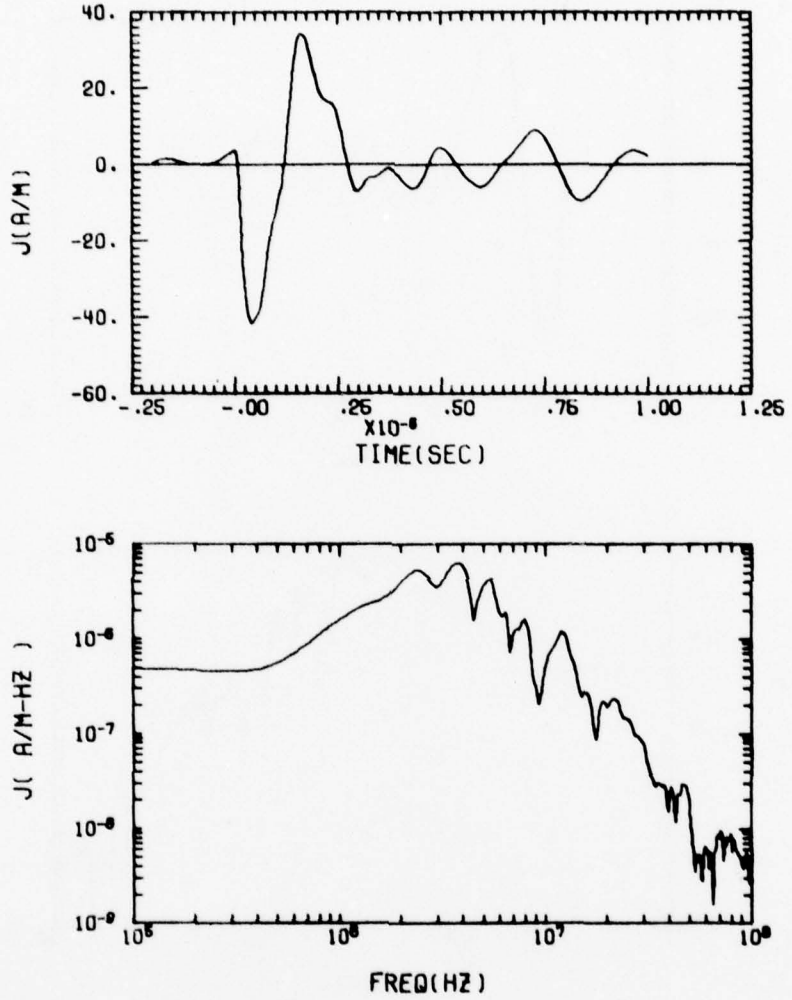

Figure 54 Time and Frequency Domain of Longitudinal Current Density on the Foremast (z=9 Meters, Port Side)

for the short circuit current has the fundamental dipole quarterwave resonance at 8 MHz. The HFM and MFM were merged between 12 to 15 MHz. The low-frequency response of the antenna was found by integrating the electric field along the antenna as described in Section III.4. The low-frequency transfer function was merged with the MFM results over the 2 to 4 MHz range. The resultant frequency domain spectrum with the EMPRESS field folded in is displayed in Figure 55 along with the time domain. The short circuit current is basically a damped sine at the quarterwave resonant frequency of the antenna and peaking at 60 A. The response is primarily that due to the incident field since there is very little scattered field at the port HF antenna. The open circuit voltage at the antenna's base was calculated by multiplying the antenna impedance by the short circuit current as a function of frequency. The open circuit voltage frequency and time domain responses are shown in Figure 56. The voltage initially follows the EMPRESS field which excites the antennas halfwave resonance current at 16 MHz resulting in a high-frequency ringing superimposed upon the EMPRESS field. The peak open circuit voltage at the base is 12.5 kV. The analysis did not consider any nonlinear effects such as dielectric breakdown or arcing which might occur before this voltage is reached.

The effect of measurement probe loading on the predicted voltage was examined and found to be negligible when the probe capacitance is within manufacturer's specifications. The high voltage measurement was done with a Tektronix type P6015, 40KV, 1000X probe. This probe has an input resistance of 100 MΩ in parallel with 3 pF. This impedance was placed in the model and found to reduce the voltage slightly. The voltage plotted in Figure 56 includes the probe loading. The effect of probe capacitance was investigated further by increasing the probe capacitance to 30 pF. The open circuit voltage is shown in Figure 57. The peak voltage is reduced and much of the high-frequency response is filtered out. Hence, if stray capacitance significantly loaded the probe, the voltage response would be reduced. The effect of the Singer 91550-2 current probe was discussed in Section III.2.

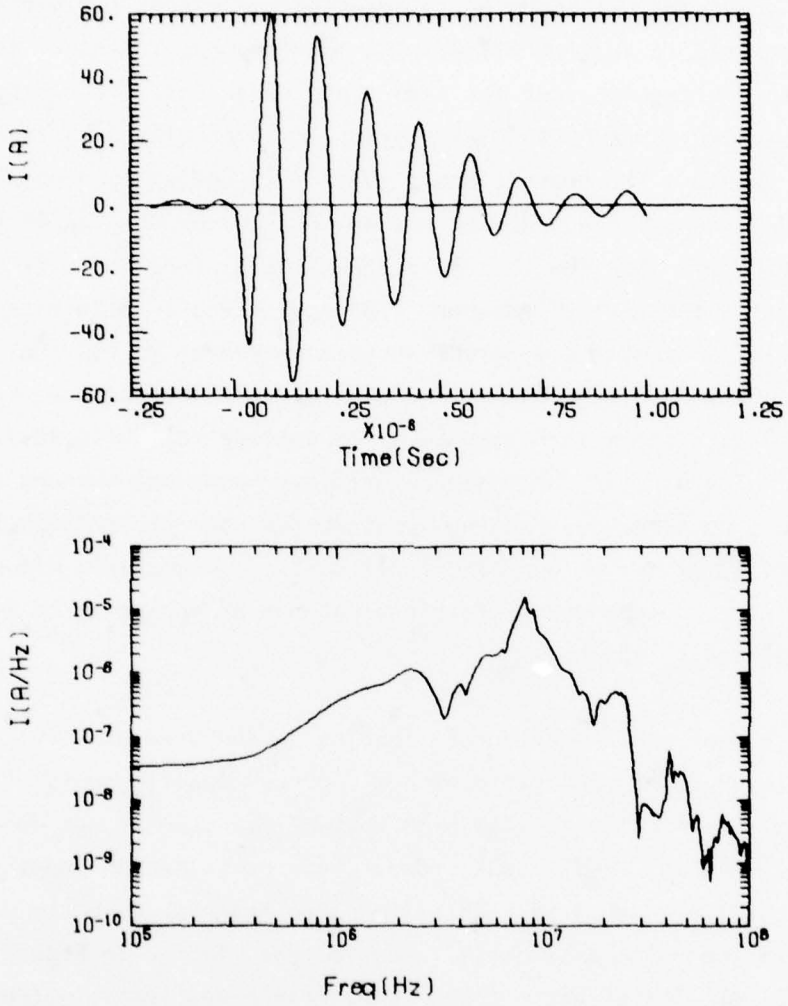

Figure 55 Time and Frequency Domain for the Short Circuit Current at the Base of the Port Side HF Transmit Whip Antenna (EMPRESS Facility Excitation)

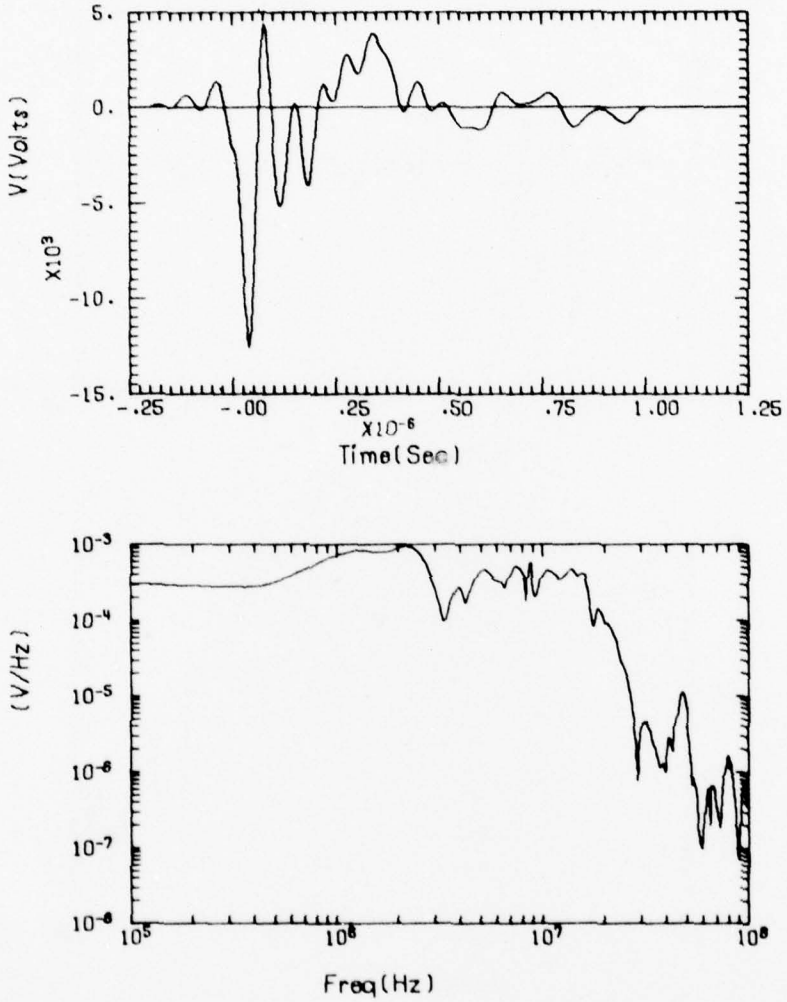

Figure 56 Time and Frequency Domain for the Open Circuit Voltage at the Base of the Port Side HF Transmit Whip Antenna

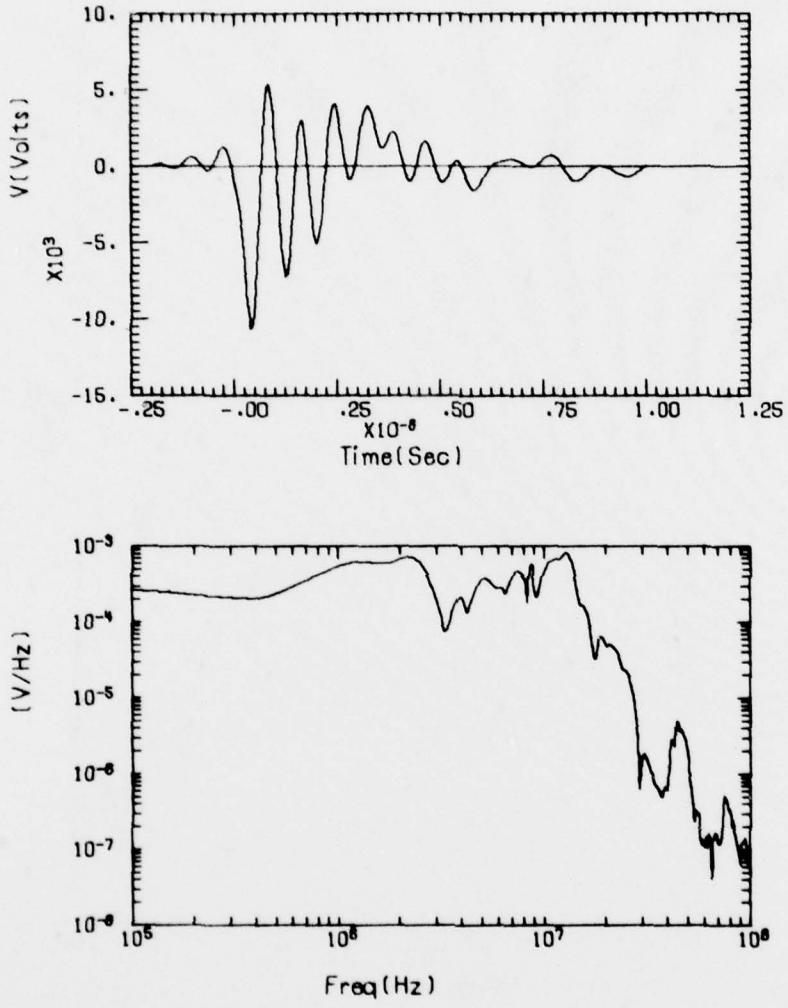

Figure 57 Time and Frequency Domain for the Open Circuit Voltage at the Base of the Port Side HF Transmit Whip Antenna Probe Capacitance = 30 pF

7. LORAN RECEIVER WHIP ANTENNA

The LORAN receiver whip antenna is a Designator British Type (AWN) with length 9.1 meters located at frame 24 1/2 starboard. Both the open circuit voltage and short circuit current at the base of this antenna were predicted. The analysis method was identical to that already described for the foremast receive and HF transmit antennas.

The LORAN receiver antenna's response is dominated by the quarterwave resonance at 8 MHz. The MFM short circuit current transfer function displays this dipole quarterwave resonance at 8 MHz with the scattered fields from the formast antenna and radar modifying the function slightly. This transfer function was merged with the LFM and HFM and multiplied by the EMPRESS spectrum. The frequency and time domains for the LORAN short circuit current are shown in Figure 58. The frequency domain is dominated by the quarterwave resonance, and the time domain displays this resonance behavior after initially following the EMPRESS field. The current peaks near 30 A and has a relatively high Q. The high Q of this response is probably due to a cavity effect created by the structure surrounding the antenna.

The open circuit voltage at the antenna base was determined by forming the product of the short circuit current and the antenna impedance. The frequency and time domains are shown in Figure 59. The voltage follows the incident EMPRESS field with the antenna's halfwave resonance ringing at 16 MHz superimposed upon it. The peak open circuit voltage is near 11 kV. The analysis did not consider any nonlinear effects such as breakdown of dielectric or arcing caused by the high voltage.

8. ACH ASTRO VHF ANTENNA

The ACH Astro antenna is a VHF EW antenna located on the lower yardarm of the aft mast as shown in Figure 60. The fan shaped ground plane is made of 3.5 foot radial tubing of 3/8 inch outside diameter. The tapered radiating

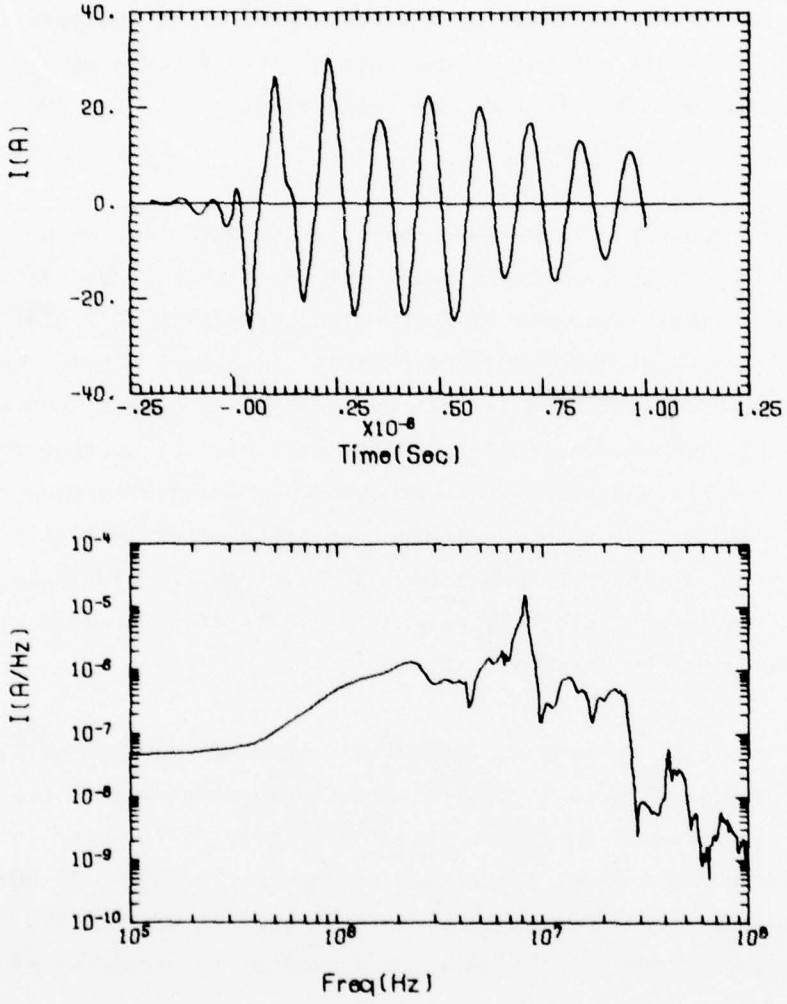

Figure 58 Time and Frequency Domain for Short Circuit Current at the Base of the LORAN Receive Antenna

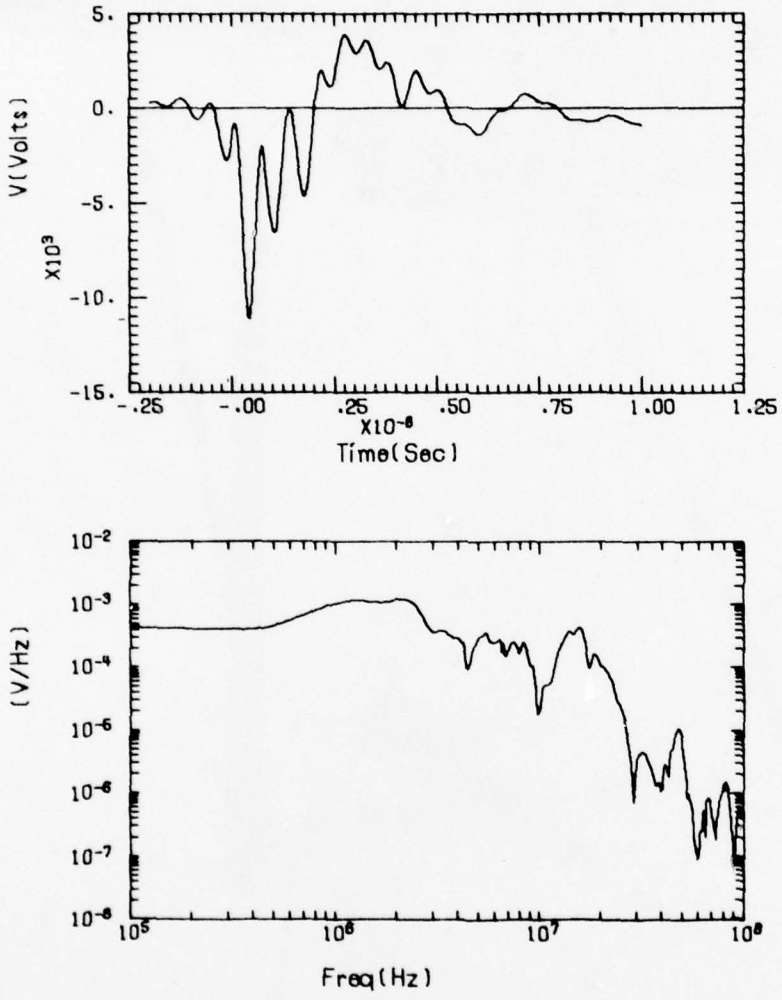

Figure 59 Time and Frequency Domain for Open Circuit Voltage at the Base of the LORAN Receive Antenna

Figure 60 ACH Astro VHF Antenna or Lower Yardarm of the Aft Mast

element, or stub, is also about 1.1 meters long and is about 10.2 centimeters wide at its base. The axis of the radiating element is 45 degrees from the vertical and 45 degrees starboard off the ship centerline. The antenna is connected to equipment in the main communications office by 61 meters of 75 ohm cable. The requirement was to predict the open circuit voltage, the short circuit current, and the matched load current at the end of the 61 meter cable. This was done by first modeling the antenna as a Thevenin equivalent source. Two separate wire grid models were used to compute the stub short circuit, I_{sc}, and the stub impedance, Z_A.

The low-frequency model of the ACH Astro antenna is part of the aft mast and yardarm model of Figure 26. In the frequency range of this model (0 to 30 MHz), the antenna responds as a short dipole, picking up the mast and yardarm resonances. Above 30 MHz, a more detailed model of the antenna by itself was developed (see Figure 61). Each of the radial arms is divided into two segments so that the upper-frequency limit is over 100 MHz. For this high-frequency model, the antenna is assumed to be in free space with no coupling to nearby structure. There is, however, some shadowing of the incident field by the mast since the antenna is on the starboard side near the shadow boundary. A hand calculation of the electric field at the antenna location, assuming the mast is an infinite cylinder, shows that the field is reduced to 40 percent of the incident field at 30 MHz. Also, by comparing the low-frequency antenna model short circuit current with the high-frequency model current, a reduction of 50 percent is required to obtain a smooth match near 30 MHz. A factor of one-half was introduced, therefore, into the high-frequency model to account for mast shadowing. The two models were merged together between 26 and 30 MHz. The high-frequency model has a resonance at 65 MHz when the stub is nearly a quarter-wavelength long.

The current into a matched load (75 ohms) at the antenna terminals is given by

$$I_M = \frac{Z_A \, I_{sc}}{Z_A + 75} \tag{17}$$

AD-A055 592 BOEING CO SEATTLE WASH F/G 20/14
EMP COUPLING ANALYSIS FOR H.M.S. SHEFFIELD.(U)
MAY 78 R S CARTER, D E YOUNG N60921-77-C-0185
UNCLASSIFIED D194-10043-1 NL

2 OF 2
AD
A055 592

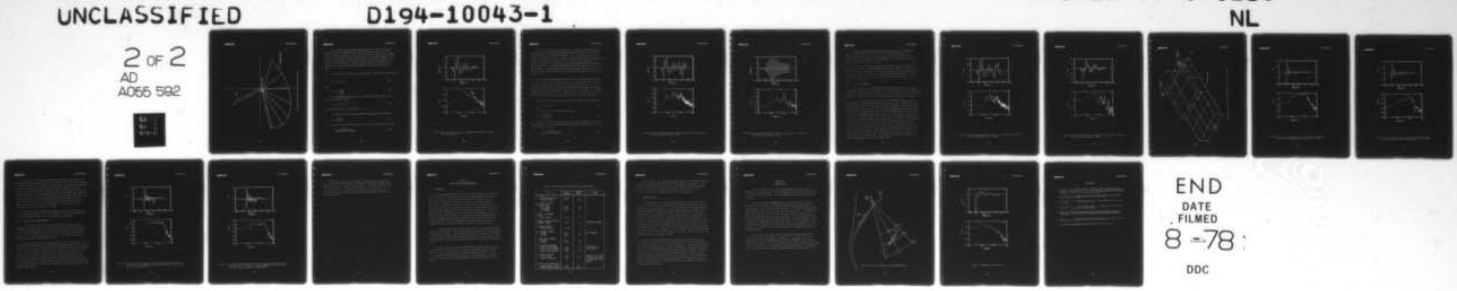

END
DATE
FILMED
8-78
DDC

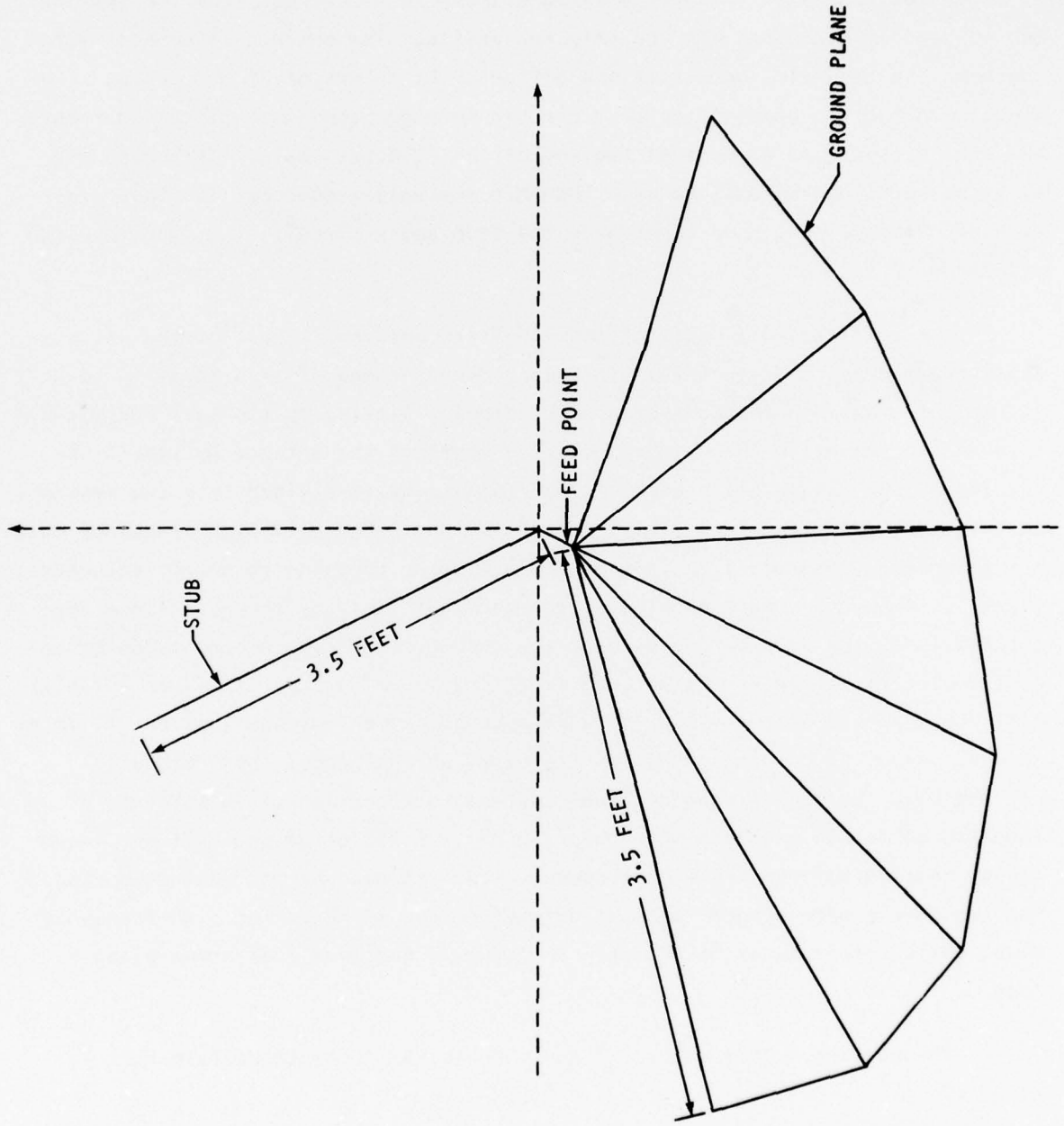

Figure 61 Wire Model of ACH Astro VHF Antenna

The time and spectral response of equation (17) is shown in Figure 62. The mast and yardarm resonances at 3.2 and 10.5 MHz are clearly seen. The antenna resonance at 65 MHz is obscured by the rapid oscillations of the EMPRESS field. The time domain response is quite similar to the lower yardarm current. The first 50 nanoseconds show a slight response to the antenna resonance. The peak current is 2.8 amperes. Since the coaxial cable loss is quite low, the matched load current of Figure 62 also applies at the end of the 61 meter cable.

When the cable is shorted, the input impedance, Z_{in}, at the antenna terminal is,

$$Z_{in} = 75 \tanh \gamma L \tag{18}$$

where

$$\gamma = \alpha + j\frac{2 f\sqrt{\varepsilon}}{3\times10^{8}} \tag{19}$$

The propagation coefficient, γ, is assumed to be similar to RG-11 which has a loss variation of [6].

$$\alpha = 7.5 \times 10^{-7} \sqrt{f} \tag{20}$$

and a relative dielectric constant of $\varepsilon = 2.3$.

The current at the antenna terminals for the shorted line condition is

$$I_{in} = \frac{Z_A I_{sc}}{Z_A + Z_{in}} \tag{21}$$

By use of transmission line equations, the current at the shorted end is

$$I = \frac{Z_A I_{sc}}{(Z_A + 75 \tanh \gamma L) \cosh \gamma L} \tag{22}$$

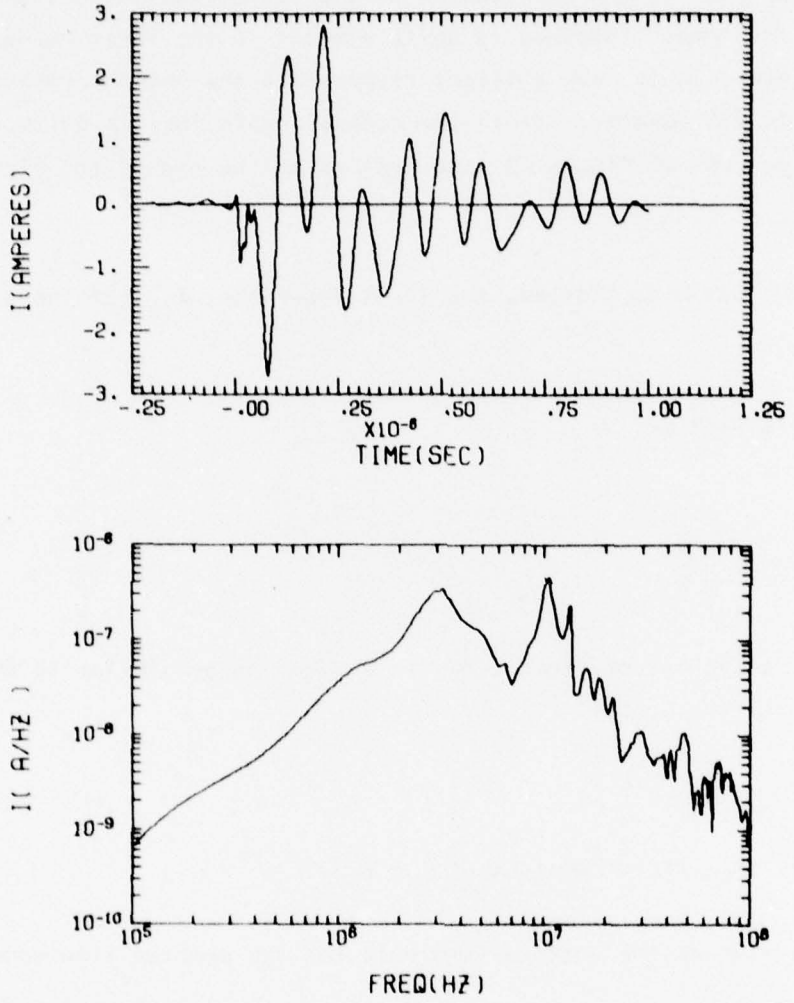

Figure 62 Time and Frequency Domain of Matched Load Current in the ACH Astro VHF Antenna

For the first 618 nanoseconds, the time it takes the signal reflected at the shorted end to travel to the antenna and return, the short circuit current is twice that of the matched load current. This is as expected since for the first 618 nanoseconds, the source impedance at the shorted end is the characteristic impedance of the cable. The short circuit current, shown in Figure 63, has a peak of 5.1 amperes. After 618 nanoseconds, the signal reflected back from the antenna appears. This reflected wave does not show the 65 MHz oscillation since this frequency is nearly matched and absorbed (radiated) at the antenna. The spectrum shows the large number of poles which are approximately due to the zeros of cosh γL.

The current was also measured up in the mast at the end of about 4 meters of cable. For the first 40 nanoseconds, the current (see Figure 64) is the same as the end of the 61 meter cable since the antenna reflected signal is not yet seen. The 4 meter cable is shorted at the one end and is approximately open at the antenna end for the dominant excitation frequency of 10.5 MHz. The resonant frequency of the cable is 11.3 MHz. Therefore, the current tends to reflect back in phase with the excitation current and builds up to a peak of 19 amperes.

When the cable is open circuited, the cable impedance at the antenna is

$$Z_{in} = 75 \coth \gamma L \tag{23}$$

The voltage at the antenna terminal, V_{in}, is

$$V_{in} = \frac{Z_A I_{sc} Z_{in}}{Z_A + Z_{in}} \tag{24}$$

The open circuit voltage at the end of the cable is obtained by dividing equation (24) by cosh γL and using equation (23). After simplification the open circuit voltage is given by

$$V = \frac{75 Z_A I_{sc}}{Z_A \sinh \gamma L + 75 \cosh \gamma L} \tag{25}$$

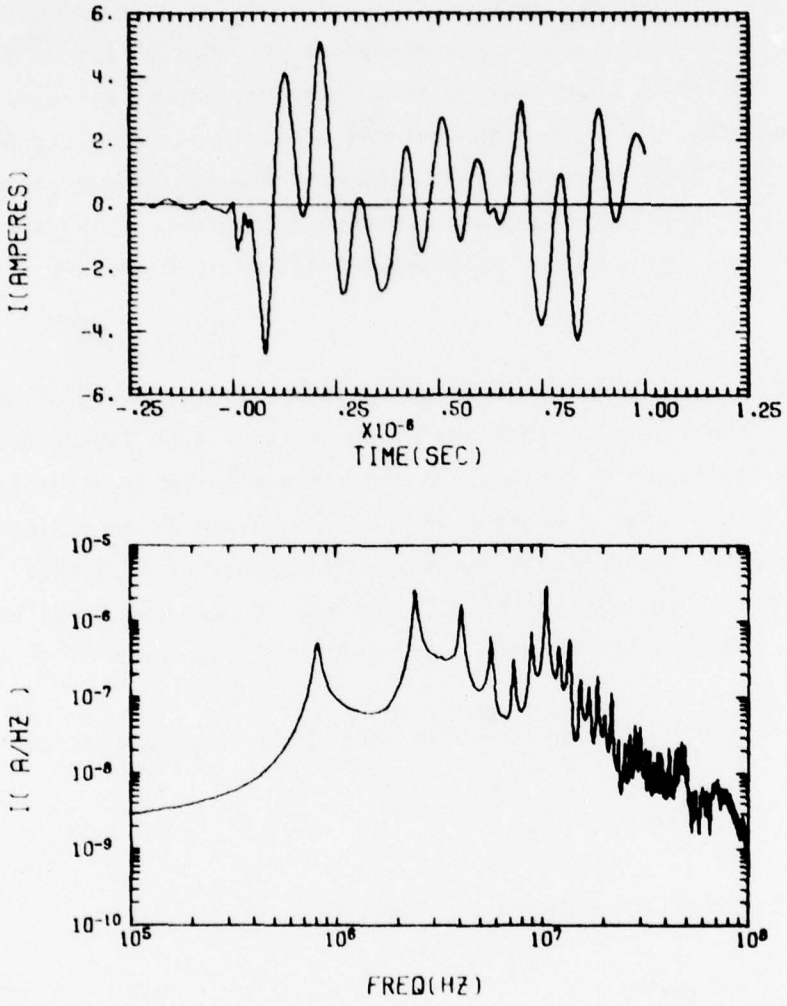

Figure 63 Time and Frequency Domain of Short Circuit Current of ACH Astro Antenna Through 61 Meters of Cable

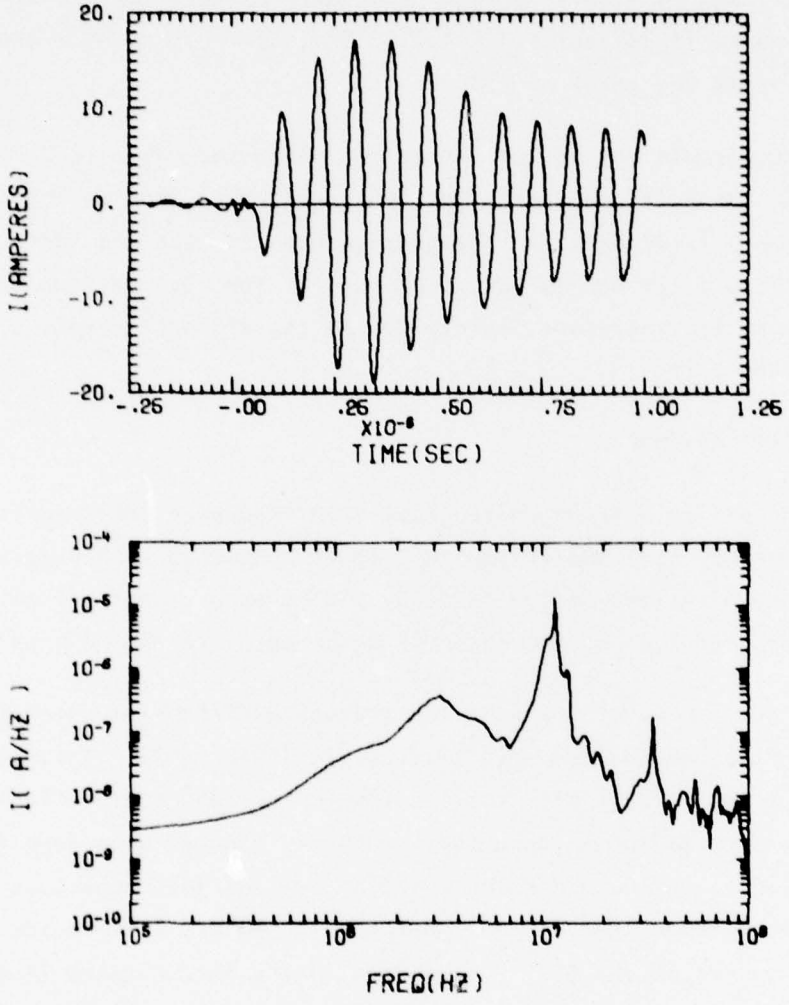

Figure 64 Time and Frequency Domain of Short Circuit Current of ACH Astro Antenna Through 4 Meters of Cable.

The open circuit voltage of the 61 meter cable is shown in Figure 65. Since the source impedance is 75 ohms for the first 618 nanoseconds, the open circuit voltage is simply 75 times the short circuit current of Figure 63. The peak value is 382 volts. Below 20 MHz, $Z_A >> 75$ so that the spectrum peaks are nearly at the zeros of sinh γL.

The open circuit voltage at the end of a 4 meter cable is displayed in Figure 66. The cable is now approximately open at both ends so that the cable resonant frequency is 22 MHz. As the voltage bounces back and forth between the two open circuits, it is nearly out of phase with the 10.5 MHz excitation. The dominant response is, therefore, mainly due to the aft mast resonance. The peak value is 440 volts.

9. UK/SRA-101 ANTENNA

This antenna is a broadband conical high frequency (HF) receiving antenna located at frame 47½ port and starboard. It is connected to a receiver patch panel in the Main Communications Office (MCO) by a 61.6 meter length of cable. The current coupled to a matched load at the receiver patch panel in the MCO was predicted.

A wire grid model of the port and starboard UK/SRA-101 antennas were constructed which included nearby ship's structure (Figure 67). These antennas are approximately 2 meters tall with top loading to increase their effective height. The coaxial cable from the antenna to the MCO was modeled as a type RG-8 using the transmission line equation and a loss term of 0.91 dB/30.5 meters at 20 MHz. The results for the matched load (50 ohm) current in the MCO (before the input filter) are shown in Figures 68 and 69. The current in the port antenna is damped sinusoidal with a 13 MHz resonance frequency and a peak value of 18 A. This response is driven primarily by the incident and scattered fields near the top of the antenna. The incident field near the antenna base is cancelled by the reflected field, while the ship's structure produces an enhancement of the electric field near the top of the antennas. These enhanced electric fields are created by the high surface charge densities which form along the edges and can be larger in magnitude than the incident field. The resultant field at the antenna is thus larger than that due to only the incident field.

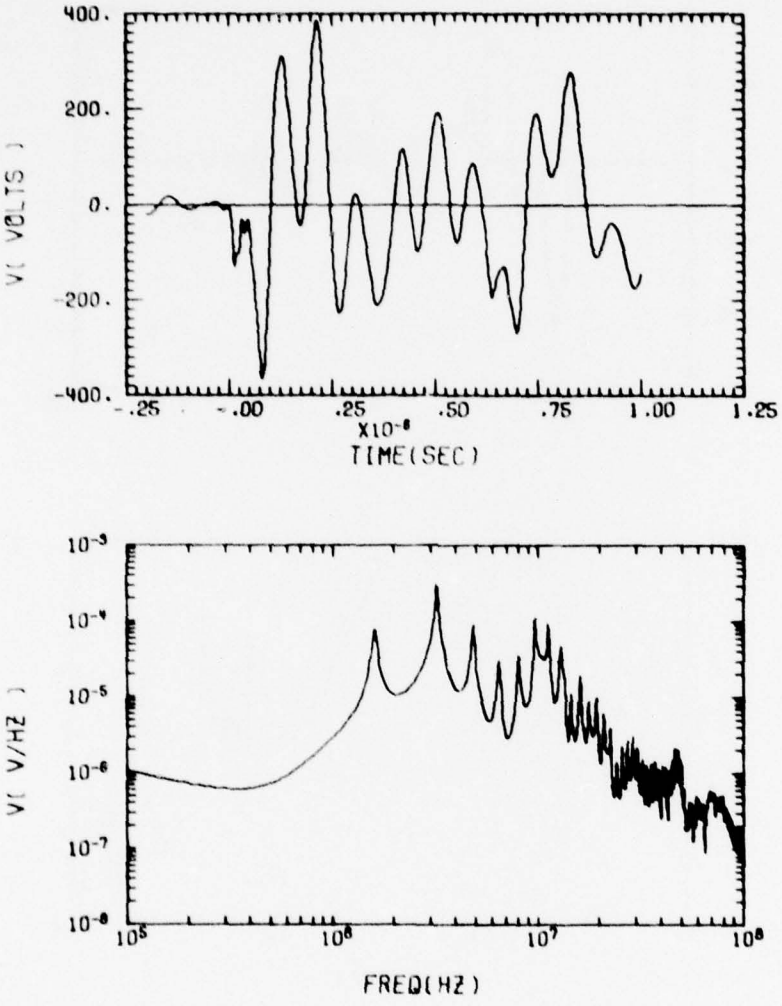

Figure 65 Time and Frequency Domain of Open Circuit Voltage of ACH Astro Antenna Through 61 Meters of Cable

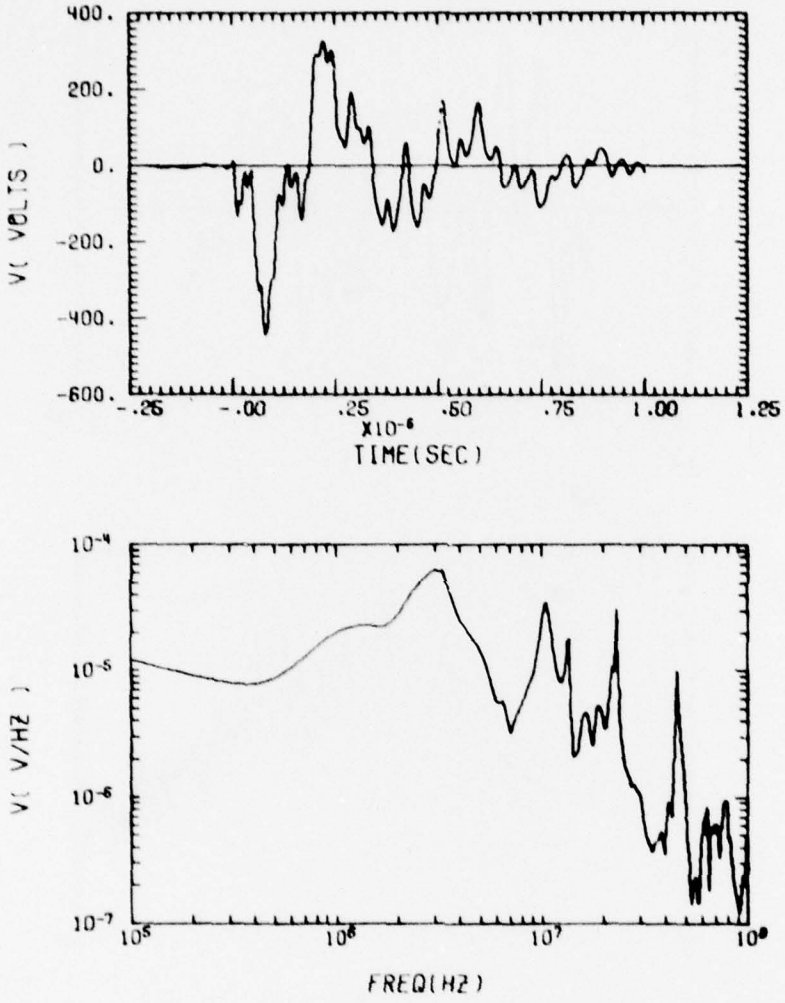

Figure 66 Time and Frequency Domain of Open Circuit Voltage of ACH Astro Antenna Through 4 Meters of Cable

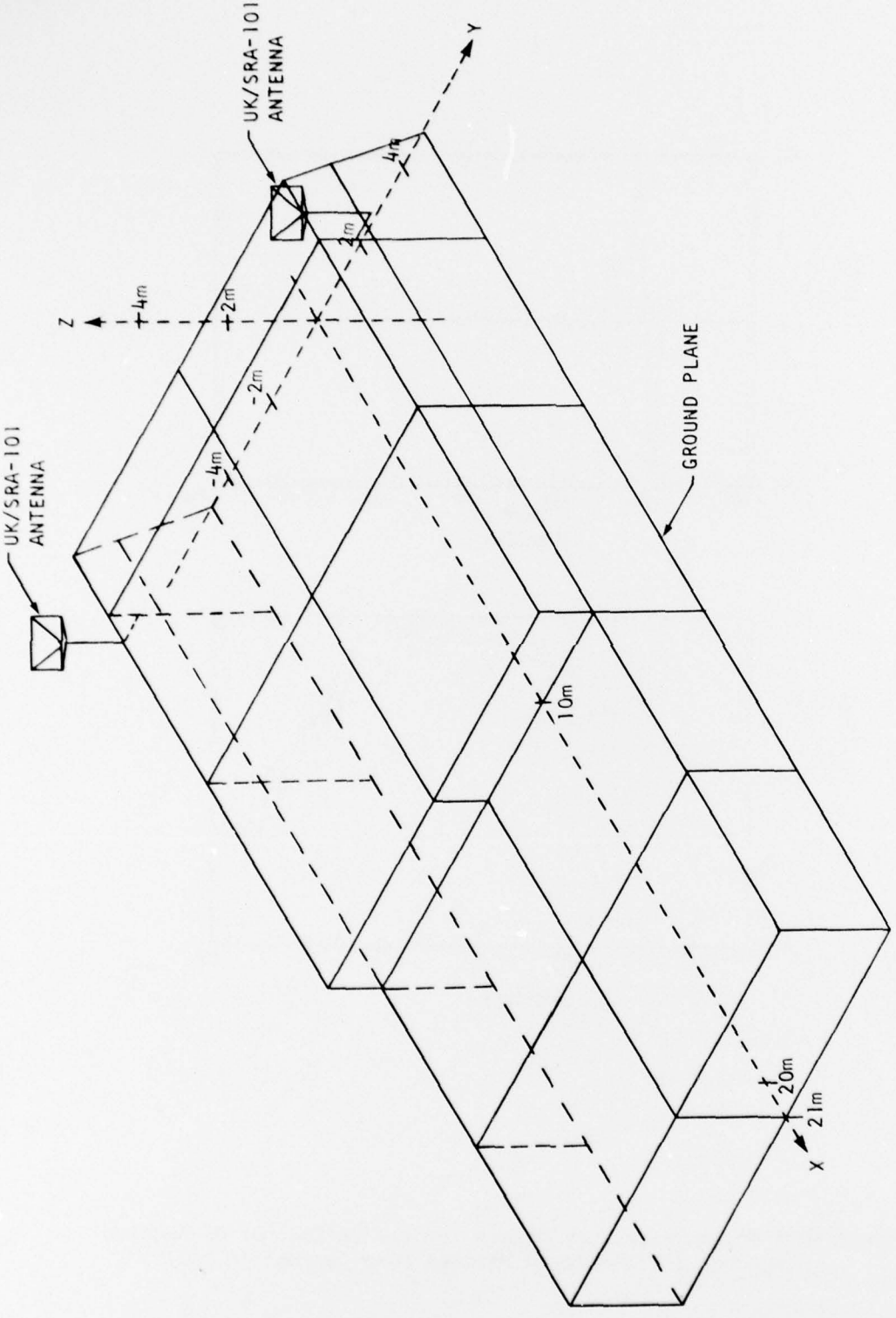

Figure 67 Wire Grid Model for UK/SRA-101 HF Receive Antennas

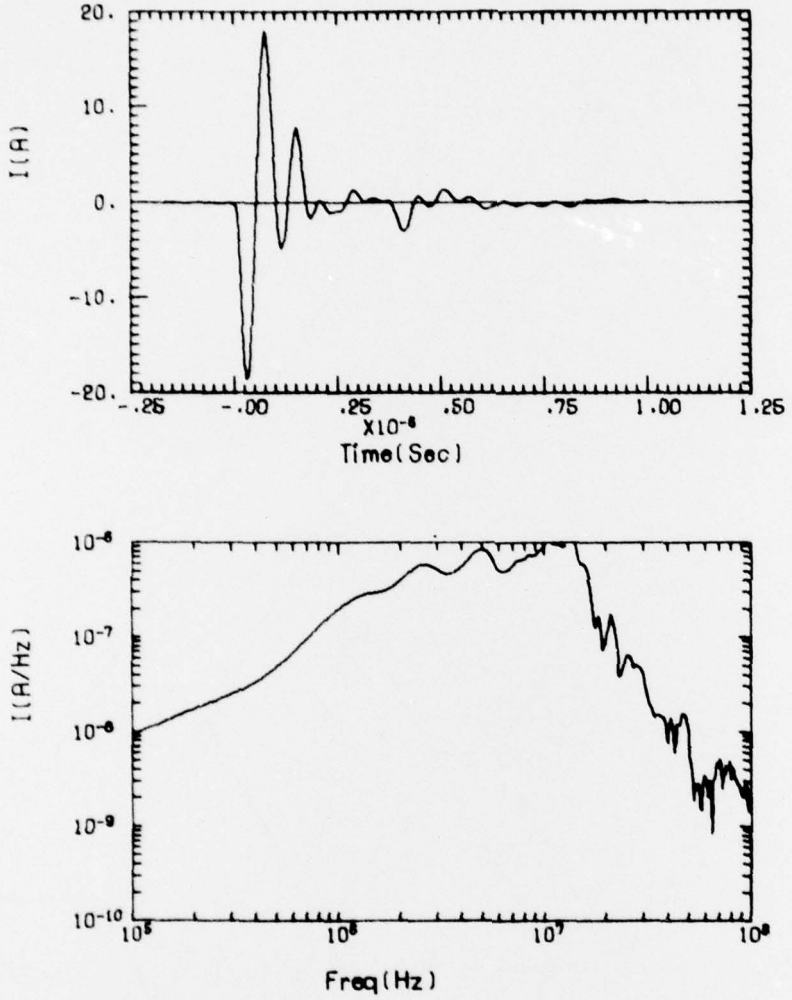

Figure 68 Time and Frequency Domain for the UK/SRA-101 HF Receive Antenna (Port Antenna Matched Load Current in MCO)

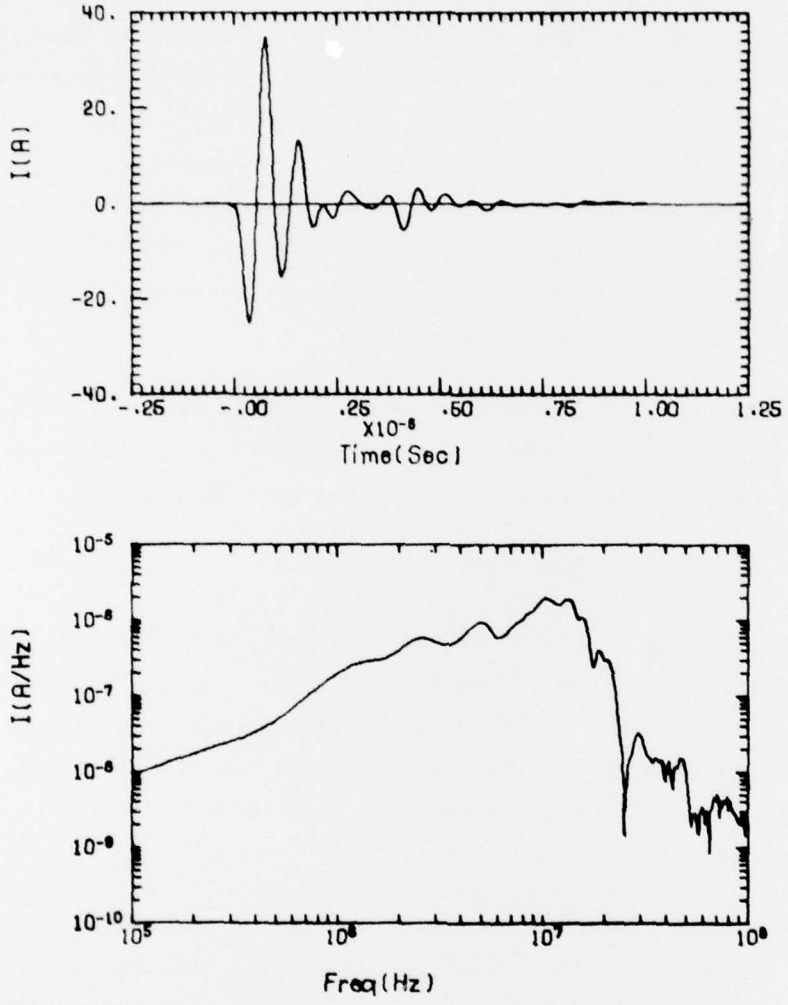

Figure 69 Time and Frequency Domain for the UK/SRA-101 HF Receive Antenna, Starboard Antenna Matched Load Current in MCO

The current in the starboard antenna exhibits the interaction with the incident field and the scattered field off the ship's edge. The current resonates at 13 MHz with a peak value near 34 A. This current is larger than that predicted for the port antenna because the incident field at the antenna base is not cancelled by a reflected field. The total current is again enhanced by the large surface charge densities which accumulate along the ship's edge. Both responses follow the incident field excitation indicating that common modes excited in the ship's structure are small. The matched load voltage can be found from the current response by multiplying the current by the load impedance of 50 ohms. Hence, the peak voltage responses would be 900 volts (port) and 1700 volts (starboard) with resonant frequency at 13 MHz.

The current at the base of each antenna can be found by translating the response back up the coaxial cable. The waveshape is essentially unaltered and the peak amplitude increases to 21 A (port) and 40 A (starboard).

10. CABLES IN THE OPERATIONS ROOM

The operations room contains many mission-essential combat systems integration equipments and their associated cabling. One large bundle of cables runs from the gun mount to the gun console on the forward side of the operations room. The currents obtained in the analysis of the gun mount antenna cable in Section III.2 were used to estimate the peak bulk cable current on a grounded and matched load cable in the operations room.

The bulk cable current at the base of the gun mount whip antenna was translated from the gun mount to the operations room using the standard transmission line equation. The transmission line parameters for this cable were defined in Section III.2. The resultant short circuit and matched load currents predicted in the operations room are shown in Figures 70 and 71. Both of these cable shield terminations were modeled because the mode of termination wasn't known. Both currents display frequency resonances at 19 MHz (gun mount antenna cable) and 2 MHz (transmission line). The time domain responses are shifted by the cable transit time and have peak currents of 5.5 A for the short circuit case and 2.75 A for the matched load circuit.

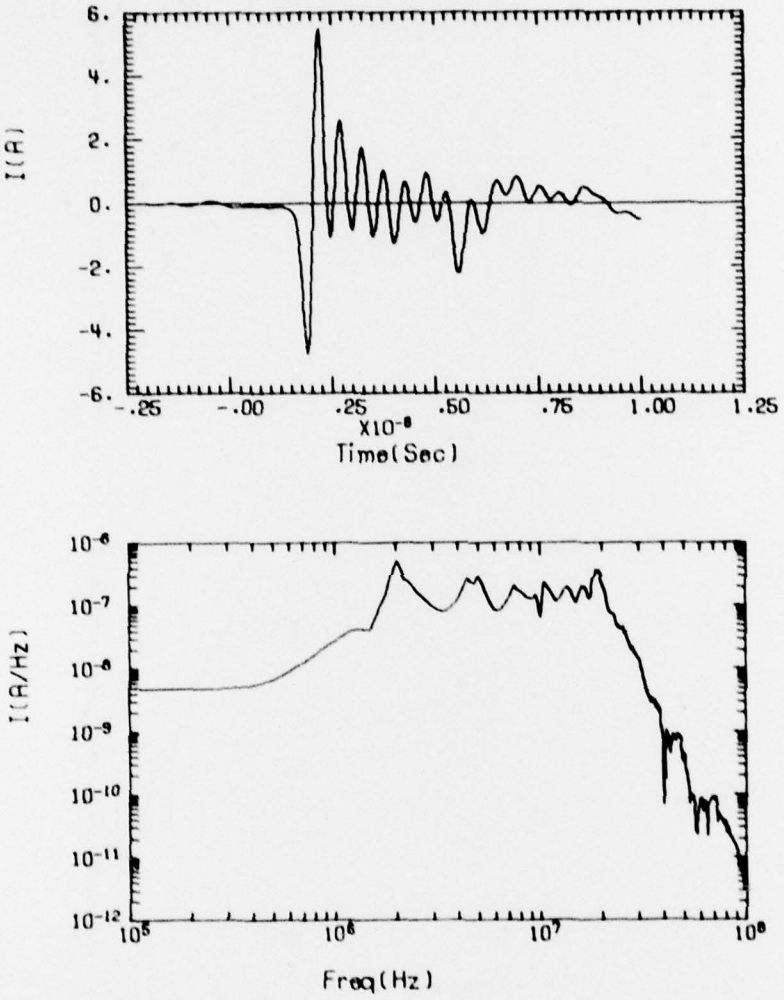

Figure 70 Time and Frequency Domain for the 4.5-inch Gun Mount Antenna Bulk Cable Current in the Operations Room, (EMPRESS Facility Excitation and Cable Shield Grounded)

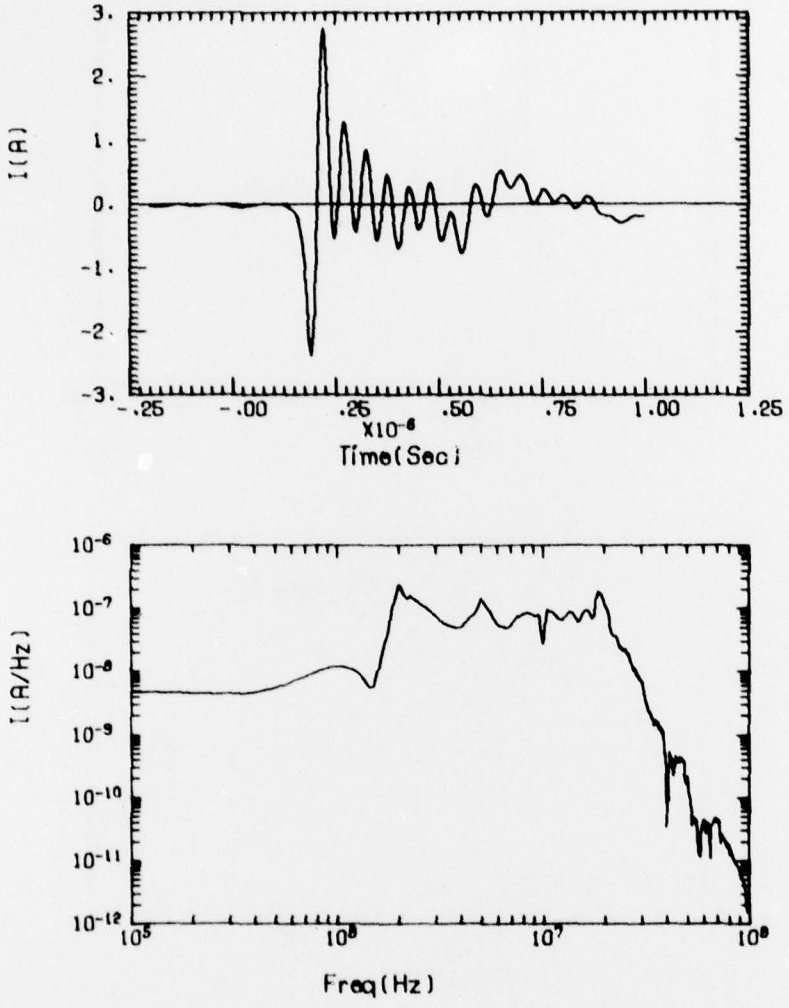

Figure 71 Time and Frequency Domain for the 4.5-inch Gun Mount Antenna Bulk Cable Current in the Operations Room, (EMPRESS Facility Excitation and Cable Shield Connected to a Matched Load)

The current predicted on this cable is expected to be an upper limit because of the many simplifications in the model. The complex loading of the cable bundle was only included in a modification of the loss term in the transmission line equation. In addition, the coupling in the gun mount was simplified to include only the primary scatters which probably overestimates the induced current.

SECTION IV
CONCLUSIONS AND RECOMMENDATIONS

1. CONCLUSIONS

Wire grid modeling techniques based on a method of moments solution have been used to predict currents, current densities, and voltages on ten ship's items. The results of these analyses are summarized in Table 1 where the peak response and dominate frequency are given for each item. Details of each analysis can be found in Section III. The maximum current density occurs on the foremast (port) 5 meters up where the mast is illuminated directly by the incident field. Maximum total current was found on the aft mast. The maximum antenna current and voltage occur on the HF transmit whip antenna. This is because the port antenna interacts directly with the incident EMPRESS field. The other antennas were partially shielded by nearby ship's structure which reduced the field. The port UK/SRA-101 antenna also interacts directly with incident field, but its effective length is shorter than the HF transmit.

It is expected that these analyses overestimate the currents and voltages induced on the Sheffield. The analytical models were by necessity simplifications of the physical situation. When simplifying the models, it was done in a manner which gave maximum coupling thus ignoring minor scatters, cross coupling to other cables, shadowing, etc., which would tend to give more loss than the simple models predict.

The analysis did not consider nonlinear effects such as dielectric breakdown in cables or arcing. Therefore, if the high voltages predicted in some of the antennas caused breakdown, these models would not include it. Also, the effect of the measurement probes was not in general included in the results because when the probe was within manufacturer's specification, the effect was small.

Table 1 Summary of H.M.S. Sheffield EMP Analysis Results

TASK	PEAK RESPONSE	FREQUENCY (MHZ)	COMMENT
AFT MAST			
MAST CURRENT DENSITY	26 A/M	3	
YARDARM CURRENT	11 A	10, 3	
4.5 INCH GUN MOUNT ANTENNA CABLE			
BASE CURRENT	9.5A	19	
MID CURRENT	7.5A	19	
TOP CURRENT	2.2A	19	
UK/SRA-102 ANTENNA CABLE			
CABLE CURRENT	1.8A	10	
FOREMAST WIRE MF RECEIVE ANTENNA CURRENT	16A	6.3	STARBOARD ANTENNA
FOREMAST SURFACE			
CURRENT DENSITY	47A/M	4	
HF TRANSMIT ANTENNA			
CURRENT	60A	8	PORT ANTENNA
VOLTAGE	12.5KV	16	
LORAN RECEIVE ANTENNA			
CURRENT	30A	8	
VOLTAGE	11KV	16	
ACH ASTRO VHF ANTENNA			
MATCHED LOAD CURRENT	2.8A	3, 10	AT END OF 200 FOOT CABLE
SHORT CIRCUIT CURRENT	5.5A		
OPEN CIRCUIT VOLTAGE	400V	3, 10	
UK/SRA-101 ANTENNA			
CURRENT PORT	18A	13	MATCHED LOAD CURRENT AT END OF 202 FOOT CABLE BEFORE FILTER IN MCO
CURRENT STARBOARD	34A	13	
CABLE IN OPERATIONS ROOM			
CURRENT SHORT CIRCUIT	5.5A	19, 2	
CURRENT MATCHED CIRCUIT	2.75A	19, 2	

In conclusion, it is found that computer aided wire grid modeling techniques can be used to predict EMP-induced currents on naval ship's structures. The modeling technique requires the division of the problem into several submodels in order to perform the calculations. However, sufficient detail can be incorporated into these models to predict the major coupling.

2. RECOMMENDATIONS

All analyses done in this report were performed without access to any of the H.M.S. Sheffield test data and without participation in the test program. Although this approach allows one to verify the adequacy of the computer aided wire grid modeling technique, a more beneficial approach to the solution of EMP coupling problems is to combine the analysis and test efforts. Calculated responses to simulated EMP on past programs have often times revealed errors in test data, caused by accidental interactions between test instrumentation and test item, or produced during the data reduction process. When a pretest analysis is performed on a system, the number of test points can be limited to only the most advantageous ones. Predicted magnitude and frequency responses can be used to select the measurement equipment, and one can identify those test points where protection of the test or system equipment is necessary. The test data can then be used to improve the analytical models.

When test data are compared to the pretest analysis predictions, the analysts understanding of the interaction will be verified and/or improved so that the system models can be corrected, if necessary. These models can then be used with increased confidence to predict responses for items at which measurements were not made and for environments that cannot be simulated. In addition, when the theoretical understanding of the EMP interaction with the system is enhanced, a better test procedure can be written. Hence, it is recommended for future ship test programs that an analytical effort be conducted in parallel with it, and that the analysis and test activities be intimately associated for optimum program performance.

APPENDIX A
EMPRESS FIELD

The Electromagnetic Pulse Radiating Environment Simulator for Ships (EMPRESS) is a subthreat level simulator capable of generating either horizontally or vertically polarized fields. For the Sheffield test, only the vertical mode was used.

The vertical mode of EMPRESS consists of a 30.5 meter high, 30 degree half-angle conical antenna, top loaded by the 396.2 meter long horizontal line. (See reference 7 for a detailed system description.) The Sheffield was anchored about 375 meters from the vertical cone as shown in Figure A-1. The EMPRESS field was incident upon the port side of the ship at an angle of 62 degrees from the bow. In the absence of the ship, the time domain electric field was measured at the ship anchor point, 4.27 meters above the water. The peak resonance, as shown in Figure A-2, is 2800 volts-per-meter. The rise time is 13 nanoseconds. The time waveform was digitized and transformed to generate the spectrum as shown in Figure A-2. A computer listing of this spectrum (real and imaginary parts) was provided by NSWC.

At the ship anchor location, the angle between the horizon and tip of the vertical cone is 4.5 degrees. The wavefront is far enough away from the source that is can be approximated as a sum of two planewaves; a direct and a water reflected wave. Since the measurement point is near the water, the reflected vertical electric field is nearly equal to the direct wave with a 2.3 nanosecond delay. The measured data, therefore, is approximately twice the direct wave.

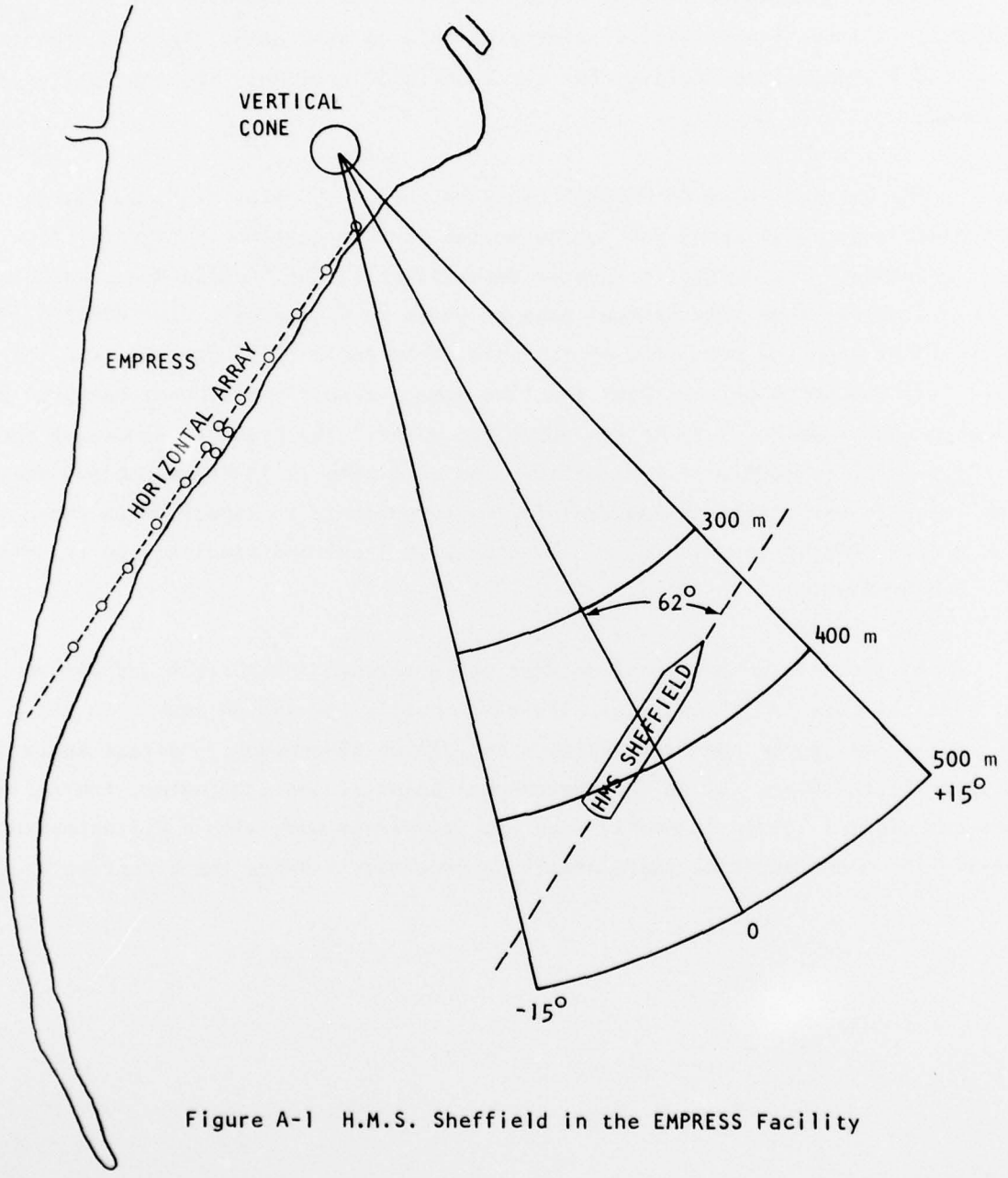

Figure A-1 H.M.S. Sheffield in the EMPRESS Facility

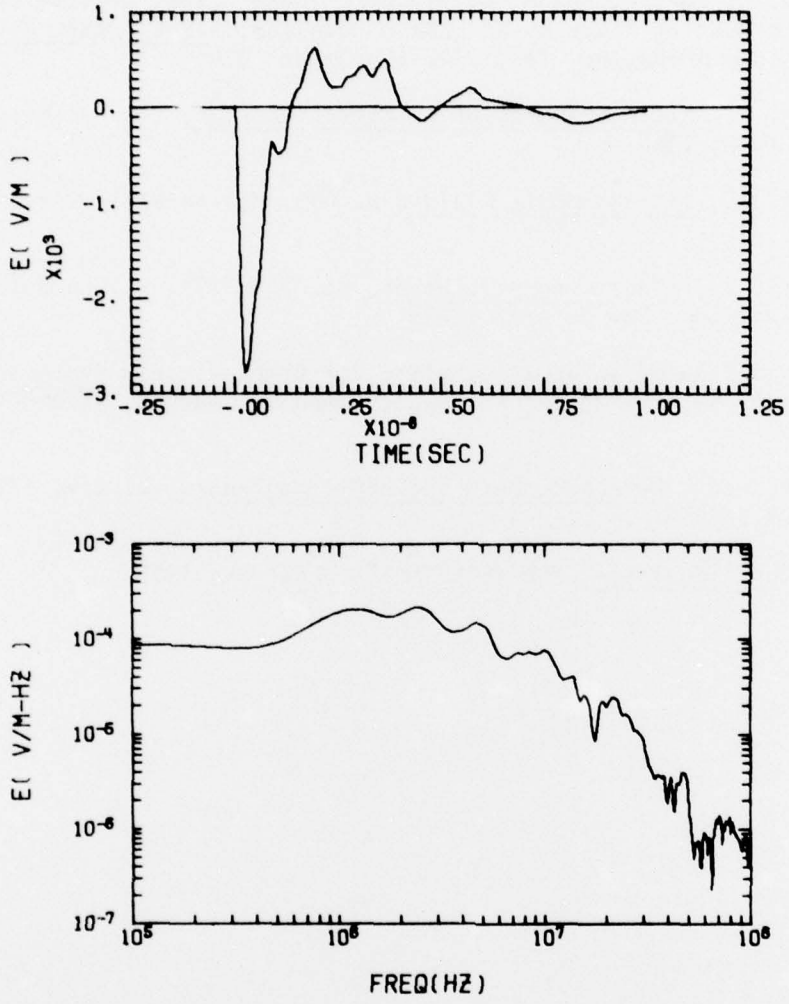

Figure A-2 EMPRESS Incident Field

REFERENCES

1. Lin, J. L., W. L. Curtis, and M. C. Vincent, "Radar Cross Section of a Rectangular Conducting Plate by Wire Mesh Modeling," IEEE Trans. Antennas Propagat., Volume AP-22, pp. 718, 720, September 1974.

2. Harrington, R. F., Field Computation by Moment Methods, the Mac Millan Company, New York, 1968.

3. Harrington, R. F., Time-Harmonic Fields, p. 233, McGraw-Hill, Inc., New York, 1961.

4. Schelkunoff, S. A., Electromagnetic Waves, pp. 369, 371, D. Van Nostrand Co., Inc., Princeton, New Jersey, 1943.

5. Single Line Modeling of Internal Coupling for Complex Cable Systems, D224-13061-1, p. 59, the Boeing Aerospace Company, Seattle, Washington, July 1975.

6. Westman, H. P., ed., Reference Data for Radio Engineers, p. 614, ITT Corp., New York, N. Y., 1956.

7. Valcour EMP Coupling Tests, NSWC/WOL/TR-103, February 1975.